Non-specific Low back pain : Exploratory analysis and clustering for a new paradigm

Lucien Robinault

▶ **To cite this version:**

Lucien Robinault. Non-specific Low back pain : Exploratory analysis and clustering for a new paradigm. Biomechanics [physics.med-ph]. Université Polytechnique Hauts-de-France, 2023. English. NNT : 2023UPHF0007 . tel-04284156

HAL Id: tel-04284156

https://theses.hal.science/tel-04284156v1

Submitted on 14 Nov 2023

HAL is a multi-disciplinary open access archive for the deposit and dissemination of scientific research documents, whether they are published or not. The documents may come from teaching and research institutions in France or abroad, or from public or private research centers.

L'archive ouverte pluridisciplinaire **HAL**, est destinée au dépôt et à la diffusion de documents scientifiques de niveau recherche, publiés ou non, émanant des établissements d'enseignement et de recherche français ou étrangers, des laboratoires publics ou privés.

Thèse de doctorat

Pour obtenir le grade de Docteur de

l'UNIVERSITÉ POLYTECHNIQUE HAUTS-DE-FRANCE

et de l'INSA HAUTS-DE-FRANCE

Discipline, spécialité selon la liste des spécialités pour lesquelles l'École Doctorale est accréditée :
Sciences pour l'Ingénieur, Biomécanique et bio-ingénierie

Présentée et soutenue par ROBINAULT Lucien

Le 19/09/2023, à Valenciennes

École doctorale :
École Doctorale Polytechnique Hauts-de-France (ED PHF n°635)

Unité de recherche :
Laboratoire d'Automatique, de Mécanique et d'Informatique Industrielles et Humaines (LAMIH – UMR CNRS 8201)

Lombalgie: Analyse exploratoire et partitionnement de données pour un nouveau paradigme

JURY

Président du jury

- Emilie Simoneau, Professeure, INSA Hauts-de-France/UPHF

Rapporteurs

- Bernadette Murphy, Professeur, Ontario Tech University
- Ernest Kamavuako, Professeur titulaire, King's College London

Examinateurs

- Emilie Simoneau, Professeure, INSA Hauts-de-France/UPHF

Directeur de thèse

- Jimmy Lauber, Professeur, INSA Hauts-de-France/UPHF

Membres invités

- Sylvain Crémoux, Maître de Conférences, Université de Toulouse
- Imran Khan Niazi, Professeur, NZCC, AUT, AA
- Heidi Haavik, Professeure, New Zealand College of Chiropractic

More information on:
https://creativecommons.org/licenses/by-nd/4.0/

PhD Thesis

Submitted for the degree of Doctor of Philosophy from

UNIVERSITÉ POLYTECHNIQUE HAUTS-DE-FRANCE

And INSA HAUTS-DE-FRANCE

Subject:

Engineering Sciences, Biomechanics and Bioengineering

Presented and defended by ROBINAULT Lucien

On 19/09/2023, Valenciennes

Doctoral school:

Doctoral School Polytechnique Hauts-de-France (ED PHF n°635)

Research unit:

Laboratory of Industrial and Human Automation control Mechanical engineering and Computer science (LAMIH – UMR CNRS 8201)

Non-Specific Low Back Pain: exploratory analysis and clustering for a new paradigm

JURY

President of jury

- Emilie Simoneau, Professor, INSA Hauts-de-France/UPHF

Reviewers

- Bernadette Murphy, Professor, Ontario Tech University
- Ernest Kamavuako, Senior lecturer, King's College London

Examiners

- Emilie Simoneau, Professor, INSA Hauts-de-France/UPHF

Thesis director

- Jimmy Lauber, Professor, INSA Hauts-de-France/UPHF

Invited members

- Sylvain Crémoux, Associate professor, Université de Toulouse
- Imran Khan Niazi, Professor, NZCC, AUT, AAU
- Heidi Haavik, Professor, New Zealand College of Chiropractic

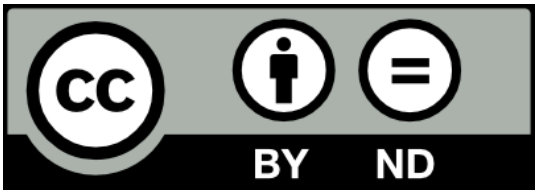

More information on:
https://creativecommons.org/licenses/by-nd/4.0/

Abstract-English

Non-specific low back pain (NSLBP) is a major public health issue and is a concern in most if not all contemporary societies. Despite NSLBP being so widespread, our understanding of its underlying causes, as well as our capacity to provide effective treatments, remains limited due to the high diversity in the population that does not respond to generic treatments. Clustering the NSLBP population based on shared characteristics offers a potential solution for developing personalized interventions. However, the complexity of NSLBP and the reliance on subjective categorical data in previous attempts present challenges in achieving reliable and clinically meaningful clusters.

This work features to goals :

1. First objective : Provide an exploratory work to better understand the influence and importance of the selected variables in regards to NSLBP and our sample population, and gather information to prepare subgrouping
2. Second objective : Provide an attempt at clustering our population sample in order to discriminate valuables subgroups

Data were acquired from 46 subjects who performed six simple movement tasks (back extension, back flexion, lateral trunk flexion right, lateral trunk flexion left, trunk rotation right, and trunk rotation left) at two different speeds (maximum and preferred). High-density electromyography (HD EMG) data from the lower back region were acquired, jointly with motion capture data, using passive reflective markers on the subject's body and clusters of markers on the subject's spine.

An exploratory analysis was conducted using a deep neural network and factor analysis. Based on selected variables, various models were trained to classify individuals as healthy or having NSLBP in order to assess the importance of different variables. The models were trained using different set of data : full data set, anthropometric data set, biomechanical data set, neuromuscular data set, and balance and proprioception data set. The models achieved high accuracy in categorizing individuals as healthy or NSLBP. Factor analysis revealed that individuals with NSLBP exhibited different movement patterns to healthy individuals, characterized by slower and more rigid movements. Anthropometric variables (age, sex, and BMI) were significantly correlated with NSLBP components.

Clustering was attempted on our full data set, and reduced data set, using PCA or the insights gather in the exploratory analysis part. The data set were either movement agnostic or movement specific. Results showed viable clustering using spectral algorithm, with the RBF kernel and the discretize label assignment's algorithm, expressing a spectrum of low back pain as did similar work before. The data set used was the full data set with spine cluster of marker data, after dimension reduction using principal component analysis.

In conclusion, different data types, such as body measurements, movement patterns, and neuromuscular activity, can provide valuable information for identifying individuals with NSLBP. To gain a comprehensive understanding of NSLBP, it is crucial to investigate the main domains influencing its prognosis as a cohesive unit rather than studying them in isolation. Simplifying the conditions for acquiring dynamic data is recommended to reduce data complexity, and using back flexion and trunk rotation as effective options should be further explored. The importance and probable usefulness of meta data, such as anthropometric data for the biophysical domain, was also noted. In the light of those results, we formulated the following new paradigm hypothesis : low back pain yields adaptations common to every subject, but due to inter-subject differences in the 5 main domains known to have a major influence on low back pain prognosis (biophysical, comorbidities, social, psychological and genetic) those adaptations are expressed in very unique way for each subject.

Keywords : Non Specific Low Back Pain, Cluster analysis, Factor Analysis, Deep Learning, Motion Capture, High Density Electromyography.

Abstract-French

La lombalgie non spécifique (LNS) est un problème majeur de santé publique vastement répandu dans les sociétés contemporaines. Malgré la prévalence importante de la LNS, notre compréhension des causes sous-jacentes à la LNS, ainsi que notre capacité à fournir des traitements adaptés et efficace pour tous les patients, reste limitée en raison de la grande diversité de la population qu'englobe la LNS et qui ne répond pas à des traitements génériques. Le regroupement de la population atteinte de LNS en fonction de caractéristiques communes offre une solution potentielle pour développer des interventions personnalisées. Cependant, la complexité de la LNS et la dépendance aux données catégoriques subjectives dans les tentatives de regroupement précédentes posent des défis pour parvenir à des regroupements fiables et cliniquement significatifs.

Ce travail à pour visée deux objectifs :

1. Premier objectif : Fournir une étude exploratoire pour mieux comprendre l'influence et l'importance des variables sélectionnées par rapport à la LNS et à notre population d'échantillonnage, et recueillir des informations pour préparer la création de sous-groupes.
2. Deuxième objectif : Tenter de regrouper notre échantillon de population afin d'identifier des sous-groupes précieux.

Les données ont été acquises sur 46 sujets. Notre protocole se basait sur un jeu de mouvement simple effectué à différentes vitesses : extension du dos, flexion du dos, flexion latérale du tronc (à droite et à gauche), rotation du tronc (à droite et à gauche), à vitesse maximum et naturelle. Des données d'électromyographie haute densité (EMG HD) de la région lombaire ont été collectées, conjointement à des données de capture de mouvement à l'aide de marqueurs réfléchissants passifs sur le corps du sujet ainsi que grâce à des groupes de marqueurs sur la colonne vertébrale du sujet.

Une analyse exploratoire a été réalisée à l'aide d'un réseau neuronal profond et d'une analyse factorielle en se basant sur des variables sélectionnées préalablement grâce à une étude la littérature. Différents modèles d'apprentissage profond ont été entraînés pour classifier les individus entre sujets sains ou atteints de LNS, afin

d'étudier le pouvoir d'information des différentes variables utilisées. Les modèles ont été entraînés en utilisant différents sets de données : jeu de données entier, variables anthropométriques, jeu de données biomécaniques, jeu de données neuromusculaires ou jeu de données liées à l'équilibre et la proprioception. Les modèles ont atteint de hauts résultats de classification. L'analyse factorielle a révélé que les individus atteints de LNS présentaient des schémas de mouvement différents de ceux des individus en bonne santé, caractérisés par des mouvements plus lents et plus rigides. Les variables anthropométriques (âge, sexe et IMC) étaient significativement corrélées avec les composantes de la LNS.

Des tentatives de regroupement ont été réalisées sur notre ensemble de données complet et un ensemble de données réduit en utilisant l'ACP ou les informations recueillies dans la partie de l'analyse exploratoire. Les ensembles de données étaient soit agnostiques au mouvement, soit spécifiques au mouvement. Les résultats ont montré un regroupement viable en utilisant un algorithme spectral avec le noyau RBF et l'algorithme d'assignation d'étiquettes discretize, comme dans des travaux similaires antérieurs. L'ensemble de données utilisé était l'ensemble de données complet avec les données de marqueurs de la colonne vertébrale, après réduction de dimension à l'aide de l'analyse en composantes principales.

En conclusion, différents types de données, tels que les mesures corporelles, les schémas de mouvement et l'activité neuromusculaire, peuvent fournir des informations précieuses pour identifier les individus atteints de LNS. Pour obtenir une compréhension globale de la LNS, il est crucial d'étudier les principaux domaines influençant son pronostic comme une unité cohérente plutôt que de les étudier isolément. Il est recommandé de simplifier les conditions d'acquisition des données dynamiques pour réduire la complexité des données, et l'utilisation de la flexion du dos et de la rotation du tronc comme options efficaces devrait être davantage explorée. L'importance et l'utilité probable des métadonnées, telles que les données anthropométriques pour le domaine biophysique, ont également été notées. À la lumière de ces résultats, nous avons formulé la nouvelle hypothèse de paradigme suivante : la lombalgie engendre des adaptations communes à tous les sujets, mais en raison des différences inter-sujets dans les cinq principaux domaines connus pour avoir une influence majeure sur le pronostic de la lombalgie (biophysique, comorbidités, social, psychologique et génétique), ces adaptations s'expriment de manière très unique pour chaque sujet.

Keywords : Lombalgie Non Specifique, Partitionnement de données, Analyse factorielle, Apprentissage profond, Capture de mouvement, Electromyographie Haute Densité.

Contents

List of Figures

List of Tables

Glossary

AP Action Potential

BW Baseline Wander

BMI Body Mass Index

CCA Canonical Correlation Analysis

COP Center Of Pressure

CNN Convolutional Neural Networks

DNN Deep Neural Network

EMG Electromyography

ES Erector Spinae

FA Factor Analysis

FRR Flexion Relaxation Response

GCS Global Coordinate System

GFR Ground force reaction

HDBSCAN Hierachical Density-based Spatial Clustering of Applications with Noise

HAC Hierarchical Agglomerative Clustering

HDEMG High Density Electromyography

LCS Local Coordinate System

ML Machine Learning

MOCAP Motion Capture

MUAP Motor Unit Action Potential

MLP Multi-Layer Perceptrons

NSLBP Non-Specific Low Back Pain

OI Obliquus Internus abdominis

PLI Power Line Interference

PCA Principal Component Analysis

PNR Pulse to Noise Ratio

RBF Radial Basis Function

ROM Range of Motion

RNN Recurrent Neural Networks

RMS Root Mean Square

RMSE Root Mean Square Error

SFAP Single Fiber Action Potential

STA Soft Tissue Artefact

TrA Transversus Abdominis

WGN White Ground Noise

YLD Years Lived with Disabilities

Introduction

Non-Specific Low Back Pain (NSLBP) is a symptom that is characterized by pain for more than one day located between the lower rib margins and the buttock creases. The pain does not have a definite cause and cannot be traced to a specific event or affliction (Maher, Underwood, and Buchbinder 2017). NSLBP is a significant public health problem around the world (Hoy et al. 2014). Despite the best efforts of researchers and public health officials over a number of decades our body of knowledge about this symptom doesn't grow as fast as the problem is getting worse (Hodges, Cholewicki, and Van Dieën 2013). A new approach is therefore needed to tackle this problem in order to reduce the crippling burden of NSLBP on the healthcare system, and society in general (Hodges, Cholewicki, and Van Dieën 2013).

A promising area of research for NSLBP is the subtyping of the NSLBP population. It is believed and likely that once sub-divided in smaller and more homogeneous sub-population, it will become easier to design specific, and therefore more effective, treatment approaches, based on each patients' individual needs (Hodges, Cholewicki, and Van Dieën 2013; Haskins, Osmotherly, and Rivett 2015b, 2015a). The first step, is to find a clinically valid framework for clustering the NSLBP population. Clustering that large population will enable the study of more homogeneous sub-populations, which would lead to a better comprehension of the symptom and of the differences between sub-population. Which in turn, would help design adapted and effective treatments for every sub-population.

But the task is not an easy and straight forward one. So far, the clustering task has not yield major success, and we therefore think a new approach should be taken. But before being able to define adapted cluster models, important preliminary work needs to be done in order to identify which variables are the most relevant and specific to NSLBP, and at discriminating between the potential subgroups inside this population.

This is where this work start: by first running an exploratory analysis to improve our understanding of discriminating variables in relation to the symptom. After this exploratory work, attempt at clustering our NSLBP population sample at hand will be made, using the insights from previous works and ours. This foundation work

will pave the way for subsequent clinical trials and should provide improvement in our understanding of NSLBP and where to focus future research.

Chapter 1

Non Specific Low Back Pain

1.1 Definition

Non-Specific Low Back Pain (NSLBP) is an idiopathic symptom that is characterized by pain for more than one day located between the lower rib margins and the buttock creases, as shown in Figure 1.1. It is either acute or chronic (more than 3 months per year). It might or might not limit the usual activities or change the daily routine of the person (Dionne et al. 2008).

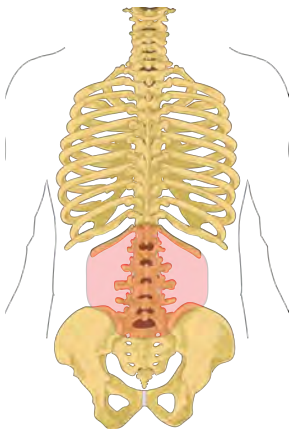

Figure 1.1: Low back pain area.

1.2 Clinical representation

NSLBP is a complex symptom which encompass multiple aspects that can be classified into 5 categories: biophysical, comorbidities, social, psychological and genetic factors (Hartvigsen et al. 2018). The main characteristic of NSLBP, is its idiopathic nature: the sources of the pain can not be traced to a specific event or affliction (Maher, Underwood, and Buchbinder 2017). People subjected to NSLBP often present pain in one or both legs, and less frequently, also present neurological disorders afflicting the lower limbs (Hartvigsen et al. 2018). Even if a large majority, 72% of the patients subject to acute NSLBP, recover in 12 months (Henschke et al. 2008), 33% of them relapse in the following 12 months (Stanton et al. 2008). If they were subject to a persistent form of the symptom, less than half of the patients recovered in that 12 months period (Costa et al. 2009). As we do not accurately understand the cause, or causes, and mechanisms that drive NSLBP, it is not possible to design specific and adapted treatments for it, treatments that would dramatically increase the chance of recovery of the afflicted patients (Maher, Underwood, and Buchbinder 2017).

1.3 Epidemiology

NSLBP is a symptom that is extremely prevalent worldwide, with a one-year point prevalence of 38% (Hoy et al. 2012), as shown in Figure 1.2, and a global point prevalence of 7.3%. This translates to an estimated 540 million of people affected at any time in the world (Hartvigsen et al. 2018). Out of all the LBP diagnosed, between 90% to 99% are deemed nonspecific, meaning that the cause of it is unknown or cannot be pinpointed (Koes, Van Tulder, and Thomas 2006; Deyo and Weinstein 2001; Henschke et al. 2009b; Enthoven et al. 2016; Downie et al. 2013). A large majority of the patients, 80%, face moderate to severe pain, and 76% of those patients see their daily function being moderately, to extremely, affected by the symptom and the associated pain (Hartvigsen et al. 2018). It has to be said that NSLBP is a long lasting and, often, recurring symptom: 76% of people complaining about NSLBP, be it acute or chronic, have already suffered previous episodes (Henschke et al. 2009a).

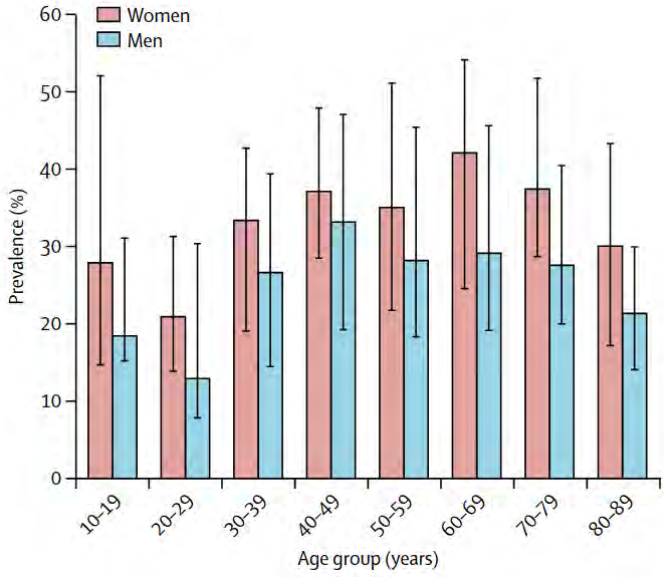

Figure 1.2: Median prevalence of low back pain, with IQR, according to sex and midpoint of age group, reproduced from Hoy and collaborators.

1.4 Impact on society

NSLBP is a significant public health problem all around the world as it is the leading cause of disability worldwide (Hoy et al. 2014) and costs governments and insurance providers billions of dollars in treatment and workers compensation costs each year (Hoy et al. 2014). As of today, NSLBP is the number 1 affliction when it comes to disabilities with 60.1 million years lived with disability worldwide (YLD) in 2015, which is an increase of 54% since 1990 (DALYs et al. 2016), as shown in Figure 1.3. The NSLBP problem is present in developed country and developing one, but exhibit different issues in each: in developed countries, the impact and burden of NSLBP is put on the healthcare and social system first. Whereas in developing countries, the burden is predominantly put on the people impacted by LBP and their support systems (Hartvigsen et al. 2018). Nonetheless, one common problem, faced by both type of countries, is the age associated disabilities which are aggravated by NSLBP, or aggravate the symptom and the associated consequences (Hoy et al. 2014). This is especially concerning in ageing societies, a common phenomenon in developed countries.

Reliably estimating the cost of NSLBP on society is a very complex task. The real cost tends to be underestimated as a lot of expenses are indirect and are not, or cannot be, taken into account in the estimates (Hartvigsen et al. 2018). But even without accounting with those underestimations, the cost on society, as a whole, is high. As an example, in 1996, the cost of NSLBP for the USA was estimated to be

between US$18.5 billion and US$28.2 billion (Dagenais, Caro, and Haldeman 2008). To put the impact of NSLBP on society in perspective, NSLBP is responsible for more early retirement of old workers than the combined effect of heart disease, diabetes, hypertension, neoplasm, asthma and respiratory diseases all together (Schofield et al. 2008), a fact even more concerning in ageing countries.

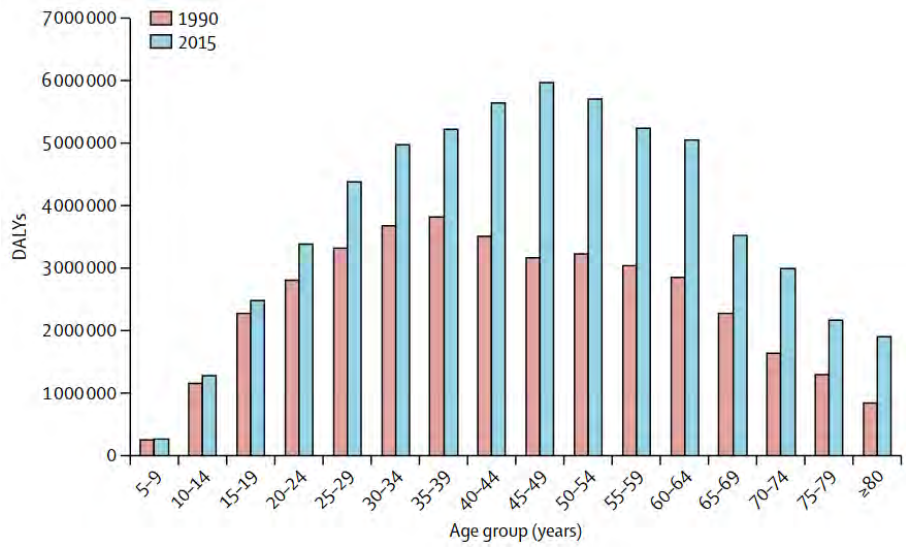

Figure 1.3: Global burden of low back pain, in disability-adjusted life-years (DALYs), by age group, for 1990 and 2015, from Hartvigsen and collaborators.

1.5 The problem of NSLBP

The major problem of NSLBP encompass a very large and variable population, a fact that make the symptom hard to study, to understand and to treat. As this large population has, so far, not be subdivided reliably, it is therefore relatively hard to design treatment and rehabilitation protocol that are effective for all patients. Currently, NSLBP is an epidemic that is both costly and socially debilitating (Hoy et al. 2014), and despite the best efforts of researchers and public health officials the problem is getting worse (Hoy et al. 2014).

A new approach to tackling this problem is required in order to reduce the crippling burden of NSLBP on the healthcare systems and societies (Hodges, Cholewicki, and Van Dieën 2013). Previous research efforts into NSLBP rehabilitation have been hampered by research designs using narrow theoretical frameworks, poor diagnostic and classification systems, unresponsive or inappropriate outcome measures, and treatment providers who may lack the necessary tools or training to obtain the best clinical outcomes (Hodges, Cholewicki, and Van Dieën 2013; Bouter, Tulder, and Koes 1998; Synnott et al. 2015). One promising area for NSLBP research,

involves subtyping NSLBP patients, so that the most appropriate treatment can be provided based on the patients' individual needs rather than the current "one size fits all" approach (Hodges, Cholewicki, and Van Dieën 2013; Haskins, Osmotherly, and Rivett 2015b, 2015a). It is likely that different subgroups of NSLBP patients will respond best to specific treatment approaches. If we can find a way to determine the subgroup of a NSLBP patient clinically, in order to allocate him to the rehabilitation protocols that will be the most beneficial to their particular needs, a major leap in treating NSLBP and understand the symptom will have been made.

1.6 Characteristics of NSLBP population

Even if the NSLBP population is broad and diverse and present inconsistent differences between itself, it still showcases consistent changes when compared against the healthy population. The changes are seen on multiple aspects, whether it be biomechanical behavior, neuromuscular control, cyclic repetitions pattern etc... In this part, we will take a look at the changes that are seen in a consistent manner in the NSLBP population.

1.6.1 Balance and proprioception

The balance ability of the NSLBP population is negatively impacted by the symptom. For example, it has been shown that patients with NSLBP exhibit greater postural instability than healthy controls. This translates to greater center of pressure (COP) excursions, and higher mean velocity of the COP. While the decreased postural stability in NSLBP subjects appears to be associated with the presence of pain, it seems to be unrelated to its exact location or the duration the patient had pain for (Ruhe, Fejer, and Walker 2011). Nonetheless, the COP amplitude still seems to be correlated with the pain location (Della Volpe et al. 2006), while the COP mean velocity seems to be correlated with the pain intensity (Corbeil, Blouin, and Teasdale 2004). But the correlation between the pain intensity and the magnitude of COP excursions alteration, is not always clearly seen. Indeed, some studies managed to find a correlation between the COP alterations and the pain intensity (Corbeil, Blouin, and Teasdale 2004), while other did not (Ruhe, Fejer, and Walker 2011). This discrepancy might be linked to the diversity of the NSLBP population: due to the different population samples studied, the studies were probably just looking at different spectrum of NSLBP, as it is very unlikely that those studies recruited the same subjects.

In addition, it is thought that NSLBP impairs or damages the patients proprioceptive system (Hodges, Cholewicki, and Van Dieën 2013). For example, when standing on foam the NSLPB population presented a more irregular COP behavior, presenting higher frequency of sway. This hypothesis of a damaged, altered, or at least deficient

proprioceptive system has been tested via trunk re-positioning tasks. The goal of those tasks was for the subject to accurately position his trunk to a specific position, and then go back to his original position. Both times aiming for optimal precision. In those studies, it was shown that LBP subjects performed much less accurately than their healthy counterpart which seems to go along the hypothesis of a damaged or altered proprioceptive system (Gombatto et al. 2015; Ruhe, Fejer, and Walker 2011; MacDonald, Moseley, and Hodges 2009). Due to this potential proprioceptive impairment from NSLBP, it is believed that NSLBP patients have a higher reliance on visual cue for postural control compared to healthy subjects. A belief that seems to be confirmed by other studies (Sipko and Kuczyński 2013).

In order to look further into it, studies using vibration were conducted (Goossens et al. 2018). Indeed, vibration applied to the muscles perturbs the muscle sensorimotor abilities. During a tracking task where the subject was to follow a path with his trunk, when no vibrations were applied to the lumbar muscles, NSLBP subjects showcased 27.1% more tracking errors than their healthy counterparts. When vibrations were applied to the lumbar muscles, the healthy subjects tracking error increased by 10.5%, while the NSLBP subjects did not show any changes (Willigenburg et al. 2013). As NSLBP subjects were not affected by the vibrations, this result seems to confirm the hypothesis of a damaged or altered sensorimotor system in NSLBP subjects.

1.6.2 Trunk movements

As could have been thought from the damaged or altered proprioceptive system hypothesis, just like the balance and proprioception, NSLBP population presents altered trunk movements in all plan and altered trunk control in general. It was shown that NSLBP patients presented more forward trunk inclination during static postural analysis, compared to healthy subjects, or that NSLBP subjects perform basic trunk movements, such as forward and backward bending, lateral flexion or rotation, with diminished amplitude compared to healthy subjects, accompanied with a diminished average angular speed (Bourigua 2014). But the opposite is also found: NSLBP subjects having higher amplitude of the lumbar spine movement. Indeed, the NSLBP population is very broad and diverse, and if it mostly consistently showcases changes compared to healthy population, those changes are inconsistent across the NSLBP population (Villafane et al. 2016). Other studies on lateral trunk flexion have shown that trunk passive elastic energy asymmetry is predicted by a gender and a muscle factor in NSLBP subjects, whereas only the gender factor had predictive power in healthy subjects (Gombatto et al. 2013).This could be explained by the alteration of the non-contractile structures (Goossens et al. 2018;Willigenburg et al. 2013), as motor schemes and control rely on those structures, partly explaining the source of the trunk control differences between healthy and NSLBP.

These alterations in NSLBP patients are also found in other movements tasks. For example, during box lifting, NSLBP subjects presented different motor strategies compared to their healthy counterparts (Sanderson et al. 2019). Those variations might stem from the significantly reduced mobility that was expressed by NSLBP subjects, which called for various strategies to compensate for it. However, the contribution of the lumbar spine relatively to the contribution of the hip was found to be similar in both healthy and NSLBP. While the NSLBP subjects had a substantially altered lumbar spine-hip joint coordination, in particular, in those with a positive straight leg raise sign (Shum, Crosbie, and Lee 2007).

Another example from the literature is with the sit-to-stand task. During such task, the NSLBP population performed at slower speed, showed counter-rotation between thorax and pelvis on the transverse axis, and an overall lack of mobility around the spine and hips joints compared to the healthy subjects. These differences were accompanied with alteration of the coordination of the lumbar spine-hips joint. Nonetheless, it wasn't possible to isolate a generic compensation strategies for the NSLBP group (Shum, Crosbie, and Lee 2005).

NSLBP patients are more likely to adopt a strategy of trunk stiffening via coactivation of agonist and antogonist muscle while reducing their reliance on deep muscles. This is thought to be done in order to prevent nociceptive input and to maximize perceived benefits. One of the drawbacks of this stiffening strategy, is that it may work in the short term, but it might also be detrimental in the long term (J. Dieën, Reeves, and Kawchuk 2018). It was reported that for a trunk forward bending, NSLBP subjects presented larger moments affecting their spine at smaller flexion angles and smaller moments at the end range of the movement when compared with healthy subjects (Shum, Crosbie, and Lee 2010). This might also explain the higher average moments in compression forces usually measured on the discs of the spine of NSLBP subjects (Hasegawa et al. 2018).

The work of Laird and collaborators summarize nicely some of the other biomechanical differences that can usually be seen in NSLBP compared to healthy peoples. On average, people with NSLBP display (Laird et al. 2014):

- No difference in lordosis angle (8 studies)
- Reduced lumbar range of motion (ROM) (19 studies)
- No difference in lumbar relative to hip contribution to end-range flexion (4 studies)
- No difference in standing pelvic tilt angle (3 studies)
- Slower movement (8 studies)
- Reduced proprioception (17 studies)

1.6.3 Variability and adaptability of the movements

A very noticeable difference in NSLBP subjects is the difference in movement variability and adaptability. Indeed, NSLBP subjects showed on average more variability in standalone repetitions, a repetition which is isolated from any other by a pause. This increased variability was, for example, shown in sit to stand tasks regarding each independent repetitions in NSLBP subjects when compared to healthy ones (Ippersiel, Robbins, and Preuss 2018). Another display of a lack of adaptability can be seen in the fact that LBP subjects do not increase their base of support by widening their stance in preparation to execute a faster movement. Something healthy subjects do in order to perform optimally (Bourigua 2014). On the other hand, NSLBP subjects showed on average less variation between repetition during cyclic movement, such as walking, or while executing multiple repetitions of the same movement. Again, those results must be put in perspective. Indeed, some studies have shown that, even if movement speed and range of motion displayed greater variability for people with LBP during trunk flexion, lateral flexion or rotation, at the same time, other movement characteristics did not display greater variability, like the pelvic tilt angle for example (Laird et al. 2014). For example, even if walking is a cycling activity, a study showed that NSLBP subjects had higher stride to stride variability compared to healthy ones (Vogt et al. 2001). Nonetheless, in general, LBP subjects, tend to present a more variable proportional motion of the spine, that is the sharing of bending across spinal segments, compared to healthy subjects (Cholewicki et al. 2019). These alterations in variability of repetitions and movement adaptability seems to indicate again alterations to the proprioceptive systems. These alterations would translate to a decrease of adaptation capabilities to the conditions in which the movement is performed, be it the starting conditions or to perturbations during the actual movement (Asgari et al. 2015). Some of these changes might stem from neuromuscular control adaptations, as NSLBP subjects tend to show less within-subject variance in activation pattern of the trunk muscles (J. Dieën, Reeves, and Kawchuk 2018), maybe due, or the cause, to their trunk stiffening strategies (J. Dieën, Reeves, and Kawchuk 2018). But during cyclic activities, such as walking, the opposite seems to be seen with more cycle-to-cycle variability in the Erector Spinae (ES) activity (Vogt, Pfeifer, and Banzer 2003).

An interesting fact to be aware of is that higher motor variability was observed in the upper limb or in the trunk in the presence of acute pain, whereas the variability was lower under chronic pain conditions (Madeleine 2010; J. H. van Dieën, Flor, and Hodges 2017), which tends to suggest adaptations to chronic NSLBP in the affected subjects, like a dose-response relation between NSLBP and adaptations.

1.6.4 Neuromuscular control

Neuromuscular control in NSLBP subjects, mainly regarding the trunk muscles, has been somewhat overlooked till recently. Today, study of the neuromuscular control of the spine is thought to be a promising area of investigation as differences are being seen between healthy and NSLBP population. It is thought that valuable knowledge could be gained about NSLBP, and yield direct improvements in the clinical field (Hodges, Cholewicki, and Van Dieën 2013). Indeed, one of the most important mediators of NSLBP is now thought to be alterations in neuromuscular control (Hodges, Cholewicki, and Van Dieën 2013). Control of the spine relies on mix between passive support, from the connectives tissues and other passive structures, and active support, from the muscles coordinated by the nervous system (Panjabi 2003). In addition, increased knowledge on neuromuscular control could help model symptomatic trunks and investigate the consequences from NSLBP more freely and easily via the use of models.

Clear examples of such differences in neuromuscular control between healthy and NSLBP subjects can be seen during lumbar extension where the centroid of the muscle activity of the lumbar muscles was systematically more cranial for the NSLBP participants compared to the healthy subjects (Sanderson et al. 2019). During the same type of movement, regression analysis showed that the extent of the distribution of the erector spinae (ES) activity was associated with more endurance: the more the muscular activity was distributed through the ES, the more endurance the subject had. NSLBP participants seemed to have used a different motor strategy to perform an endurance task. A strategy characterized by a greater activation of the more cranial regions of the ES and a more localized muscular activity of the ES through the task (Sanderson et al. 2019). In another study, NSLBP subjects showed on average a higher activity of the paraspinal muscles compared to healthy subjects (Sanderson et al. 2019). This higher activity of the paraspinal muscle in NSLBP subjects was correlated with a deficit in muscle endurance compared to healthy subjects (Villafane et al. 2016). At the same time, hypoactivity of the deep intrinsic spinal muscles was consistent in LBP population when compared to healthy subjects (Hodges and Moseley 2003).

Very explicit differences in neuromuscular control between healthy and LBP subjects can be seen when they are subjected to perturbations, such as a delay in activation of stabilizers muscles (MacDonald, Moseley, and Hodges 2009) or of the transversus abdominis during a voluntary perturbation task in NSLBP patients (Hodges and Richardson 1996). For example, during a balance task against external perturbations, when the perturbations happened, healthy subjects showcased a shut-off of agonist muscles, with a reaction time of 53 milliseconds, which occurred before the switch-on of antagonist muscles, with a reaction time of 70 milliseconds. On the other end, NSLBP subjects exhibited a pattern of co-contraction, with agonist and antagonist muscles remaining active through the task, while at the same time having longer

reaction times activate or deactivate those muscles. Furthermore, their individual reaction times showed greater variability between repetitions (Radebold et al. 2000). Similarly, when subjected to sudden load release, NSLBP subjects demonstrated significantly different muscle activation patterns compared to healthy subjects (Radebold et al. 2000). In another study, when performing upper limb movements, healthy control subjects showcased early activation of transversus abdominis (TrA) and obliques internus abdominis (OI) in the majority of the trials, be it for movements performed at fast or intermediate speeds. In contrast, subjects with NSLBP failed to recruit TrA or OI when performing the movement at a fast pace, as well as in the majority of the intermediate speed trials (Hodges and Richardson 1999). It is to be noted that no differences between the two groups was identified when the movements were performed at slow speed. This yields the question of long-term consequences of NSLBP subjects' adaptations, as here for example, the results let us believe that the adaptations don't hold against a demanding task such as compensation for a sudden and fast load which could predispose the NSLBP patient to greater risk of relapse.

An intriguing fact is that pain intensity, fear of movement and disability from NSLBP seemed to be all unrelated to the observed changes in coordination. This tends to suggest that the observed changes in trunk coordination and ES activity were a direct consequence of NSLBP symptom on the different physiological structures (Lamoth et al. 2006).

1.6.5 Walking

Walking is a very interesting condition to study for NSLBP as it seems that there is less inter variability in the adaptations showcased by NSLBP subjects in this condition (Gombatto et al. 2015). But also as walking is an activity consistently to people afflicted by this symptom during their rehabilitation.

As we said earlier, NSLBP subjects present higher stride to stride variability, but also increased fluctuations in dynamic thoracic and pelvic oscillations (Vogt et al. 2001). It has also been shown that NSLBP subjects presented more variability in the timing of the segments in the frontal plane during a walking cycle. The gait of the NSLBP participants was characterized by a more rigid and less variable kinematic coordination in the transverse plane, and a less tight and more variable coordination in the frontal plane, accompanied by poorly coordinated activity of the lumbar ES (Lamoth et al. 2006). This seems to agree with the trunk stiffening strategy via co-contraction of the trunk muscles and associated higher muscle activity and done while relying less on deep muscles for stabilization, as discussed earlier. Indeed, the impaired coordination during walking for NSLBP subjects, seems to be the direct consequence of this more rigid, less flexible pelvis-thorax coordination of the trunk. At the same time, there was no significant differences in the kinematics of the rotations component (Lamoth et al. 2002; Gombatto et al. 2015). This happened in

addition to significant differences in hip joint range of motion, stride time and onsets of the lumbar spine and hip extensors, which were activated earlier, in the NSLBP population compared with the healthy one (Vogt, Pfeifer, and Banzer 2003).

In addition, it is to be noted that the change from in phase to anti phase pelvis-thorax coordination, when increasing walking speed, is diminished in NSLBP subjects compared to healthy subjects (Lamoth et al. 2006; Gombatto et al. 2015). Another example of the lack of adaptability from the LBP subjects, an issue already discussed earlier. Related to this, comfortable walking velocity was significantly lower in the NSLBP participants and was limited, or provocative of pain, in more than 25% of the subjects with the symptom. This again, bring us to the question of the long-term consequence of the patients' adaptation to NSLBP. Adaptations based on perceived benefits by the subject, but which objectively do not benefit the patient's long-term quality of life (Gombatto et al. 2015).

1.7 Summary

NSLBP is a major concern in today's world: be it for the nations due to the important spending in healthcare, for the private sector with the cost on production and loss of income due to worker being absent or incapacitated, and obviously for the individuals, due to the impact of the symptom on their life and its quality, their capacity to work and to provide for oneself and the people dependent on them. To this day, little is known about the NSLBP symptom and subsequently on the NSLBP population. We are faced with a very large and diverse population where, most of the time, standard and generic rehabilitation protocols showcase little to no benefit to the patient. This brings to the table the need to try to subgroup the NSLBP population into smaller subset, in order to more easily design better suited rehabilitation protocol, but also to gain a better understanding of the symptom.

Chapter 2

Problematic and objectives

2.1 Research gap

NSLBP is a concerning problem, this extremely prevalent symptom (Hoy et al. 2012; Hartvigsen et al. 2018) costing up to billions in direct and indirect cost to society (DALYs et al. 2016; Dagenais, Caro, and Haldeman 2008) or in the number of lost working day and compensation (Hartvigsen et al. 2018). But most importantly it cost the individuals, by the long lasting (Henschke et al. 2009a) pain and associated impact on one's quality of life (Hartvigsen et al. 2018) and the extreme impact on early retirement rate (Schofield et al. 2008).

A large proportion of the people afflicted by an acute episode of NSLBP recover within 12 months (Henschke et al. 2008). But 12 months is quite a long period which is susceptible of affecting one's life in a dramatic way, especially if the symptom leads to a decreased working time or capacity, or simply one's quality of life. And above that, the symptom showcase a relapse rate of 33% (Stanton et al. 2008), which means two things:

- The people afflicted by NSLBP recover slowly, if at all.
- Around half of the people afflicted by NSLBP goes into a pervasive chronic state

Treatments are barely better than placebo for acute episode (Hartvigsen et al. 2018), and with the over reliance on pain killer, especially opioids, make so that the management of pain can be extremely detrimental for the individual (Massaly, Morón, and Al-Hasani 2016). Same goes for chronic NSLBP were, to date, no effective treatments exist (Maher, Underwood, and Buchbinder 2017), not even accounting for the potential deleterious effect of pain management in long term cases (Massaly, Morón, and Al-Hasani 2016).

Despite its high and global prevalence (Hoy et al. 2012; Hartvigsen et al. 2018), NSLBP is not yet clearly understood. The changes induced by NSLBP, while most of the time swerving from the norm, are not consistent across the population and the nature and the magnitude of those changes are unpredictable. But this lack of knowledge on the symptom does not come from a lack of research or clinical effort, but from the complexity of the task. As seen earlier, up to more than 90% of the diagnosed LBP are idiopathic ones (Koes, Van Tulder, and Thomas 2006; Deyo and Weinstein 2001; Henschke et al. 2009b; Enthoven et al. 2016; Downie et al. 2013), meaning that no specific cause or causes for those LBP can be defined, making the NSLBP population is extremely diverse and heterogeneous. As the practitioners and researchers are faced with a very large, broad and diverse population. which makes it extremely hard for them to work with patients and study the symptom. It is hard to generalize findings, understand or simply study the symptom, and even more to design adequate treatments for the patients (Maher, Underwood, and Buchbinder 2017; Hartvigsen et al. 2018). In order to circumvent this issue, one solution that is making consensus, is the clustering of the LBP population (Hartvigsen et al. 2018). If working, clustering of the population would divide the complexity of the problem. Indeed, if the NSLBP population can be divided from a single entity, into to multiple more homogeneous and definite groups, practitioners and researchers would be dealing with clusters of patients with less variance and more commonality. This would render the research and ground work much easier, and hopefully be the first step to answer the NSLBP question. But as of today, the research community as yet to find valuables answer to this task (Laird et al. 2014; Maher,Underwood, and Buchbinder 2017; Hartvigsen et al. 2018).

Some attempt at investigating subgroups and designing personalized treatments for them have already been tried, but without great success. For example, the Quebec task force tried to divide the NSLBP population in three arbitrary distinct groups (O'Sullivan 2005). This was done using a theoretical framework encompassing multiple aspects of the NSLBP (Hartvigsen et al. 2018). A lot of different types of classification techniques have been tried along the years (Karayannis, Jull, and Hodges 2012; McCarthy et al. 2004) using conceptual framework, movement examination, questionnaire, imaging or even electromyography (Marras et al. 1999; Karayannis, Jull, and Hodges 2012). None of which yielded actual significant improvement in research or clinic.

Today, most attempts at NSLBP classification rely on the use of categorical data. Most of the current classification models that work, do so using questionnaire data, or variables in general, that are categorical at the time of acquisition (Laird et al. 2014; Koppenaal et al. 2023). The categorization, as well as answering those categorical variables, are subjective acts. This arbitrary aspect might limit the extrapolation of the clusters found through those categorical models, into actual useful groups in a clinical setting, the work of the Quebec Task Force being a good example of this

(Loisel et al. 2002). Some experiments have tried, to circumvent the difficulties of designing classification models using strict continuous data, by categorizing those continuous variables. Some with appreciable results (Laird, Keating, and Kent 2018). While still better a better solution than having to rely on a subjective assessment from the subject, still poses the issue of subjectivity: the categorization relies on an educated guess of the operator, and is therefore tied to his judgment, appreciation and subjectivity. Being able to design classification models that work on non-arbitrary data, for example based on continuous data, would ground those classification models into a solid foundation based on objective data.

As of today, it can be argued that a lot of the classification models are not used in a clinical setup, or even usable in the field. The clinically usable classification models have a very variable usage rate: between 7% to 70% (Byrne, Doody, and Hurley 2006; Poitras et al. 2005; Hamm et al. 2003; Foster et al. 1999; Battié et al. 1994; Jackson 2001; Gracey, McDonough, and Baxter 2002). Some of the reasons for this lack of use are the unfamiliarity professionals have with those type of tools, and the perceived usefulness of those classification models, while those classification models compete with other, more popular and, or, useful tools (Karayannis, Jull, and Hodges 2012). Therefore, there is a lot of room for improvement in the domain of subgrouping NSLBP. This is in this context that our work ground itself: where attempt to clustering the LBP population, in a clinically meaningful way, has yet to be found, and more exploratory work, in order to help the creation of those meaningful clustering framework, is needed.

2.2 Project objectives

As we discussed above, little is really known about NSLBP population characteristic aside that there display differences from the healthy population. Therefore, before attempting any clustering work, there is a need for an exploratory work, our first objective in this work, to have a better understanding of how NSLBP affects the patient population, and to help us outline more clearly the variables that seem to be of greater importance. Once that exploratory work is done, it should become clearer how to go on about subgrouping the NSLBP population, our second objective. Our approach is therefore summarized in those two objectives:

1. **First objective: Provide an exploratory work to better understand the influence and importance of the selected variables in regards to NSLBP and our sample population, and gather information to prepare subgrouping**

2. **Second objective: Provide an attempt at clustering our population sample in order to discriminate valuables subgroups**

2.3 Research plan

Contrary to previous works, we will focus on the use of continuous variables in order to try to subgroup our NSLBP population sample. As discussed earlier, there are numerous domains, like the ones talked about earlier or more generally, the meta-domains enumerated by Hartvigsen and collaborators (Hartvigsen et al. 2018), in which the LBP population differ from the healthy population: biophysical factors, comorbidities, genetic factors, psychological factors, social factors. We will therefore focus our attention on those domains. In order to assess those aspects for each participant, we based our protocol on movements tasks and tools that have been previously tested in other works. We weren't able to investigate subjects' walking in this work, despite the amount of potential information it could yield, due to the lack of instrumented treadmill at our disposal.

Consequently, we focused our efforts on the movement strategies, the variability intra and inter-subjects and the neuromuscular domains. Data was acquired using motion capture and high-density electromyography. According to our objectives, our work was divided into two parts: exploratory analysis, cluster analysis.

Once our variables were extracted from the acquired signals and pre-processed, we started with the exploratory analysis. The objective here, is to help us understand the relation between the continuous variables acquired and NSLBP. Deep neural networks (DNN) and factor analysis (FA) were used for this. The goal of the DNN was not the categorization itself, as it is fairly easy and robust to know if somebody have back pain simply by asking them, but to help us know which variables are more important when it comes to NSLBP, and to tell us more about the amount of information in the variables we chose. After this, we used factor analysis to perform a R-type analysis to get a better understanding of the importance of our selection of variable, each of them representative of some of the main domains driving the NSLBP prognosis, in relation to the NSLBP symptom.

Once the exploratory analysis was done, we used classic and well tested clustering algorithms in order to investigate the presence of subgroups inside our population sample. Different algorithms were used due to their different behavior so that we maximized our chance of finding clusters, and at the same time to test the results from the clustering algorithms against each other. K-means clustering, spectral clustering and hierarchical agglomerative clustering were used in this step. First our whole data set was used, with or without dimension reduction via principal component analysis, as null models. Following that, we used the insights gained from the exploratory analysis to define movement specific data sets, using for each movement the variables highly correlated to the symptom, in order to use them to subgroups our population sample.

To summarize, our protocol is built up on basics movement tasks performed by the subject, while we acquire data on the participant biomechanic and neuromuscular control via the use of motion capture and high-density EMG. We then use different tools for exploratory analysis in order to gain information on the relation between acquired variables and the symptom, to then investigate the presence of clusters, subgroups, in our population sample.

2.4 Summary

NSLBP is a concerning problem. As of today, what is known about the symptom, and what can be done to treat it is limited. One of the main obstacles in improving our knowledge and our clinical practice is that the symptom encompasses as large and diverse population. To work around that problem, one solution that is thought to yield significant potential is to subgroup the NSLBP population. Subgrouping the NSLBP population should allow to discriminate more homogeneous groups. This homogeneity should help better understand the symptom, and consequently improve our capacity to treat the symptom in the field, by helping design appropriate rehabilitation protocol for each group. Our approach to the present problematic of NSLBP can be summarized in two steps: exploratory analysis, and cluster analysis.

Chapter 3

Method

3.1 Design and location

Our study was approved by the Health and Disability Ethics 158 Committees on November 6, 2019 (Approval: 19/CEN/187). It was conducted at the Centre for Chiropractic Research, Auckland, New Zealand, and Auckland University of Technology, Auckland, New Zealand. A picture of the MOCAP lab from AUT, used for the data acquisition can be found in Figure 3.1. The study involved 2 groups, Healthy subjects and NSLBP subjects. Participants were not blinded to group allocation. Outcomes assessors and data analysts remained blinded to group allocation throughout the data collection and data processing steps.

Figure 3.1: AUT MOCAP laboratory.

3.2 Population

53 subjects have been recruited in total. The subjects were divided into 2 groups:

- Healthy: 17 subjects
- LBP: 36 subjects

A total of 7 subjects were excluded post-acquisition due to issues during the data collection:

- Healthy: 3 subjects
- LBP: 4 subjects

This brought the total number of participants kept for data analysis to 46 subjects:

- Healthy: 14 subjects
- LBP: 32 subjects

The subjects were recruited via advertising within the New Zealand College of Chiropractic community. The participant interested in the study were to contact the person in charge of the recruitment via e-mail or telephone. They were then received for a quick interview to assess if they fitted the inclusion criteria of our study. During the interview, it was made mention that a 20 NZD$ petrol voucher was offered to the participant at the end of the acquisition session for his time and effort if he partook in the study. Participants included students, staff, faculty, and previous patients of the College's chiropractic center and also family, friends and acquaintances of the New Zealand College of Chiropractic community. The experimental protocol was advertised by inviting volunteers to get in contact with our team in order to participate in a scientific study, whether they have experienced low back pain and have, or not, received treatment (the NSLBP group) or they have not experienced back pain (healthy group).

The population inclusion/exclusion criteria were as follow:

- English speaking
- Age between 18 and 50
- In case of LBP, no identifiable cause for it
- Not suffering from a current lower limb disorder/dysfunction
- No recent history of inner ear infection with associated balance or coordination problems
- No history of cerebral trauma with unresolved sensorimotor symptoms
- No recent history of vestibular disorder
- No previous spinal surgery
- No involvement in specific balance or stablization training in the past 6 months
- Not currently on pain medication

- Below 3/10 on the pain scale on the day of the data collection (Hawker et al. 2011)

NSLBP was defined as pain located between the lower rib margins and the buttock crease (Dionne et al. 2008) and for which the pathoanatomical cause of the pain was not determined (Maher, Underwood, and Buchbinder 2017). The low back pain must have been present at least 3 months in the last year to be counted as chronic (Bernell and Howard 2016).

Our population sample was composed of a total of 46 individuals, 11 of which were female participants and 35 were male participant. The healthy group was composed of 14 subjects, and the NSLBP group of 32 subjects. More detailed characteristics of the population can be found in the Table 3.1 below. Distribution of the anthropometric data, age, height, weight and BMI are found in the figures below, respectively Figure 3.2, Figure 3.3, Figure 3.4 and Figure 3.5.

Population	Age (year)	Weight (kg)	Height (cm)	BMI
General	31.2 ± 9.2	74.4 ± 13.8	172.9 ± 8.5	24.9 ± 4.3
Healthy	29.6 ± 9.1	69 ± 12.7	172.5 ± 8	23.1 ± 3
LBP	31.8 ± 9.3	76.7 ± 13.8	173 ± 8.9	25.6 ± 4.6

Table 3.1: Population characteristics.

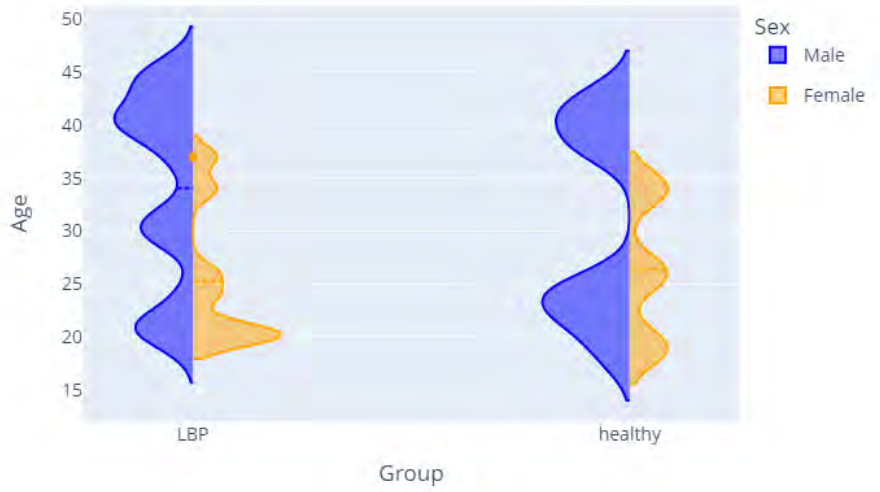

Figure 3.2: Age distribution by groups.

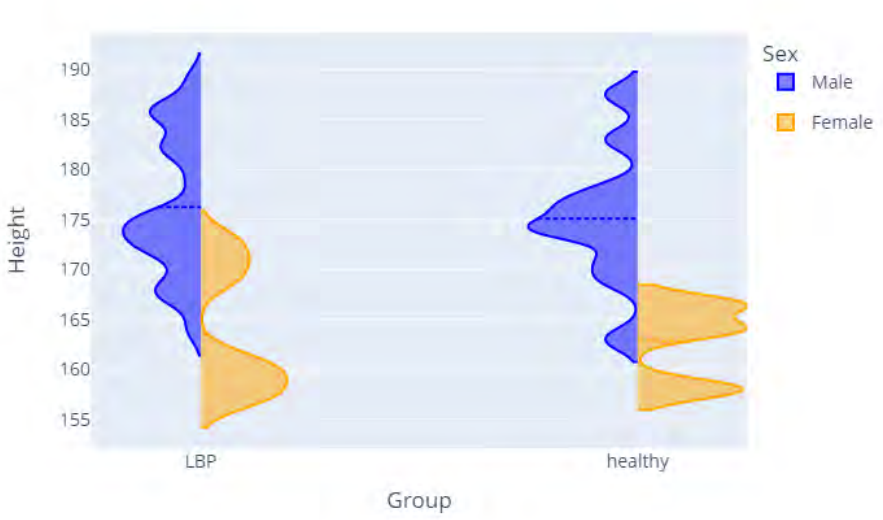

Figure 3.3: Height distribution by groups.

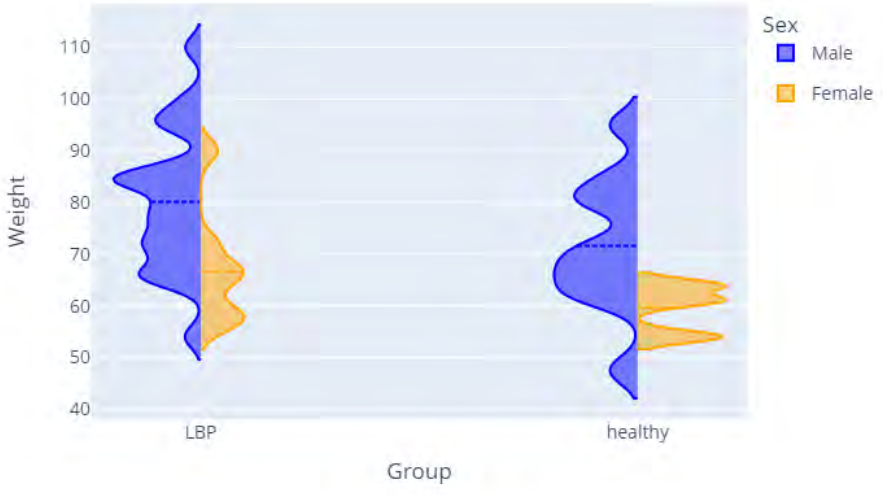

Figure 3.4: Weight distribution by groups.

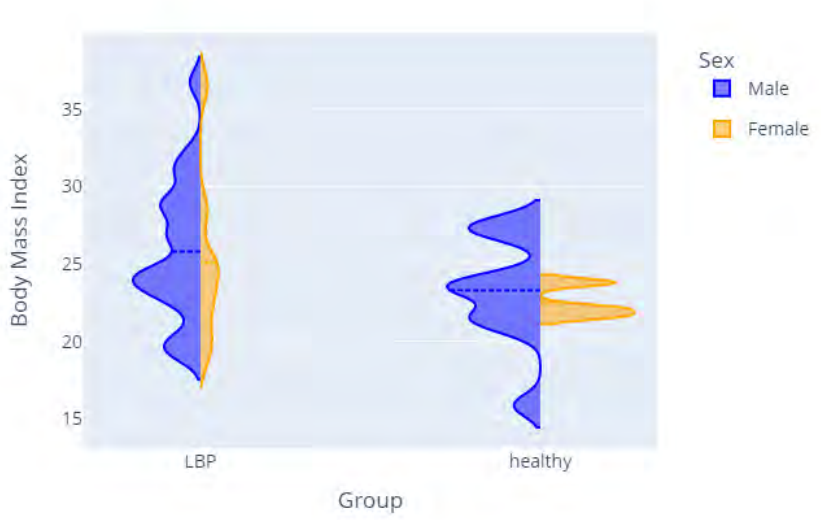

Figure 3.5: BMI distribution by groups.

3.3 Data acquisition tools

3.3.1 Motion Capture

A motion capture (MOCAP) system, is a system which aim to record the position of elements in space. There are different types of systems, which can be regrouped into 2 main categories:

- Optical systems
- Non-optical systems

As our project used an optical system, we will not dwell into the non-optical systems, but the interested reader can turn to the book *Understanding motion capture for computer animation* (Menache 2011) for more information on those. The optical systems can in turn be divided into 2 groups:

- Markerless
- Passive marker
- Active marker

Markerless systems do not rely on markers to track bodies in space, and only require cameras. Competitive markerless systems are fairly recent, but still suffer from two mains problems. Firstly, their accuracy. Even if major leaps forward have been made in the domains, their accuracy is still relatively poor when put against systems using

markers. Indeed, the latter showcase a precision that is still two orders of magnitude better. Secondly, they are tied to a very rigid framework: they are only able to track bodies that they have been trained to recognize. Their models cannot be adapted to the needs of the experiment as easily as it can be with optical systems using markers, and esoteric models cannot be reliably studied with them.

Passive and active marker systems both use markers to track one or multiple bodies in space. The difference between the two comes from the fact that in the passive marker system, the infrared light is produced by the camera, which will light up the volume of capture. The light will bounce back on the passive markers, either a sphere, demi-sphere or disc of reflective material, as shown in Figure 3.6a. Then the light reflection will be picked up by the cameras to allow for triangulation of the marker position. Whereas, in active marker systems, the marker itself generate the infrared light that will be picked up by the cameras, as shown in Figure 3.6b. It is to be noted that at least two cameras need to capture the light from a marker, be it reflection or produced light, to allow for the triangulation of the position of said marker. The mathematics behind those computation won't be covered here but can be found in the work of Parent R. and collaborators (Parent et al. 2009).

(a) Passive marker system diagram.

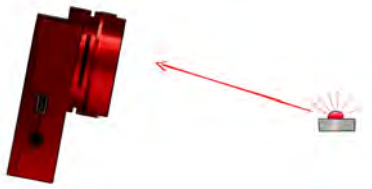

(b) Active marker system diagram.

Figure 3.6: Motion capture marker types

In order to track a body in space, marker have to be placed at key landmarks of that body that will best describe its structure and movements. When it comes to human bodies, numerous models have been used, but some standard have been suggested by the International Society of Biomechanics (ISB) to facilitate reproducibility of the studies (Wu et al. 2002, 2005), and therefore we made our setup as compliant as possible to the ISB standards. Marker position on the subject was chosen to limit as much as possible skin artifact or soft tissue artefact (STA) (Cappozzo et al. 1995). The STA is the slight displacement of marker due to the elasticity of the soft tissue the marker is put on, here the skin, and which is not due to the displacement of the underlying bone structure of interest.

Once the position data of the marker acquired, and their trajectory aggregated, the markers all appears identical to the software. For the trajectories to be usable, they need to be labeled first. This operation can be automated to a certain extent, but the results are never complete or 100% accurate and a significant part of labeling work still needs to be done by a human operator. Once the trajectories are labeled, they need to be cleaned in order to be used for processing. Cleaning the data mean filling the gap that might have happened during the recording due to occlusion of the marker, and correct artifacts and noise issues. Indeed, during recording it usually happens that, either the camera loses track of some markers due to obstruction of the line of sight, or simply would misinterpret markers which are close to each other, associating the trajectory data of one marker with the other marker's trajectory. Therefore, before using the trajectory data, they need to be cleaned, either by filtering or by a human operator. But as of today, correcting those errors and filling those gaps can only be made manually in most case, and is a time consuming activity.

The motion capture acquisition system used in our study was a Qualisys system (Qualisys AB, Göteborg, Sweden, version 2021.2, build 6940), of 9 Oqus 500+ series camera acquiring data at 120Hz, with two Amti force platform, of the S464508 series (Watertown, Massachusset, USA) connected via an analog interface USB-2533 (Measurement Computing Corporation DAQ) using an acquisition rate of 1000Hz.

3.3.2 High Density Electromyography

The electromyography (EMG) signal that is recorded from the surface of the skin via the surface EMG, spring from the superimposition of the multiple electrical potential created by the cellular depolarization of the muscle fiber. The electrical signal coming from a single muscle fiber is named Single Fiber Action Potential (SFAP), and the superimposition of the SFAP linked to a same Motor Unit (MU) is called Motor Unit Action Potential (MUAP) (Farina and Holobar 2016). To be noted that the superimposition can be constructive or destructive due to the nature of the SFAP signal, which can be either of positive or negative amplitude. The Figure 3.7 (Farina and Holobar 2016) show a graphical representation of the surface EMG signal generation.

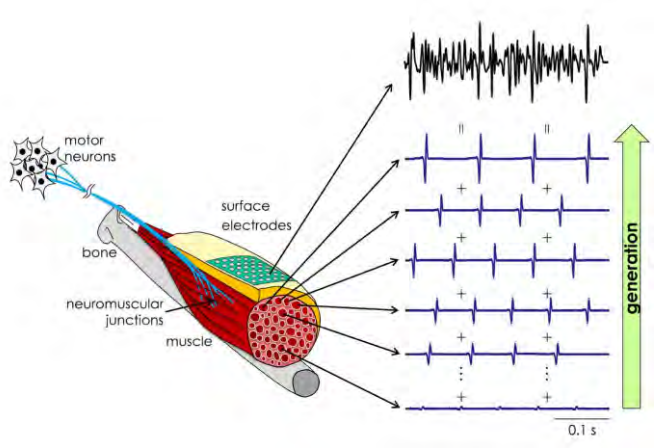

Figure 3.7: EMG signal generation (from Farina and Holobar, 2016).

The signal that we get via EMG recording is not the direct representation of the MUAP signals superimposition. It is the MUAP signals superimposition after it has been influenced by numerous factors. This also prevent direct interpretation of the surface EMG signal as a direct representation of the muscle activity or behavior. Some of the factors of utmost importance in shaping the recorded EMG signal are (Dimitrov and Dimitrova 1998; Farina, Cescon, and Merletti 2002):

- MUAP signals superimposition
- Muscle anatomy
- Subcutaneous tissues and the related volume conductor effect
- Electrode positioning

To simplify, a surface EMG setup is composed of an EMG amplifier and an electrode setup. In classic surface EMG setup, this electrode setup can be made of 1, 2, 3 or 4 electrodes, not accounting for any of the reference electrodes. Usually this or these electrodes are usually used in a monopolar or bipolar mode (Barbero, Merletti,

and Rainoldi 2012). Tri or quadripolar mode a usually reserved to more specific application, for example ECG (Weiss, Weiss, and Silver 2021).

One of the major downsides of these classic setups are the very low spatial resolution: only one spot is being looked at one time. To circumvent this, high density EMG (HDEMG) systems have been developed in recent years. Those systems rely on the same principles as the classic ones, but differ from their electrode setup. Instead of recording at one points only, they will assess the EMG activity on a relatively large surface thanks to grid, or grids, of electrodes, which are composed of a number of electrodes, from a couples of electrodes to many dozens. As stated earlier, a HD EMG system is composed of one or more electrode grids which are placed on the skin, over a muscle, and connected to an amplifier, similarly to a classic EMG system. These HD EMG grids are a matrix of multiple small EMG electrodes separated by an equal distance from each other and organized in rows and column. HD EMG gives the researcher a higher definition of the muscle activity, providing spatial information in addition to time information, thanks to a larger recording area. This yield much more information than a classic EMG setup, allowing for more complex data processing on the data recorded, and providing richer information about the muscles studied, and some information on the system directly related to them.

To record HD EMG signals in our study we used the HD EMG Quattrocento amplifier, as shown in Figure 3.8b, from the company OT Bioelettronica (Turin, Italia) with semi-disposable adhesive matrix from the same company, model GR08MM1305, 63 sensor grid electrodes, 5 columns, 13 rows architecture with electrodes diameter of 1mm and inter electrodes distance of 8mm, as shown in Figure 3.8a. AD64 HD EMG adaptor (OT Bioelettronica, Turin, Italia) were used to connect the patches of electrodes to the amplifier. All the parameters were manipulated from the interface of the OT Bioelettronica software. The signals were acquired using the software OTBiolab+ (version 1.5.7.3, OT Bioelettronica, Turin, Italia). The settings used were:

- Bandpass filter: 10-500 Hz
- Sampling frequency: 2048 Hz
- Gain: 2000

(a) GR08MM1305 electrode grid.

(b) Quattrocento HD EMG amplifier.

Figure 3.8: HD EMG acquisition setup from OT Bioelettronica, Turin, Italia.

3.4 Protocol

3.4.1 Subject preparation

As the patient arrived at the experiment location, they went through an explanation of their rights, the experimental procedures, security and safety rules, as well as the goal of the study was given orally and were also accompanied by a written document stating and explaining all of this. The participants would then provide informed consent if they accepted to participate in the study. Following this, they were to complete a questionnaire to identify symptoms and dysfunctions. Once the questionnaire was answered we determined the handedness of the subject by asking him which hand they used to write.

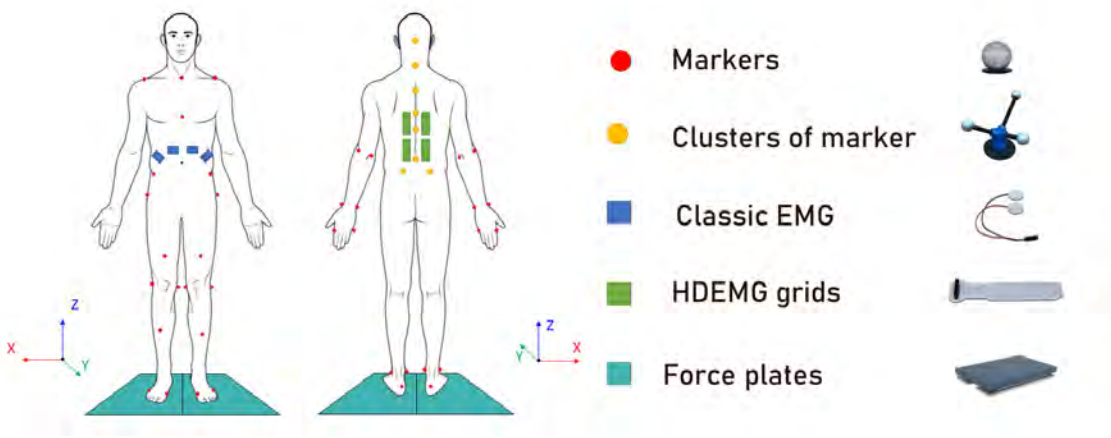

Figure 3.9: Experimental setup.

Spherical reflective surface markers (7 mm), and clusters of markers, custom made from Optitrack (NaturalPoint, Inc. DBA Optitrack) 6 mm markers, were placed on anatomical landmarks according to the international society of biomechanics recommendation (Wu et al. 2002, 2005) to make up a model of 38 markers on the body, and 8 clusters of markers placed on the spine as shown in Figure 3.9. The cluster of markers allowed for the creation of multiple segments of the spine, as shown in Figure 3.10. The full set divided the spine in 5 segments, Hips-L5, L5-T12, T12-T6, T6-T3 and T3-C7. These positions for the cluster were chosen as they allow for a fine representation of spinal kinematics with a minimal number of clusters of markers (Papi, Bull, and McGregor 2019; Schinkel-Ivy and Drake 2015). It should be noted that previous studies have shown that this type of cluster of markers is appropriate for assessing spinal kinematic, despite the presence of skin artifacts (Mörl and Blickhan 2006; Zemp et al. 2014).

Figure 3.10: Spine segments created by the clusters. On the left side, the simplified set of spine segments. On the right side, the full set.

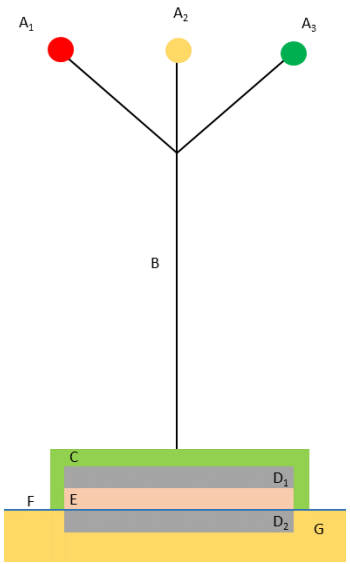

Figure 3.11: Structure of a cluster of marker used during our experiment. A_1, A_2 and A_3 respectively, the left, middle and right marker. B the aluminium sticks which are tightened together using tape. C the epoxy and D_1 and D_2 neodymium magnets. E the acryclic sheet. F, tape used to stick the D_2 magnet on the skin of the participant. G the skin of the participant.

The clusters of markers were home made using the following structure: a base made of a thin acrylic square, to which a neodymium magnet and 3 aluminum sticks were bound to via the use of epoxy. At the end of the sticks, 6mm diameter passive reflective markers were attached, as shown in Figure 3.11. The structure made of the sticks was reinforced with tape. It was made sure that each pair made by combining markers of the cluster did not end up forming a parallel axis. Magnets were used for the cluster fixation on the spine of the subject. The magnets were placed on the respective spinous processes via the use of double-sided tape (Vicon Motion Systems Ltd, United Kingdom).

For high density electromyography (HD EMG), the area of skin where the electrodes were to be placed, was prepared by gentle abrasion using abrasive paste (Everi, Spes Medica, Italy), then the area was cleaned with alcohol wipes, as to follow recommendations (Merletti and Farina, 2016). To record HD EMG signals, we used the HD EMG Quattrocento amplifier (OT Bioelettronica, Turin, Italia) alongside semi-disposable adhesive electrodes matrix from the same company, model GR08MM1305, 5 columns, 13 rows architecture for 63 electrodes with a diameter of 1mm and inter electrodes distance of 8mm. GR08MM1305 patches of electrode were prepared by first applying an adhesive foam on top of them, which was filled with conductive and adhesive paste AC Cream (Spes Medica S.r.l., Genova, Italia). The electrode grids were placed at either side of the low back, always starting precisely, for the lower pair, from L5, up to L2 depending on the subject morphology, and for the upper pair, from L1 to T8, again depending on the subject morphology (Martinez-Valdes et al. 2019; Falla et al. 2014; Murillo et al. 2019). The grids were placed around 2 cm away from the spine as to cover the back extensors and paraspinal muscles (Sanderson et al. 2019). Figure 3.9 and Figure 3.13a display the grid of electrodes placement.

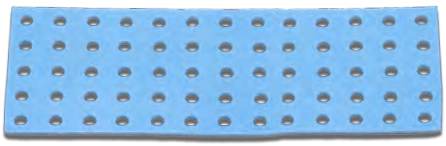

Figure 3.12: Adhesive foam for semidisposable matrix, 8mm i.e.d (13 rows - 5 columns).

Classic bipolar EMG electrode were applied on the Rectus Abdominis, just below the navel, on the left and right side, and Abdominal External Obliques, at equal distance from the last floating rib and the iliac crest, on both sides of the subject. Those electrodes are here to provide information about the activation onset of these muscles we aim to study (Radebold et al. 2000; MacDonald, Moseley, and Hodges 2009; Hodges and Richardson 1996). The electrodes used were Ag/Cl electrodes, placed with a 20 mm inter-electrodes distances and placed parallel to the muscles fibers of the muscle of interest (Barbero, Merletti, and Rainoldi 2012), as shown in Figure 3.13b, according to SENIAM recommendations (Stegeman and Hermens 2007).

(a) HD EMG electrodes position.

(b) Classic EMG electrodes position.

Figure 3.13: EMG electrodes placement.

Once the patches of electrodes and the classic electrodes were placed, Pretaping Adhesive Spray Grip (D3, London, England) was sprayed on the spine area to increase the adhesive power of the X6.0 D3 tape (D3, London, England) used to secure the magnets on the spine of the subject. The same X6.0 tape was applied around the waist of the subject to secure the patches of electrodes to the subject's body, in order to minimize the displacements of these during the subject's movements. The references electrodes were placed, on the crest of the spine of the scapula. The subject's reference for the amplifier was fixed on the ankle of the subject.

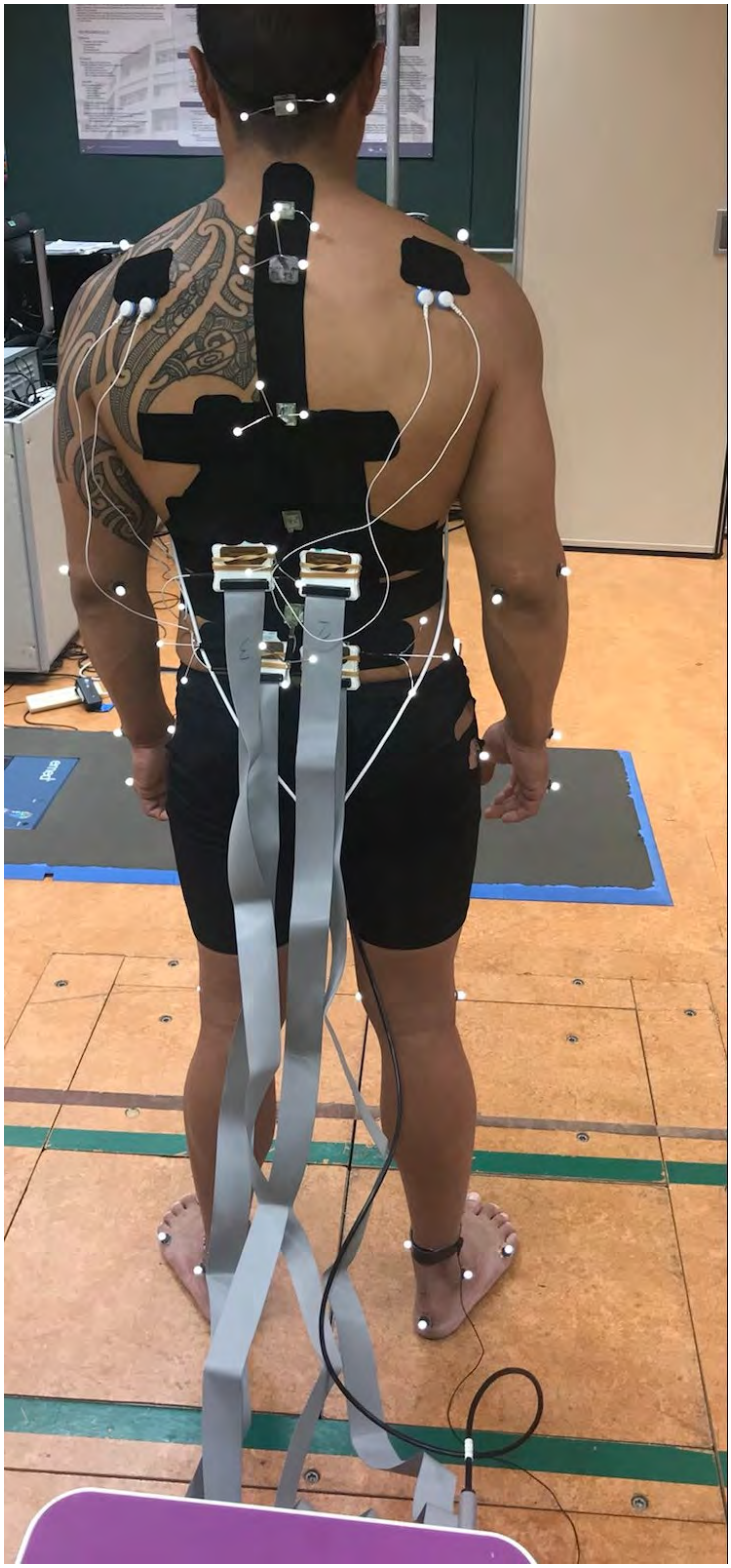

Figure 3.14: Fully prepared subject, back view.

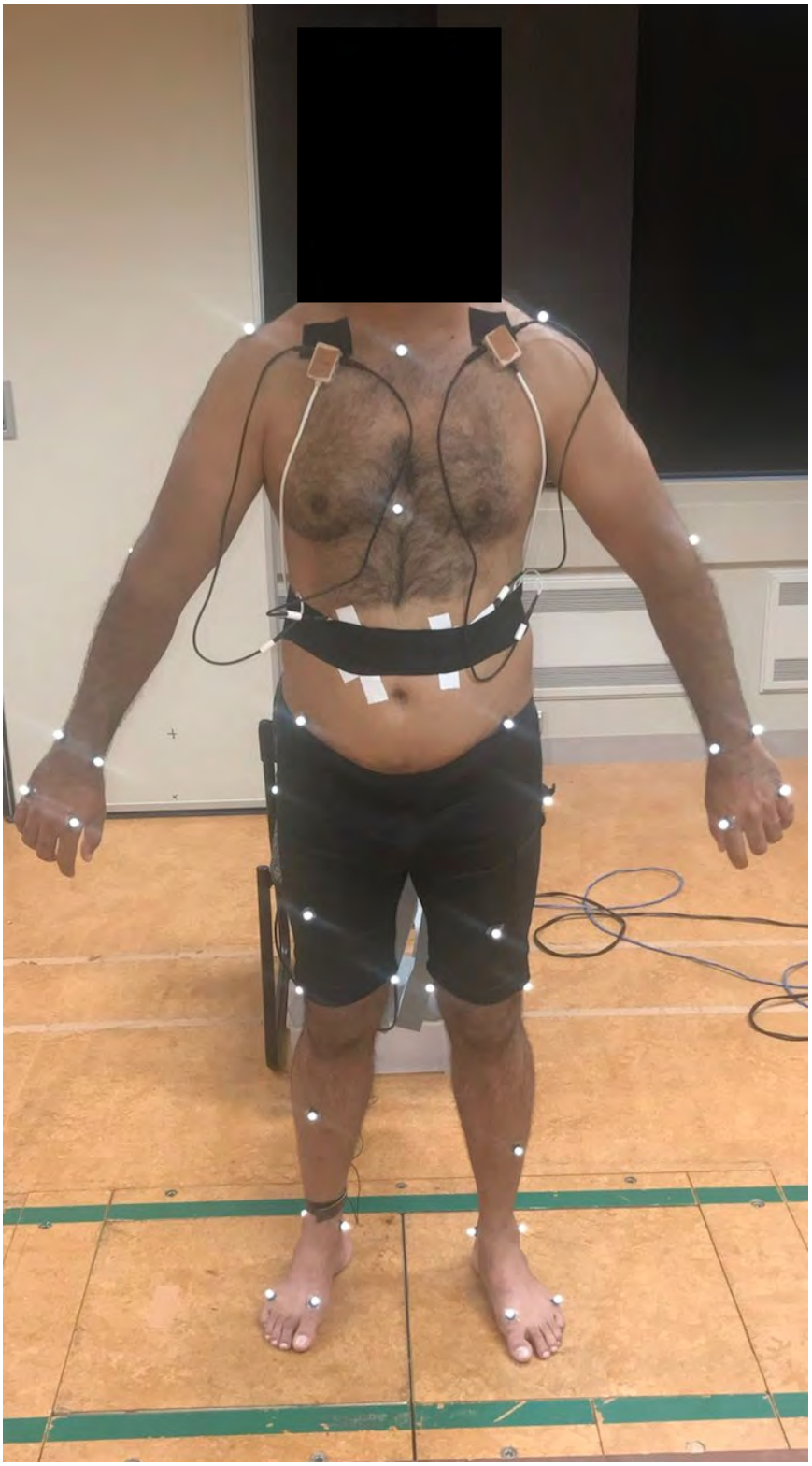

Figure 3.15: Fully prepared subject, front view.

3.4.2 Data recordings

Once the subject was prepared, he was set in the center of the acquisition volume of the MOCAP system. Each foot on a separate force plate. The subject was instructed to take a natural foot stance. Aside from the fact that each foot had to remain on its respective force plate, the foot stance was not controlled (Bourigua 2014). Indeed, foot stance is subject to difference between healthy and NSLBP subjects (Koch and Hänsel, 2019).

Once the subject was in position, he was given instructions on how to perform each movements:

- Static postural recording, 90 seconds eyes open and 3 x 90 seconds eyes closed.
- Movement tasks, 10 repetition with eyes closed, at preferred velocity and maximal velocity
  - Back extension
  - Back flexion
  - Lateral trunk flexion, left and right
  - Trunk rotation, left and right

The static postural task consisted of the subject standing upright, straight, relaxed, and to not move for the duration of the task. Two static postural recordings were performed first, one eyes closed and one eyes open, then another recording with eyes closed after the movements at preferred speed had been performed, and a last recording with eyes closed after the movements at maximal speed were performed. The movement tasks were performed in a random order, different between preferred and maximal. All conditions, except for the first static postural recording, were executed with the eyes closed, in order to maximize difference between the two groups (Gill and Callaghan 1998; Leitner et al. 2009). Flexion, extension and abduction of the lower limb joints were monitored during movement tasks. The repetition would be invalidated if they occurred. The different movements tasks are displayed in Figure 3.16.

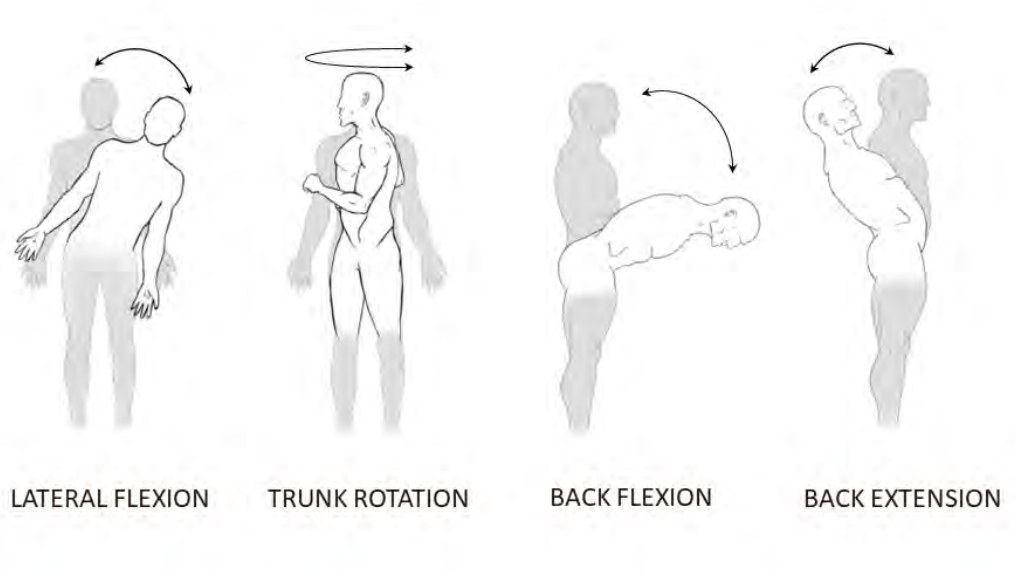

Figure 3.16: Movements performed during the experiment.

The preferred velocity was defined as:

> The speed at which the subject would perform the movement in a day-to-day life scenario.

And the maximal velocity was defined as:

> The maximal speed at which the subject can perform the movement safely.

For the lateral bending, participants were asked to bend their trunk laterally from an upright posture to maximal lateral flexion, without engaging the hip joint or bending their knees.

For the trunk rotation, participants were asked to rotate their trunks from the starting position, without engaging the hip joint or bending their knees. For the back extension, the participants were asked to extend their back backward, without bending their knees.

For the forward bending condition, participants were asked to bend the trunk, without moving their hip joints or bending their knees. The forward bending condition had a slightly different execution than the other movement conditions when performed at preferred speed, in order to study the Flexion Relaxation Response (Solomonow et al. 2003). To do so, the subject performed the actual trunk flexion movement, from a standing position to maximum amplitude, in 3 seconds. Once the maximum amplitude was reached, the subject stayed still in that position, for 3 seconds. The

subjects would then return to its starting standing position, again in 3 seconds.

Once explanations were given and understood, the protocol itself started. The subject was asked to perform the movements, 10 consecutive repetitions each, one after the other, first at preferred speed, then at maximum speed. The repetitions were made to be as independent as possible by waiting till stabilization of the participant at the end of each repetition, before engaging in a new repetition. This was controlled by the MOCAP operator via the force plate readings. The movements were performed in a randomized order. The randomized order was different for the preferred and maximum speed movements.

3.5 Protocol rational

We relied on a combination of dynamic movements conditions in our study over static conditions as the dynamics ones seems to showcase more opportunities to find differences between the two population, which should be intensified by the fact that the tasks will be performed eyes closed. Indeed, as discussed in our first chapter, numerous variables were shown to differ between NSLBP and healthy population. Our focus will be driven on the domains developed in our first chapter that are known to present significant and consistent difference between healthy and NSLBP:

- Adaptability of the movement
- Balance and proprioception
- Movement strategies
- Metadata
- Neuromuscular control
- Variability of movement

As the proprioceptive abilities of the NSLBP population seems to be negatively impacted by the symptom, probably due to damage or alterations in the related systems (Hodges, Cholewicki, and Van Dieën 2013; Gombatto et al. 2015; Ruhe, Fejer, and Walker 2011; MacDonald, Moseley, and Hodges 2009) and, or, deficit in the integration of the proprioceptive information (Brumagne, Lysens, and Spaepen 1999; Gill and Callaghan 1998; Leitner et al. 2009; Pijnenburg et al. 2015). Due to this deficit, NSLBP subject seems to rely more heavily on visual cue to compensate for it, as discussed in our first chapter (Sipko and Kuczyński 2013). Previous works already highlighted bigger differences between healthy and NSLBP subject while performing tasks with eyes closed for example when performing trunk inclination (Brumagne et al. 2008), during postural sway (Mientjes and Frank 1999; Nies and Sinnott 1991) or simply balance performance in general (Radebold et al. 2001). By having the subjects perform the movement tasks with their eyes closed, we aim to highlight more easily the differences between potential subgroups groups.

These proprioception alterations will also be shown indirectly via the inter and intra-subject variability. The intra-subject variability of this kinematics and dynamics variables should provide insight on the impact of LBP (Asgari et al. 2015; Descarreaux, Blouin, and Teasdale 2005; Ippersiel, Robbins, and Preuss 2018) on the sensorimotor pathway of the subject. We expected to see an increase in variability in one-off repetitions (i.e. isolated movement) on NSLBP subjects but a decrease in the variability of repetitive movement, cyclic movement (i.e. repetition of similar movement over time, like during walking), which could indicate an inefficient proprioceptive system, as the NSLBP subject would be more affected by the initial condition of the movement, but show a decrease in adaptation capabilities (Asgari et al. 2015; Descarreaux, Blouin, and Teasdale 2005; Hamill, Palmer, and Van Emmerik 2012).

As was also developed in our first chapter we expect the NSLBP population to show differences in kinetics and kinematics (Bourigua 2014), but also at a neuromuscular level with strategies that differ from the ones used by healthy subjects (Colloca and Hinrichs 2005; Neblett et al. 2003). It is to be noted, when it comes to neuromuscular control, that when performing trunk flexion, healthy subjects present a phenomenon called Flexion Relaxation Response (FRR): when the spine is fully flexed, deactivation of the lumbar muscle is observed, the extension forces needed for spine stability being then handled by the passive structures composing the spine (Kim et al. 2013). NSLBP people shows significantly less deactivation of the lumbar muscles, which could be an indicator of passive structure change or some protection mechanisms (Kim et al. 2013; Deyo et al. 1991; Solomonow et al. 2003). A phenomenon that is not observed most of the time in the NSLBP population, hence the reason for this movement and its peculiar procedure at normal speed, which goal is to observe this FRR.

The use of HD EMG will allow us to better understand how low back muscles are controlled and activated during the different condition performed during our experiment, conjointly with MOCAP which will give us valuable kinetic and kinematic information.

3.6 Data pre-processing

3.6.1 Motion capture data

Once acquired, the marker trajectories were pre-processed: first, trajectories were labeled, then the gaps in them were filled and all the different artifacts, marker swapping or noise that could be treated were corrected for. Once it was done, the signals were exported into a `.mat` file in order to be processed in Matlab (MathWorks, Natick, MA, USA) later on. The position of the clusters was computed at that moment.

To compute the clusters position, it is first necessary to compute the measured cluster rotation against its reference. The reference being this same cluster, flat on the leveled ground, with its base aligned to the X and Y axis of the General Coordinate System (GCS) of the laboratory.

The first step was to create the Local Coordinate System of the cluster (LCS), in GCS terms, of the measured cluster of markers and its reference. This was done by executing the following steps:

1. Compute the centroid of the cluster
2. Create the LCS itself:

$$\overrightarrow{\mathrm{LCS_y}} = C_{right} - C_{left} \tag{3.1}$$

$$\begin{gathered}\overrightarrow{\mathrm{temp_{middle}}} = C_{mid} - (C_{left} + \frac{\overrightarrow{\mathrm{LCS_y}}}{2}) \\ \overrightarrow{\mathrm{temp_{LCS_x}}} = \overrightarrow{\mathrm{LCS_y}} \times \overrightarrow{\mathrm{temp_{middle}}} \\ \overrightarrow{\mathrm{LCS_z}} = \overrightarrow{\mathrm{temp_{LCS_y}}} \times \overrightarrow{\mathrm{temp_{LCS_x}}}\end{gathered} \tag{3.2}$$

$$\overrightarrow{\mathrm{LCS_x}} = \overrightarrow{\mathrm{LCS_z}} \times \overrightarrow{\mathrm{LCS_y}} \tag{3.3}$$

   with C_{left}, C_{mid} and C_{right}, respectively the left, middle and right marker position of the cluster. This was done for the measured cluster and its reference. $\times$ being the cross product of the vectors.

3. Normalization of the vectors LCS_x, LCS_y and LCS_z constituting the LCS. Knowing the LCS of the measured cluster and the LCS of its reference, the 3D rotation of the measured cluster against its reference was computed via the following steps:
4. Create the following matrices both for the measured cluster and its reference, as follows:

$$M = \begin{pmatrix} LCS_{x_x} & LCS_{y_x} & LCS_{z_x} \\ LCS_{x_y} & LCS_{y_y} & LCS_{z_y} \\ LCS_{x_z} & LCS_{y_z} & LCS_{z_z} \end{pmatrix}$$

5. Compute the rotation matrix:

$$\mathbf{R} = \mathbf{M_{control}} \times \mathbf{M_{measured}}^{\mathsf{T}} \tag{3.4}$$

The **R** matrix is then applied to the reference translation offset to rotate it in order to match the rotation of the measured cluster. The offset being the translation vector $\overrightarrow{\text{Offset}} = Reference - Centroid$, from the centroid of the cluster of marker, to the actual position of the base of the cluster, were the cluster actually connect to the skin of the subject. Once the offset translation was rotated, we used it in order to get the actual position of the cluster on the spine.

6. If needed, compute the rotation angles for each axis, using the following equations:

$$\mathbf{R} = \begin{pmatrix} R_{11} & R_{12} & R_{13} \\ R_{21} & R_{22} & R_{23} \\ R_{31} & R_{32} & R_{33} \end{pmatrix}$$

$$R_x = -\arcsin R_{32} \tag{3.5}$$

$$R_y = -\arctan \frac{-R_{31}}{R_{33}} \tag{3.6}$$

$$R_z = -\arctan \frac{-R_{12}}{R_{22}} \tag{3.7}$$

3.6.2 Electromyography data

First the portion of interested of the raw HD EMG and classic EMG signals was extracted using the trigger data broadcasted from Qualysis Track Manager via the acquisition board, and acquired via a connection to the Quattrocento. The trigger outputed by the Qualisys acquisition board being subject to noisy oscillation, a function `trigBound()` was designed to select the poriton of interest in spite of those unwanted oscillations. The function filtered out the trigger signal via two bandstop filter: a first one for the 48-52 Hz band and a second one for the 148-152 Hz. This noise was most probably due to the power line inference (PLI) of the New Zealand electrical grid which use an alternative current oscillating at 50 Hz. The second filter was added to filter this peculiar harmonic of the 50 Hz PLI and to improve the sharpness of the trigger signal. The `bandstop()` function from the `Signal Processing toolbox` from Matlab was used for the filtering. Following this, the trigger boundaries were found, and trimmed for accuracy purpose. The details of this stage can be found in the appendix `trigBound()`.

Following this, the HD EMG and EMG signals were filtered for baseline wander (BW) noise also called baseline fluctuation, as shown in the example of Figure 3.17 and Figure 3.18. To do so a filter has been implemented, based on the work of A. Fasano and V. Valeria (Fasano and Villani 2014) to which an automatized function of our own design was added to, in order to find the optimal lambda for that filter.

To summarize, the filter uses the quadratic variation as a measure of the variability of the signal. This measure helps us find the high variability part of the measured signal: the actual signal, as the BW noise is a low frequency additive noise. Once the actual signal is estimated this way, we can subtract from it the rest of the measure signal: the BW noise (Fasano and Villani 2014). More ample details about the reasoning and mathematics of the filter can be found in the article of A. Fasano and V. Valeria (Fasano and Villani 2014). The implementation of this filter in Matlab can be found in appendix `BWfilt()`

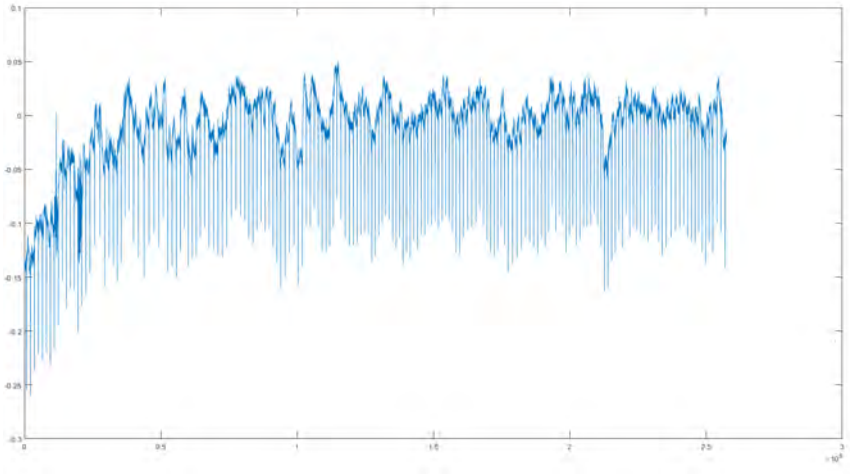

Figure 3.17: Original classic EMG signal before BW filtering.

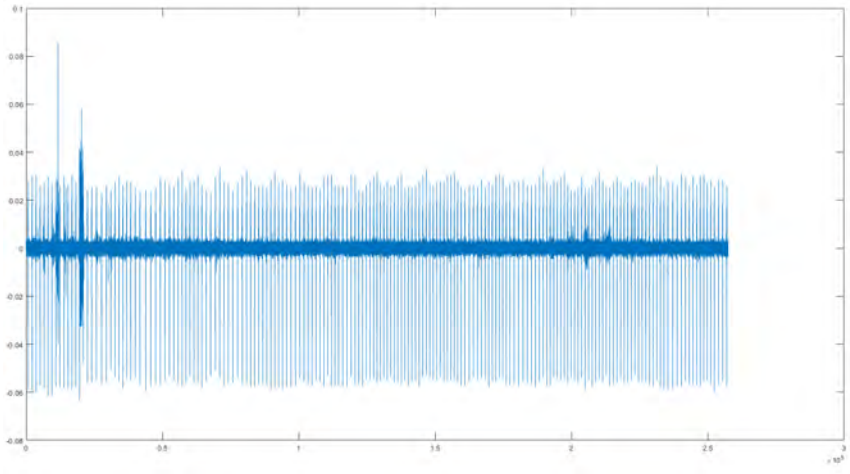

Figure 3.18: Original classic EMG signal after BW filtering.

After that, the HD EMG signals were filtered for ECG noise. Indeed, as the measurements were made on the trunk region, ECG signals were also picked up along the EMG during acquisition, as shown in Figure 3.19.

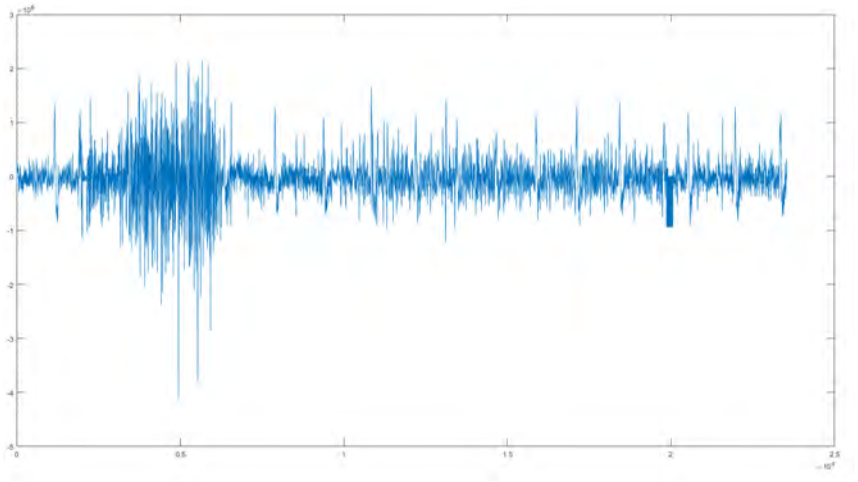

Figure 3.19: Signal from an HD EMG electrode showing the ECG artifacts.

To take care of that issue, a filter based on the work of J. Mak, Y. Hu and K. Luk (Mak, Hu, and Luk 2010) was implemented. The filter as described by Mak et al., wasn't working optimally on our HD EMG data set, maybe due to the low Pulse to Noise Ratio (PNR) of the signals. To circumvent that issue, a moving average filter of window 102 samples was added before the actual filter, and a 10% error in the second step of the ECG component identification algorithm has been added. This was added based on empirical evidence on our data set, yielding adequate filtering. Nonetheless, this choice might not be generalizable to other EMG data set contaminated with ECG.

The filter works by first, running an ICA on the HD EMG signals in order to extract independent component from the signals. The next step is to go through the components and automatically detect if they correspond to the ECG artifact or not. This step is done in two stages: first, Peaks Detection, and second, identification of the ECG component perse via the characteristics of the detected peaks.

The Peak Detection algorithm works in 5 stages (Mak, Hu, and Luk 2010):

1. Scan the signal for peaks, and determine the maximum peak value s_{max}
2. Define the threshold, Th, as a fraction of the maximum, $0.6s_{max}$

3. Convert the signal into binary format:
$$\begin{cases} s_1(n) = 1, s(n) \geq Th \\ s_1(n) = 0, s(n) < Th \end{cases}$$

4. Calculate the first derivative of $s_1(n)$, in order to get the rate of change of the signal $s_1(n)$, using the following equation:
$s_2(n) = s_1(n) - s_1(n-1), n = 2, 3, \ldots, N$
With N the number of samples

5. Select the samples for which the corresponding $s_n(n) = 1$ which means that they have a positive rate of change, following the equation:
$\mathbf{P} = n | s_2(n) = 1$
$\mathbf{P}$ containing the indices of the peaks in $s(n)$

The identification of ECG source components is done using 3 criteria that must be met (Mak, Hu, and Luk 2010):

1. Number of peaks:
$(200\ bpm/60\ s) \cdot d \geq |\mathbf{P}| \geq (40\ bpm/60\ s) \cdot d)$
where $|\mathbf{P}|$ indicates the number of elements in the set $\mathbf{P}$, that is the number of peaks detected, and d represents the length of the component signal in seconds. The limit of BPM is set to be between 40 and 200 in order to stay within physiological ranges.

2. Peak intervals:
$1.5s \geq \mathbf{P}(n+1) - \mathbf{P}(n) \geq 0.3s, n = 1, 2, \ldots, N$
where $\mathbf{P}(n)$ represents the time information of the n^{th} peak detected. N is the number of peaks detected. $1.5s$ is the averaged peak interval value for a \$40 bpm \$ heart rate, and $0.3s$ is the averaged peak interval value for a 200 bpm heart rate. An error of 10% has been allowed, from empirical evidence, so that the filter works optimally on our data set.

3. Variance of peak intervals:
$[\mathbf{P}(n+2) - \mathbf{P}(n+1)] - [\mathbf{P}(n+1) - \mathbf{P}(n)] \geq R \cdot (1.5s), n = 1, 2, \ldots, N$
where $1.5s$ is the upper limit of the peak interval value. A scaling factor R of 0.5 was adopted for this study.

The components that meet those 3 criteria are labeled as ECG components and are then discarded when reconstructing the signal. Figure 3.20 shows the effect of the filter when applied on the signal shown in Figure 3.19.

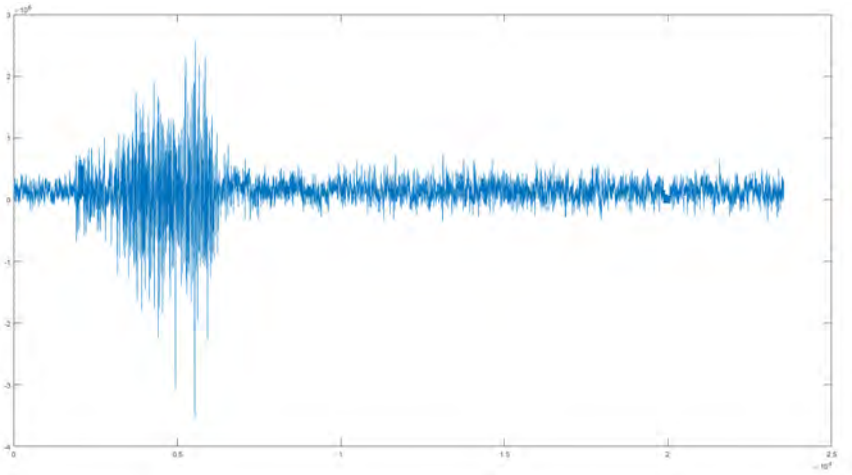

Figure 3.20: Signal from an HD EMG electrode after the ECG artifacts have been filtered out via the use of the ECG filter.

Details about the Matlab implementation used can be found in the appendix `ACGartRm()`.

After the ECG filtering step, the HDEMG signal was filtered for noise artifact of extreme amplitude that were left after the previous filtering steps. First the distribution of the signal's values was acquired. Then the 0.05% of the extreme values from the upper and lower range of the distribution were replaced by the median value of the signal. Details on the implementation of this filter can be found in the appendix `distriFilter()`.

The next step was to filter for PLI, white ground noise (WGN) and movement artifacts (MA) in order to improve the signal PNR. To do so, we implemented a filter based on the work of Al Harrach et al. (Al Harrach et al. 2017). This filter is based on the use of Canonical Correlation Analysis (CCA) (Hassan et al. 2011; Sweeney, McLoone, and Ward 2012) in order to rank estimated sources of the signal, which allow to design an adequate thresholding paradigm to select wanted and unwanted signal sources (Al Harrach et al. 2017). This filter works in 3 stages:

1. Canonical Correlation Analysis
2. CCA Component Thresholding:
   For each component obtained via the CCA, an intensity ratio is computed using the equation:

$$r_j = \frac{\sum_{i=1}^{N} |S_j(i)|}{N} \times \frac{P}{\sum_{i=1}^{P} |b_{s_j}(i)|} \tag{3.8}$$

   where r_j is the intensity ratio of the j^{th} estimated source, $S_j(i)$ the i^{th} sample of the j^{th} estimated source, $b_{s_j}(i)$ the corresponding noise obtained from the first 0.5 s period of the $S_j(i)$ which has to be devoid of muscle contraction, in order for this step work.
   Then, we reconstruct the signal with only the component(s) that have an intensity ratio above 1. The correlation value between the reconstructed signal and the original signal is then checked. If the correlation is ≥ 0.8, we reiterate the previous step by increasing the threshold for the intensity ratio value by 0.1. We keep on as long as the correlation value between the reconstructed signal and the original signal is ≥ 0.8. When the correlation drops below 0.8, it means we found the threshold. The components that have an intensity ratio below the found threshold are therefore discarded from the reconstruction of the filtered signal.
3. Selective CCA:
   This step is here in order to prevent contamination of the signal by high PNR component. We check if the filtered signal has a higher PNR than the original signal. If not, we discard the filtering. This step is done electrode by electrode.

The Figure 3.21 shows the effect of the CCA filtering on the signal shown in Figure 3.20.

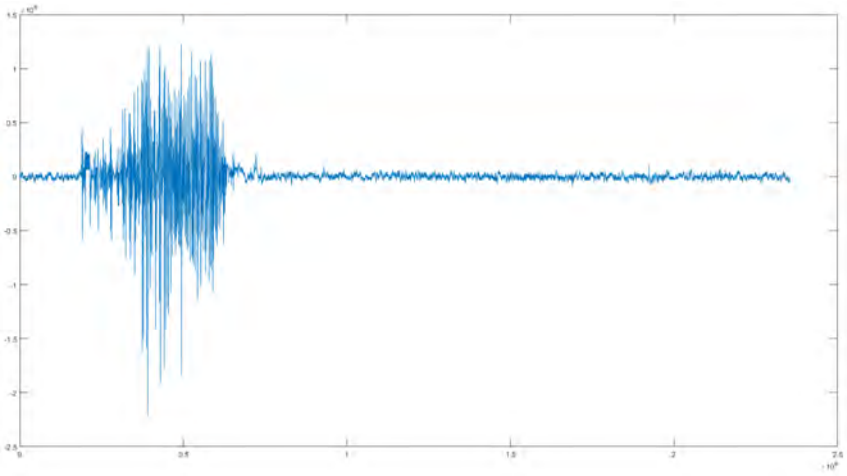

Figure 3.21: Signal from an HD EMG electrode showing the effect of the CCA filter.

Details about the Matlab implementation used can be found in the appendix `EMGccaFilt()`.

All the filter's Matlab implementation can be found on https://github.com/TSS-22/EMG-preprocessing-tools (Robinault 2021).

3.7 Data processing tools

3.7.1 Principal component analysis

PCA is based on the works of multiple mathematicians from the 19th century (Abdi and Williams 2010), dating as far back as 1829 with the work of August-Louis Cauchy (Cauchy 2009), but it was named and developed into its modern form by Harold Hotelling later during the 1930s (Hotelling 1933). Explaining how PCA works and all its intricacy is beyond the scope of this work but the goal of PCA can be summarized as "extract the most important information from the data set" (Abdi and Williams 2010. A goal achieve using the following three steps:

1. Reduce the size of the data set
2. Simplify the data set
3. Help analyze the structure of the variables and observations

There are multiple different methods to compute PCA results. We will explain the method described by Hotelling in 1933 (Hotelling 1933), due to the simplicity of the calculus which help visualize and understand the process of PCA. Each component is a combination of the variables, and the importance of each variable can be estimated from the factors loading associated to that variable.

Each component is computed from an eigenvalue and an associated eigenvector. The eigenvalue associated to a component corresponds to the sum of the squares of the factor loading, and also represent the variance that this component explains.

An eigenvector is a vector that bear weights each associated with one of the variables used. They represent the importance of each variable in the computation of the component. The factors of each variable in the component can be obtained by multiplying this vector by the square root of the associated eigenvalue.

The eigenvalues and vectors are computed via an iterative method, which stops when the computed $\overrightarrow{V_n}$ eigenvectors is deemed to be the same as the $\overrightarrow{V_{n-1}}$ eigenvectors, when this happen, the solution is to said to have converged and the iteration is stopped.

To compute the components is done by first computing the eigenvalues and eigenvectors (Paul Kline 2014):

1. Compute the correlation matrix $\mathbf{C}$ of the variables, of dimension $v \times v$, where v is the number of variables used:

$$\mathbf{C} = \begin{pmatrix} C_{x_1x_1} & C_{x_1x_2} & \cdots & C_{x_1x_{v-1}} & C_{x_1x_v} \\ C_{x_2x_1} & C_{x_2x_2} & & & C_{x_2x_v} \\ \vdots & & \ddots & & \vdots \\ C_{x_{v-1}x_1} & & & C_{x_{v-1}x_{v-1}} & C_{x_{v-1}x_v} \\ C_{x_vx_1} & C_{x_vx_2} & \cdots & C_{x_vx_{v-1}} & C_{x_vx_v} \end{pmatrix}$$

2. Compute each vector $\overrightarrow{\mathrm{U}_1}$ such as:

$$\overrightarrow{\mathrm{U}_1}(j) = \sum_{i=1}^{v} \mathbf{C_{ij}} \tag{3.9}$$

where $\overrightarrow{\mathrm{U_j}}$ is the sum vector of the j^{th} columns of the correlation matrix $\mathbf{C}$, and v the number of variables.

3. Normalize $\overrightarrow{\mathrm{U}_1}$ into $\overrightarrow{\mathrm{V}_1}$ the following way:

$$\overrightarrow{\mathrm{V}_1} = \frac{\overrightarrow{\mathrm{U}_1}}{\sqrt{\sum_{i=1}^{v} \overrightarrow{\mathrm{U}_1}^2(i)}} \tag{3.10}$$

where $\overrightarrow{\mathrm{V}_1}$, the normalized corresponding vector $\overrightarrow{\mathrm{U}_1}$. This is our first eigenvector.

4. To get $\overrightarrow{\mathrm{U}_2}$, we proceed the following way:

$$\mathbf{M} = \mathbf{C} \times \overrightarrow{\mathrm{V}_1}\overrightarrow{\mathrm{U}_2}(j) = \sum_{i=1}^{v} \mathbf{M}(i,j) \tag{3.11}$$

5. To get $\overrightarrow{\mathrm{V}_2}$ we normalize $\overrightarrow{\mathrm{U}_2}$ the following way:

$$\overrightarrow{\mathrm{V}_2} = \frac{\overrightarrow{\mathrm{U}_2}}{\sqrt{\sum_{i=1}^{v} \overrightarrow{\mathrm{U}_2}^2(i)}} \tag{3.12}$$

This is our second eigenvector.

6. We then compare $\overrightarrow{\mathrm{V}_1}$ and $\overrightarrow{\mathrm{V}_2}$ for similarity. If they are deemed not similar, we repeat the step 4 and 5 to get $\overrightarrow{\mathrm{V}_3}$ from $\overrightarrow{\mathrm{V}_2}$, compare them, and we stop the iterative algorithm when $\overrightarrow{\mathrm{V_n}}$ is deemed similar to $\overrightarrow{\mathrm{V_{n-1}}}$. $\overrightarrow{\mathrm{V_n}}$ is then discarded. The choice of the similarity criterion is up to the subjective choice of the researcher, and generally is below 0.00001 decimal accuracy. We can now compute the components, their eigenvalues and the associated vector loadings.

We compute the component using the following sequence (Paul Kline 2014):

1. The eigenvalues of the first component is computed as:

$$E_1 = \sqrt{\sum_{i=1}^{v} \overrightarrow{\mathrm{U_{n+1}}}(i)} \tag{3.13}$$

2. The factors loading of the first components are computed as:

$$\overrightarrow{\mathrm{F_1}} = \overrightarrow{\mathrm{V_n}} \times \sqrt{E_1} \tag{3.14}$$

3. We then compute the residual matrix as:

$$\mathbf{R_1} = \mathbf{C} - \begin{pmatrix} F_{1_1}^2 & F_{1_1} \times F_{1_2} & \cdots & F_{1_1} \times F_{1_{v-1}} & F_{1_1} \times F_{1_v} \\ F_{1_2} \times F_{1_1} & F_{1_2}^2 & & & F_{1_2} \times F_{1_v} \\ \vdots & & \ddots & & \vdots \\ F_{1_{v-1}} \times F_{1_1} & & & F_{1_{v-1}}^2 & F_{1_{v-1}} \times F_{1_v} \\ F_{1_1} \times F_{v_1} & F_{1_v} \times F_{1_2} & \cdots & F_{1_v} \times F_{1_{v-1}} & F_{1_v}^2 \end{pmatrix} \tag{3.15}$$

4. Reiterate the steps 1, 2 and 3 till there is no more component to compute.

The number of components to extract is finite, as at some point, all the variance will be explained by x amount of component, but usually components that explain too little of the variance are discarded. The threshold is usually set at 5%.

To get a deeper dive into PCA and its intricacy, we recommend to the reader to take a look at the very complete article of H. Abdi and L. Williams (Abdi and Williams 2010) and to the tutorial from R. Bro and A. Smilde (Bro and Smilde 2014). The a very thorough work of C. Nunally (Nunally and Bernstein 1978) or P. Kline (P. Kline 1992) will satisfy the most curious reader.

3.7.2 Factor Analysis

The factor analysis (FA) is a variant of the PCA. It differs from it in the construction of the correlation matrix used to compute the components and find the factors loading on those components. A R-type exploratory analysis was run for each movement of the protocol to look for an "NSLBP" component and study its factor loadings (Paul Kline 2014). The technique used in our work for the R-type analysis, was the Maximum Likelihood , developed by K. Joreskog and collaborator (Jöreskog 1970). The mathematics of this method being fairly complex, we will not detail them here, but the work of S. Mulaik (Mulaik 2009) is recommended for the curious reader. This technique was developed by A. Comrey (Comrey 1962) and H. Harman (Harman 1976). The component rotation algorithm used was the `varimax` one. It

was choosen in order to simplify the structure found by the FA, the simpler structure being thought to be the optimal result (Thurstone 1947; Cattell 2012). We used the R function `fa()` from the R package `psych` to run the FA analysis. The reader looking for more details on FA is recommended to read the book **Easy Guide to Factor Analysis** from P. Kline (Paul Kline 2014).

3.7.3 Deep Neural Network

Deep Neural Network (DNN) is a technique from the family of the Deep Learning domain, which is itself a subset of Machine Learning (ML) (Deng 2014). The ideas at the base of DNN where already developed a couples of decades ago (LeCun et al. 1989; Ivakhnenko et al. 1967; Fukushima, Miyake, and Ito 1983), but were only "re-discovered" recently (Tappert 2019), and really put to use in the last decade. It is in large part due to the increase of available data, especially labeled data, in conjunction with the dramatic increase in computing power, especially with the advances in matrix processing with the use of graphics processing unit which dramatically increased the speed and processing capacity for this type of calculus (Bartlett et al. 2012). Deep Learning, and DNN are a vast, broad and complex subject, therefore we will only explain the basics of the tools we used here. The avid reader is referred to the very complete and thorough book of I. Goodfellow and collaborators (Goodfellow, Bengio, and Courville 2016), which will answer most, if not all, questions that he might have on the subject.

The DNN domain is very broad, and there exist numerous types of family of DNN, the main ones being (Goodfellow, Bengio, and Courville 2016):

- Multi-Layer Perceptrons (MLP)
- Convolutional Neural Networks (CNN)
- Recurrent Neural Networks (RNN)

In this project we used a MLP type DNN. Those type of DNN are composed of multiple layers: at least one input layer and one output layer and in most cases, one or multiples hidden layers, that interconnect with each other in a linear sequence (Goodfellow, Bengio, and Courville 2016). The model is associated to a loss function and an optimizing function that work together to train the model by changing the weight values linked to the perceptron, also called neurons, that are composing the layers of the model (Francois Chollet 2021). Each layer is composed of perceptron, hence the name Multi-Layer Perceptron. In the present work, the training of our DNN was supervised, meaning that the input we were feeding our DNN were linked to answers the DNN is supposed to give us back (Bengio, LeCun, et al. 2007).

Each neurons act as an object that is composed of the following parts, as shown in Figure 3.22 (Abraham 2005):

- Input(s)
- Weight(s)
- Non-linear activation function
- Output

The weights are first applied to the inputs, then those inputs are fed to the neuron, which will apply its activation function to the sum of the input. In most case the activation function is a nonlinear one. This function, applied to the sum of the input of the neuron, will give the output.

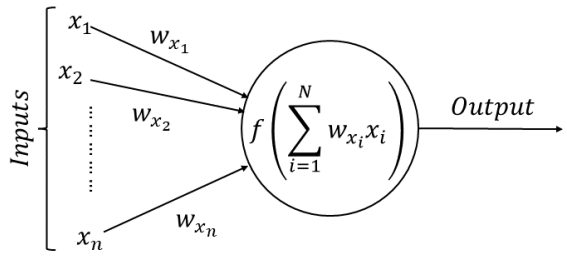

Figure 3.22: Diagram of a neuron.

Each layer is constituted of one or multiple neurons. There exists multiple type of layers, so we will only detail the one used in this project:

- Dense layer
- Dropout layer

The dense layers connect every neurons of a layer to every other neurons of the next layer, as shown in Figure 3.23 (Francois Chollet 2021). On the other side, dropout layers connect layers like a dense layer first, then a set amount of those connections, in most case randomly, are discarded, as shown in Figure 3.24. The use of dropout layers helps in preventing model over-fitting (Srivastava et al. 2014).

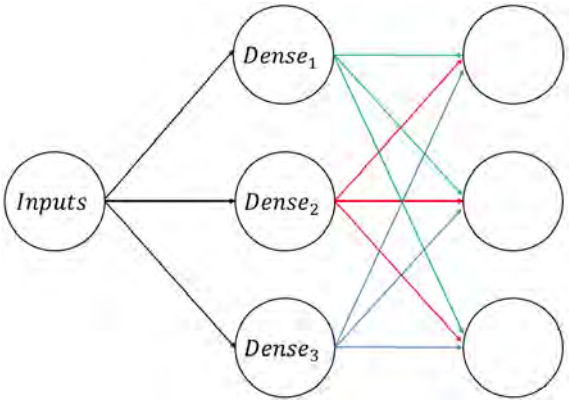

Figure 3.23: Diagram of a dense layer behavior.

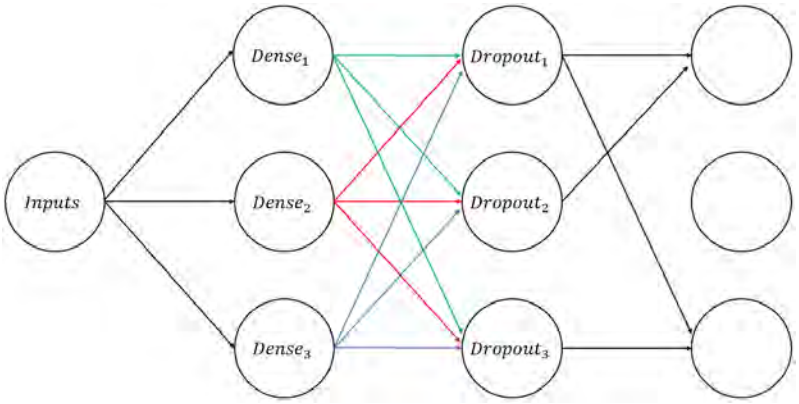

Figure 3.24: Diagram of a dropout layer behavior.

The DNN is trained accordingly to the process summarized in Figure 3.25 (Francois Chollet 2021). The model is first created with random weights, then the inputs are fed to the input layer, which will process those inputs accordingly to the rules that apply to the neurons it is composed of. Then those neurons output will be fed to the neurons of the next layer $n + 1$, according to the connection rule of the layer n. This will be done until we get to the output layer. The output layer will give a prediction of the result, which will be interpreted against the excepted result, via the loss function. This loss function will assess the quality of the prediction and give a loss score for this prediction (Goodfellow, Bengio, and Courville 2016). The loss score will then be interpreted by the optimizer, which will update the weights of the neurons that compose the model via backpropagation, according to the rules that the optimizer abides to, and the learning rate of the model. The goal of this optimizer is to optimize the loss function, via a gradient descent (Le et al. 2015).

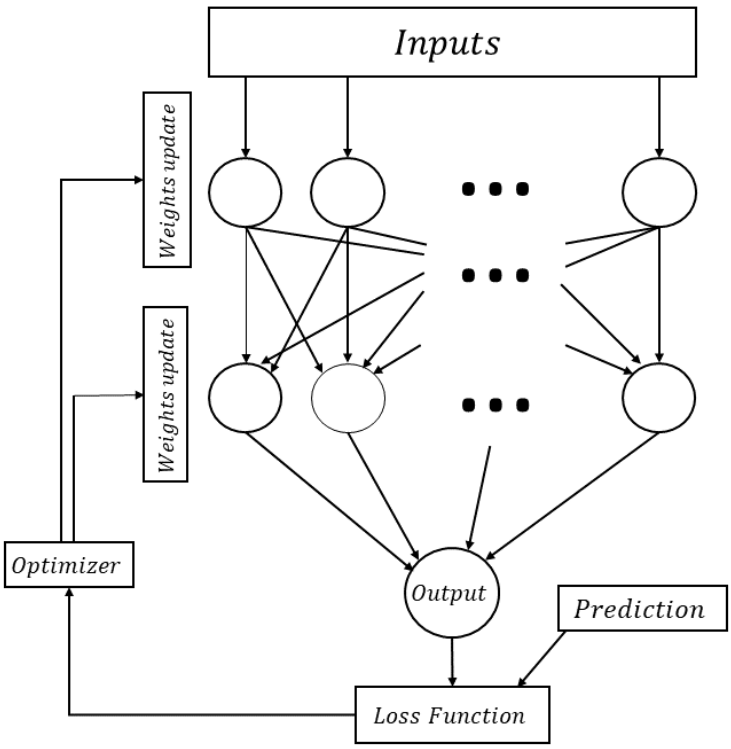

Figure 3.25: Neuron diagram.

3.7.3.1 Convolutional Neural Network

Convolutional neural network (CNN) is a special type of DNN. They were inspired by the visual processes from animal, and more particularly mammals (Fukushima 2007, 1980; Hubel, n.d.; Kosko and Mitaim 2003). They provide an efficient way to process image and video data (Wei Zhang et al. 1988, 1991; Denker et al. 1988; LeCun et al. 1989; W. Zhang et al. 1994) but also find uses in many different domains, such as natural language processing (Collobert and Weston 2008), time series (Tsantekidis et al. 2017) or brain computer interface (Avilov et al. 2020) to only give a couple of examples.

Two of the main benefits of CNN has over the DNN that we discussed earlier, is an artificially reduced size and its capacity to extract spatial features from the data, a great benefit when working on image and video data. Indeed, the number of elements in the CNN are limited by the different layers that he is made off. The Figure 3.26 shows the classic architecture of a CNN, with the main operations that compose a CNN:

- Convolution
- Pooling

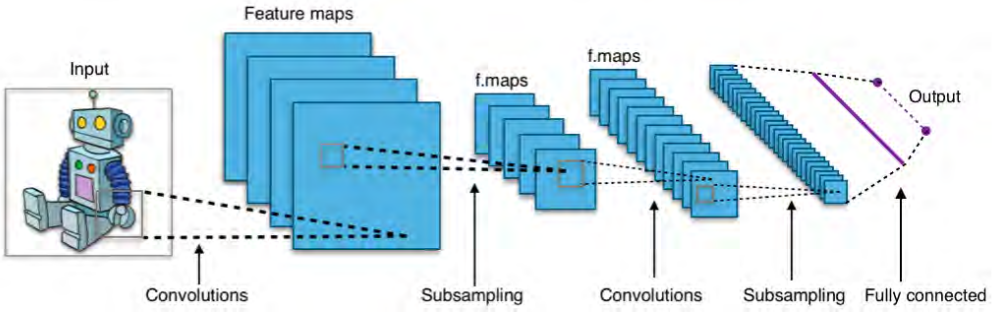

Figure 3.26: Typical CNN architecture. Gratefully provided by Aphex34.

The convolutional layers apply a convolution operation on our input data (Cao et al. 2022). To put it simply the convolution operation will be applied via a kernel of size $n \times n$ on our data, as displayed in Figure 3.27 (Goodfellow, Bengio, and Courville 2016). This results in a significant decrease of the number of connection and therefore, of parameters and size of the model. The Figure 3.28 (Goodfellow, Bengio, and Courville 2016) shows a good example of a convolution operation which act as a simple and effective edge detection.

In CNN, pooling layers are usually used in conjunction with convolution layers. They will reduce the size of our input by pooling the neighboring elements, further reducing the size of the model. The most used pooling layers are the Max Pooling and Average Pooling, which, respectively, discriminate for the maximum value read by the kernel, or the average of the value read by the kernel (Goodfellow, Bengio, and Courville 2016).

Once those operation carried out, following the needed architecture and parameters, the output of these operations are flattened, and usually feed through a fully connected layer to a rectified linear unit activation function, ReLu, which will categorize the input in multiple categories (Goodfellow, Bengio, and Courville 2016). Different architectures, with different input and output can be used for different purposes, so we only developed on the architecture that was used in this project.

3.7.4 Clustering techniques

Cluster analysis is part of the more global Pattern Recognition group of techniques, and use value of resemblance, or dissemblance, between objects in order to separate them in groups, called clusters (Diday and Simon 1976). After our exploratory analysis the following techniques were used:

- K-means clustering
- Spectral clustering
- Hierarchical agglomerative clustering

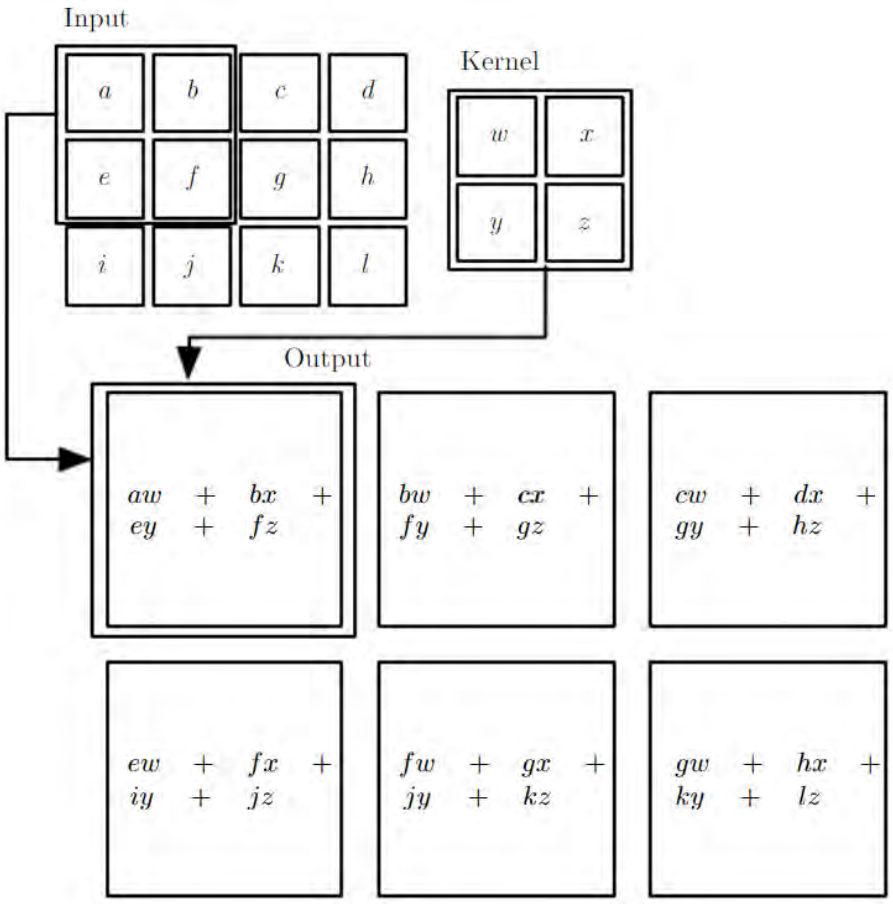

Figure 3.27: : An example of 2-D convolution without kernel-flipping (from Goodfellow, Bengio, and Courville 2016).

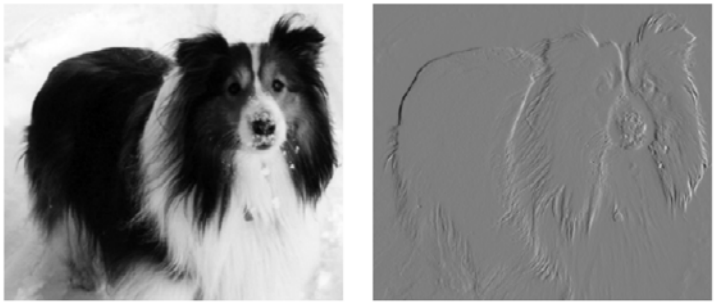

Figure 3.28: Example of a kernel subtracting the value of the neighboring pixel to the left. We can see that this kernel act as an efficient but yet simple, edge detection tool (from Goodfellow, Bengio, and Courville 2016).

3.7.4.1 K-means clustering

The K-means method was independently developed by G. Sebestyen (Sebestyen 1962) and J. MacQueen (MacQueen 1967) in the second half of the 20^{th} century. This method is designed to partition N objects containing values for P variables in K classes (Steinley 2006). Each partition, also named clusters, have a centroid which is a point of P dimensions, found by averaging the values of each variable for the occurrences within the cluster. First, clusters are initialized randomly. Then to populate them, the algorithm will allocate an object n to a cluster k, such as the distance between the centroid C_k of the cluster k and the object n is at least as small as the distance to the centroids of the other cluster k_x (Steinley 2006). To put it simply, the problem that the algorithm solve, is a minimization and optimization of a distance problem.

One of the drawbacks from the K-means clustering technique is that it will find local optimum not global one, it is not a robust solution (MacQueen 1967; Hartigan and Wong 1979). As even moderate data set have up to thousands of local optimum (Steinley 2003), this problem is very pervasive, but nonetheless, the K-means clustering algorithm exhibits usually good clustering ability (Dimitriadou, Dolničar, and Weingessel 2002; Steinley 2003).

First our data were normalized using the `sklearn.preprocessing.RobustScaler()` from the *Scikit Learn* Library (Pedregosa et al. 2011). Using Milligan and Cooper (Milligan and Cooper 1987) recommendation, would give clustering results that were poorer than with the `RobustScaler()`: even if it gave a relatively more uniform distribution of the data points among the clusters, it gave an inadequate one, and with a lower Silhouette score than using the `RobustScaler()`. We used the function `sklearn.cluster.KMeans()` (Pedregosa et al. 2011) to compute the clusters. The use of different parameters than the default ones did not yield better results, so we stuck to the default parameters for this algorithm.

The K-means clustering algorithm goes as follow (Steinley 2006):

Let there be, N objects: $n_1, n_2, \ldots, n_N$, each with P variables: $p_1, p_2, \ldots, p_P$ that we want to divide into K classes: $C_1, C_2, \ldots, C_k$.

1. Be $\mathbf{X}$ the data matrix of N row, one for each object, and P columns, one for each variable, such as:
2. Create initial seeds for each cluster, represented by a vector $S_k = (s_1^k, s_2^k, \ldots, s_P^k)$. We then allocate objects to the cluster that have the smallest Euclidean distance to them. This Euclidean distance is computed as follow:

$$d^2(i,k) = \sum_{j=1}^{P} (x_{ij} - s_p^k)^2 \tag{3.16}$$

   where d is the Euclidean distance, P the number of variables, also called dimensions here, s_j the seed coordinate for the j^{th} dimension or columns of $\mathbf{X}$, and i the i^th object, or row of the matrix $\mathbf{X}$.
3. Once allocated, the centroid of each cluster is computed as:

$$centroid_{C_k} = (\bar{x}_1^k, \bar{x}_2^k, \ldots, \bar{x}_p^k) \tag{3.17}$$

   with $\bar{x}_p^k$ the mean of the values of the p dimension of the object allocated to the cluster k.
4. Once the centroids have been established. The objects are allocated again to the cluster that have the centroid to a minimal distance from himself.
5. The step *3* and *4* are reiterated until convergence is reached: no objects are moved from one cluster to the other.

3.7.4.2 Spectral clustering

Spectral clustering uses a different idea than the distance calculation of the K-means algorithm, and rely on the use of graph Laplacian matrix to find similarity among the data (Von Luxburg 2007), and cluster it accordingly. The algorithm creates a weighted graph of the data points connection, and then divide the graph into clusters of interconnected components (Jia et al. 2014). One of the main difference of the spectral clustering algorithms is that it does not make any assumptions on the global structure of the data, which means that, contrary to K-means algorithm which will perform well mainly on convex data, the spectral algorithm will be able to provide robust clustering solution in spaces of complex shapes (Ding et al. 2014; Nascimento and De Carvalho 2011).

The spectral clustering algorithm used in this project was the normalized one (Shi and Malik 2000) due to its higher convergence capacity under general conditions (Von Luxburg, Belkin, and Bousquet 2008). We used the

`sklearn.cluster.SpectralClustering()` (Pedregosa et al. 2011) method which implement the algorithm detailed below. We used `K-means` and `Discretize` (Stella and Shi 2003), a technique less sensitive to random initialization, algorithms for the clustering step, and the `nearest_neighbors` or `RBF`, radial basis function kernel (Scholkopf et al. 1997) options to build the affinities.

The general shape of the spectral clustering algorithm can be divided into 3 stages (Verma and Meila 2003):

- Pre-processing
- Spectral Mapping
- Post-processing and grouping

The algorithm used for spectral clustering goes as follow (Ng, Jordan, and Weiss 2001; Von Luxburg 2007):

1. Be $S = \{s1, \ldots, s_n\} \in \mathbb{R}^{\lessdot}$, a set of points that we want to assign to k clusters
2. Form the affinity matrix $\mathbf{A} \in \mathbb{R}^{\kappa \times \kappa}$ defined by $\mathbf{A}_{ij} = e^{\frac{-||s_i - s_j||^2}{2\sigma^2}}$ if $i \neq j$, and $A_{ij} = 0$. σ the parameter control the the speed at which the affinity of $\mathbf{A}_{ij}$ falls off within between the distance s_i and s_j
3. Define D, the diagonal matrix where the $(i,i)^{th}$ element is the sum of $\mathbf{A}(i,:)$
4. Construct the matrix $\mathbf{L} = \mathbf{D}^{-\frac{1}{2}}\mathbf{A}\mathbf{D}^{-\frac{1}{2}}$
5. Find $x_1, x_2, \ldots, x_k$, the k largest eigenvectors of L and form the matrix $\mathbf{X} = [x_1, x_2, \ldots, x_k] \in \mathbb{R}^{n \times k}$ by stacking the eigenvectors in columns. To be noted that, in the case of repeated eigenvalues, the eigenvectors $x_1, x_2, \ldots, x_k$ are chosen to be orthogonal to each other.
6. Form the matrix $\mathbf{Y}$ to normalize each rows of $\mathbf{X}$ to have unit length, as $\mathbf{Y}_{ij} = \frac{\mathbf{X}_{ij}}{(\sum_j \mathbf{X}_{\mathbf{ij}}^{\mathbf{2}})^{-\mathbf{1/2}}}$
7. For $i = 1, \ldots, n$, let $\mathbf{Y}_{(i,:)} \in \mathbb{R}^k$ be the vector corresponding to the i^{th} row of $\mathbf{X}$
8. cluster the points $\mathbf{Y}_{(i,:)}$ into clusters using a cluster algorithm that attempt to minimize distortion, here the K-means algorithm
9. Assign the original point s_i to cluster j if $\mathbf{Y}_{(i,:)}$ was assigned to cluster j

3.7.4.3 Hierarchical agglomerative clustering

Hierarchical clustering is a method that cluster data points either from a bottom-up approach, the agglomerative one, or a top-down approach, the divisive one. One thing to note before going further, is that the hierarchical cluster technique is what is called a greedy algorithm: which means it will make locally optimal choice at each

stage (Black 2005), and the choices made at any stages are definitive and can't be altered subsequently (Yim and Ramdeen 2015). The divisive approach starts with all the data points as one cluster, and then separated them based on how dissimilar they are from each other. One of the main downsides of this approach is the heavy computational load that it infers.

The agglomerative approach used in this work start with all the data points as one cluster. It then computes a proximity matrix, also called similarity or dissimilarity matrix, depending on the methodological choices made in the parameters of the algorithm. This proximity matrix computes the distance in between each cluster, called linkage. Multiple metrics can be used to assess the distance between clusters. The following linkage metrics were used in this work:

- Manhattan, also called l_1
- Euclidean, also called l_2
- Cosine

The Euclidean distance is calculated using the following equation:

$$\sum_{j=1}^{k} = (a_i - b_i)^2 \tag{3.18}$$

With a and b two different data points, compared on the i variable, and k the total number of variable that compose a data point (Blei and Lafferty 2009).

The l_1 distance, also called Manhattan distance, due to its graphical resemblance to the way you go from one point to another in Manhattan due to its block division, is computed as the sum of the of the absolute differences of their Cartesian coordinates. It is defined using the following equation:

$$d(p, q) = \sum_{i=1}^{k} |p_i - q_i| \tag{3.19}$$

With p and q the data points, compared on the i variable, and k the total number of variables that compose a data point (Stigler 1986; Black 2019).

To be noted that Euclidean and Manhattan metrics are all part of the Minkowski distance function family.

The cosine Distance is equal to $CosineDistance = 1 - COsineSimilarity$, which is computed using the following equation:

$$CosineSimilarity = \frac{\sum_{i=1}^{k} a_i b_i}{\sqrt{\sum_{i=1}^{k} a_i \sum_{i=1}^{k} b_i}} \tag{3.20}$$

With a and b two different data points, compared on the i variable, and k the total number of variables that compose a data point. To put it simply, it computes the cosine value linked to the angle between the two data points when taken as vectors.

As the metrics above are made to be used between two points only, we need to choose a linkage criterion to compute the distance between cluster when clusters are made of more than one data points each. This criterion will let us know how to interpret the distance. Again, multiple criteria exist and only the following were used in this project:

- Single linkage
- Complete linkage
- Average linkage

The Single linkage, also called nearest neighbor linkage, define the distance between two different clusters as the smallest distance that can be found between an occurrence in the first cluster compared to an occurrence in the second cluster (Florek et al. 1951; Sneath 1957). One of the main drawbacks of this method, is that it can link clusters only due to outliers that are close to each other, while the rest of the cluster is closer to a different cluster, as shown in Figure 3.29. This is called the chaining effect (Mazzocchi 2008).

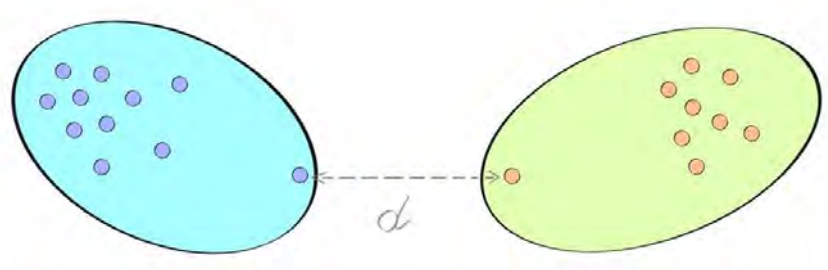

Figure 3.29: Distance using single linkage with outliers presence.

On the opposite side, the Complete linkage method, also called furthest neighbor or maximum method, define the distance between two different clusters as the largest distance between pairs of occurrences (Sokal 1958). The complete linkage is not subject to the chaining effect, but is subject itself to outliers, as outliers in the clusters could prevent an accurate measurement of the closeness of the clusters between each other, as shown in Figure 3.30.

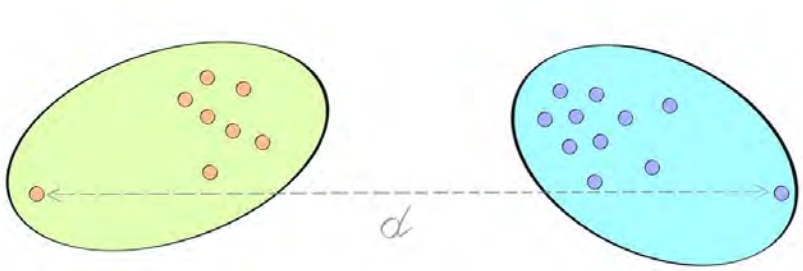

Figure 3.30: Distance using Complete linkage with outliers presence.

A middle ground can be found in the average linkage criterion. Also called Unweighted Pair-Group Method using Arithmetic Averages (Landau et al. 2011), this method computes the distance between clusters as the average of the distance of each occurrence from the first cluster between each occurrences of the second cluster (Sokal 1958). This alleviate the problems that can be found in Single and Complete linkage, by trading off robustness with heavier computational load. We used the `sklearn.cluster.AgglomerativeClustering()` (Pedregosa et al. 2011) method that is an implementation of the algorithm seen above. For the parameter `affinity` we used:

- `euclidean`
- `manhattan`
- `cosine`

For the parameter `linkage` we used:

- `single`
- `complete`
- `average`

3.7.4.4 Choosing the optimal number of clusters

The silhouette score was used to assess the optimal number of clusters, and also the quality of the clustering: quality of the separation of the cluster, and their tightness. The Silhouette Score method has been developed by P. Rousseuw in 1987 (Rousseeuw 1987). This value assesses a cluster separation from the other cluster and its tightness. The value ranges from *1*, perfectly separated and extremely tight cluster, to *-1*, misclassified observations, and *0* meaning that clusters are extremely

spread and are overlapping with others. To assess the quality of the clustering, we use the average Silhouettes score of the clusters obtained. The closer to *1*, the better. The highest average silhouette score tell us the optimal number of clusters to use. It is to be noted that the Silhouettes score is non robust to outliers, something that will appear clearly in the results described below.

3.8 Variables used

As was discussed earlier, the NSLBP population differ from the healthy population on different aspects. Different variables were chosen to represent those aspects.

3.8.1 Neuromuscular control

The back is a complex structure, that is composed of a lot of muscle. Surface EMG doesn't allow for the isolation of muscle when recording, as EMG is only recording EMG activity of a surface area. Recording is composed of a large number of data points, and it can be complex to interpret those data points in a clustering algorithm. We made the choice to use extract variables that would summarize information from the signals in order to circumvent this problem. The first variable that we used is the centroid of the EMG activity. This variable let us know where the EMG activity is concentrated, either on a specific patch or the group of patches. This variable has been chosen as it has already been proved to be discriminating among LBP and healthy populations (Sanderson et al. 2019), and as it yields information about the neuromuscular strategies of the subject. We suspect that this variable will therefore express nuances across the NSLBP spectrum, which will yield valuable information to cluster our NSLBP population sample.

The second variable used is the entropy of the EMG signal. The entropy of a signal allows us to know if the signal contain a lot of information or not. The entropy of a signal indicates to us the predictability of the data series of the signal. The higher the entropy value, the less the data series of the signal is predicable, and the other way, a low entropy value means a very predicable data series (Rényi 1961). To simplify the matter, the predictability of the signal can also be thought as the amount of information in the signal (Galar and Kumar 2017). Information can be interpreted in the case of EMG, as a representation of the strategy of the command sent by the brain. Low entropy value means that the muscle activity is much more localized, less distributed, and more predicable. On the other hand, a high entropy value would mean that the activity is much more distributed and less predicable across the recording zone. This variable will summarize information about the neuromuscular strategies of the participants by giving information about the zone of muscular activity. Contrary to the centroid of the activity which gives information about the general distribution of the muscle activity from a global standpoint, the

entropy gives us information on the relative distribution of the muscle activity from a structural standpoint.

Due to poor data quality of the classic EMG electrodes placed on the belly of the subjects, their data weren't used. The low quality of the signal acquired came from a sub-optimal placement, relatively high presence of fatty tissue in that area, and reference electrodes subjected to the weight of the EMG adapter, even after securing them with tape.

3.8.1.1 Centroid of the EMG activity

The centroid variables used were as follow:

- Centroid of the right low back electrode grid, X and Y position
- Centroid of the right upper back electrode grid, X and Y position
- Centroid of the left low back electrode grid, X and Y position
- Centroid of the left upper back electrode grid, X and Y position
- General centroid, X and Y position

X and Y being axis of focus of the location of the centroid: X sagittal axis and Y the transverse axis (Corresponding respectively to the axes X and Z displayed Figure 3.9). The centroids were computed for each repetition, then averaged to give the centroid value for the movement. This was done for each subject and for each movement.

To compute the centroid, the first thing, was to compute the Root Mean Square (RMS) value of each electrode signal, then each electrode was mapped as a matrix in which its position corresponds to its actual physical position and the grid of electrode to their physical position on the electrode grid. The weighted barycenter of the matrix was then computed for each electrode grid, using the RMS values previously calculated as weight, using the following formula (Farina et al. 2008; Nishikawa et al. 2017):

$$barycentre = \sum_{i=1}^{N} (\frac{\overrightarrow{y}}{\sum_{i=1}^{N} y_i}) \times C_i \tag{3.21}$$

With N the number of electrodes, $\overrightarrow{y}$ the mean vector of the RMS values on the transverse axis, $\overrightarrow{C_i}$ the coordinate value of the electrode, for the transverse axis $\overrightarrow{C} = [1, 2, \ldots, 8]$. The computation for the sagittal axis is the same but with the mean vector $\overrightarrow{x}$ of the RMS value on the sagittal axis and $\overrightarrow{C} = [1, 2, \ldots, 5]$. To get the general centroid, the centroid of each electrode grid was offset by the position of the grid on the back of the person. The [0,0] position corresponding the position where every grid connect. The general centroid was weighted by the sum of the RMS

values of each electrodes grid. The processing was inspired by the work of Falla et al (Falla et al. 2014).

The centroid of EMG activity gives us indication on where the centroid of the contraction is positioned, meaning where most of muscle activity seems to be distributed. A valuable information, as showed Sanderson and collaborator in his work (Sanderson et al. 2019), as NSLBP subjects tend to have a more cranial activation of their low back muscles, meaning that the muscle activity is distributed more toward the upper regions in comparison to the healthy population.

3.8.1.2 EMG entropy

The entropy variables used were as follow:

- Entropy of the right low back electrode grid
- Entropy of the right upper back electrode grid
- Entropy of the left low back electrode grid
- Entropy of the left upper back electrode grid

To compute the entropy of each EMG grid, the RMS value of each EMG signal of the grid was computed. Then the entropy of the grid was computed using the Shannon entropy equation (Shannon 1948):

$$entropy = \sum_{i=1}^{N} n_i^2 \times \log(n_i^2) \tag{3.22}$$

With N the number of electrodes, n_i the RMS value of the i^{th} electrode. The entropy values were computed for each repetition, then averaged to give the entropy value for the movement. This was done for each subject and for each movement.

The entropy of a signal indicates to us the predictability of the data series of the signal. The higher the entropy value, the less the data series of the signal is predicable, and the other way, a low entropy value means a very predicable data series (Rényi 1961). To simplify the matter, the predictability of the signal can also be thought as the amount of information in the signal (Galar and Kumar 2017). Information can be interpreted in the EMG case, as a representation of the quality, the efficiency of the command sent by the brain to the muscles. The lower the entropy value, the more the muscle activity will be constrained to a specific region and less distributed across the recording zone.

Entropy summarizes information about the neuromuscular strategies employed by the participants, by giving information about the distribution of muscular activity across the recording area. On the other side, the centroid of muscle activity gives

us information about the general position of the activity. We can summarize this difference as the entropy giving us the amount of concentration of the muscle activity, and the centroid of activity giving us the localization of this activity.

3.8.2 Variability and adaptability of the movements

Earlier, we discussed the fact that NSLBP populations had significant differences when it came to inter and intra-subject variability compared to the healthy population (Cholewicki et al. 2019; Asgari et al. 2015; Ippersiel, Robbins, and Preuss 2018). Therefore, those aspects were integrated in the present work. Inter and intra-subject variability was assessed as the error against the mean trajectory from the healthy population. Another measure, the entropy of the movement, has also been added. This measure let us know about the smoothness of the trajectory: the higher the entropy value, the more jittery the movement is. This could be interpreted, for high entropy value, as a movement that ask for a lot of readjustment. And for low entropy value, a smoother movement. And for extremely low values of entropy, the movement could even be interpreted as rigid, not adapting to the inevitable little perturbations that a subject would face.

3.8.2.1 Entropy of the movement

- Entropy of the left shoulder trajectory X, Y and Z axis
- Entropy of the right shoulder trajectory X, Y and Z axis
- Entropy of the hips cluster of marker trajectory X, Y and Z axis
- Entropy of the T6 vertebrae cluster of marker trajectory X, Y and Z axis
- Entropy of the C7 vertebrae cluster of marker trajectory X, Y and Z axis

The X, Y and Z axis correspond to the axis showed in Figure 3.9. The entropy for each axis of each shoulder marker is computed following the same logic as in EMG entropy, to the difference that the Sample Entropy (Song, Liò, et al. 2010) was used, as we are working on physiological time-series signal. The Sample entropy is computed using the implementation developed by K. Lee (Lee 2022).

3.8.2.2 Variability inter-subject

- Left shoulder trajectory X, Y and Z axis inter-variability
- Right shoulder trajectory X, Y and Z axis inter-variability

The X, Y and Z axis correspond to the axis showed in Figure 3.9. The inter subject variability, called inter-variability, is the variability of a subject against the other subjects. First the average trajectory of the healthy subjects was computed in each axis: X, Y and Z. All trajectories were re-sampled to be represented by vectors of

100 samples each before comparison. Following this, for each repetition, the RMS error (RMSE) of the trajectory of the subject against the average Healthy trajectory was computed. It was then averaged to give one error value, the inter-variability. This was done for each subject and each movement. The variability inter-subject is normalized by the height of the subject.

3.8.2.3 Variability intra-subject

- Left shoulder trajectory X, Y and Z axis intra-variability
- Right shoulder trajectory X, Y and Z axis intra-variability

The X, Y and Z axis correspond to the axis showed in Figure 3.9. The intra subject variability, called intra-variability, is the variability of a subject against himself. First the average trajectory of the subject was computed in each axis, X, Y and Z. All trajectories were re-sampled to be represented by vectors of 100 samples each before comparison. Following this, for each repetition, the RMS error (RMSE) of the trajectory of the repetition against the average trajectory of the other repetitions of the subject was computed. The errors values for each repetition were then averaged to give one error value, the intra-variability, for that movement. This, for each subject and each movement. The variability intra-subject is normalized by the height of the subject.

3.8.3 Movement strategies

As discussed earlier, compared to their healthy counterpart, the NSLBP population seems to present different movement strategies (Sanderson et al. 2019; Shum, Crosbie, and Lee 2005, 2010; Laird et al. 2014; Bourigua 2014; Villafane et al. 2016; Gombatto et al. 2013) , and diminished range of motion (Shum, Crosbie, and Lee 2010, 2007), compared to the healthy population, even if those changes are inconsistent across the NSLBP population.

Spine mechanics has been shown to be altered in NSLBP population compared to their healthy counterpart (Villafane et al. 2016). Therefore in order to get our work to take this aspect into account, we used clusters of markers placed on the back, as to assess and capture precisely the spine mechanics of the subjects. Unfortunately, due to the important work needed to pre-process the motion capture data we weren't able to use all the participant's data due to the time constraints imposed by this work. In order to circumvent this, shoulder marker was used as they are the most stables and fastest to clean and label markers that are directly linked to the trunk, and therefore to the spine position and dynamic. When possible, the spine markers were used, either the full set, or a subset, in order to use as much information as possible. Details about the markers and clusters of markers setup can be found in the part System and setup from the part Motion Capture.

According to what was discussed earlier, and the work of Laird, et al., 2014 (Laird et al. 2014), in order to investigate the different movements strategies displayed by the participant, the maximum amplitude and time to maximum amplitude of the participant was used, as well as the maximum angle and time to maximum, the latter being used when working on the rotation movement conditions.

3.8.3.1 Maximum amplitude

- Maximum amplitude of the left shoulder trajectory X, Y and Z axis
- Maximum amplitude of the right shoulder trajectory X, Y and Z axis
- Maximum amplitude of the hips cluster of marker trajectory X, Y and Z axis
- Maximum amplitude of the T6 vertebrae cluster of marker trajectory X, Y and Z axis
- Maximum amplitude of the C7 vertebrae cluster of marker trajectory X, Y and Z axis

The X, Y and Z axis correspond to the axis showed in Figure 3.9. The maximum amplitude of each marker and each axis is computed as the maximum absolute difference reached from the position in the first frame. It is done for each repetition, then average to give a value for each subject and each movement. The values have been normalized by height.

3.8.3.2 Time to maximum amplitude

- Time to maximum amplitude of the left shoulder trajectory X, Y and Z axis
- Time to maximum amplitude of the right shoulder trajectory X, Y and Z axis
- Time to maximum amplitude of the hips cluster of marker trajectory X, Y and Z axis
- Time to maximum amplitude of the T6 vertebrae cluster of marker trajectory X, Y and Z axis
- Time to maximum amplitude of the C7 vertebrae cluster of marker trajectory X, Y and Z axis

The X, Y and Z axis correspond to the axis showed in Figure 3.9. The time to maximum amplitude of each marker and each axis is computed as the time it takes for the subject to reach the maximum amplitude, defined in Maximum amplitude of the movement. It is done for each repetition, then averaged to give a value for each subject and each movement.

3.8.3.3 Maximum angle and time to maximum angle

- Maximum value and Time to maximum value of the shoulder angle on the Z rotation axis
- Maximum value and Time to maximum value of the angle between the Hips and C7 cluster of markers on the X, Y and Z rotation axis
- Maximum value and Time to maximum value of the angle between the T6 and C7 cluster of markers on the X, Y and Z rotation axis

The Z axis correspond to the axis showed in Figure 3.9. The maximum angle is computed as the maximum absolute angle reached during movement by the subject. It is only computed for the rotation around the Z axis as shown in Figure 3.31. The time to maximum value is the time it takes the subject to reach this maximum angle. The values have been computed for each repetition, then average to give a value for each subject and each movement.

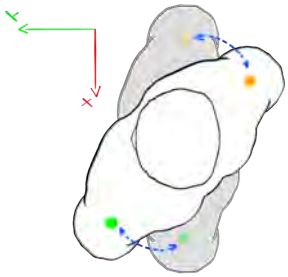

Figure 3.31: Description of the shoulder angle in Z during a trunk rotation to the right.

3.8.4 Balance and proprioception

As seen earlier, the NSLBP population showcase balance (Mok, Brauer, and Hodges 2011; Byl and Sinnott 1991) and proprioception alterations (Gombatto et al. 2015; Ruhe, Fejer, and Walker 2011; MacDonald, Moseley, and Hodges 2009). To assess this aspect, we summarized the force plate data in two variables that yield information on proprioception and balance of the participants.

The proprioception of the participant was assessed via the use of the normalized statokinesigram area (J. Oliveira 2022), the COP projection of the X and Y axis (Prieto et al. 1996). The balance was assessed by the ground force reaction ratio. This ratio tells us about the balance strategy of the subjects and how they distribute their weight in order to perform the movement conditions.

3.8.4.1 Area of the normalized statokinesigram

The statokinesigram is the projection on the horizontal plane, of the Center of Pressure (COP) of the subject on the force plates (Prieto et al. 1996). The COP is measured via the use of the force plate, which records the ground force reaction of the subject, and therefore its body sway (Directions 1983). Different variables can be extracted out of it, that have the potential to yield useful and interesting information: like the area of the statokinesigram: the ellipse that contain 95% of its values, as represented in Figure 3.32. We do not use 100% of the values in order to increase the robustness of the measure against outliers (J. M. de Oliveira 2017). One of the drawbacks of the statokinesigram is its high inter and intra-variability, indeed repeated measurement showed high intra-day and intra-subject variability (Chiari, Rocchi, and Cappello 2002; Samson and Crowe 1996). To circumvent this issue, normalization of the statokinesigram have been recommended, in order to improve inter and intra-reliability of the associated variables (Chiari, Rocchi, and Cappello 2002). We therefore implemented the self-normalization technique of J. M. de Oliveira (J. M. de Oliveira 2017), using the function that he designed (J. Oliveira 2022). Once the statokinesigram is normalized, the area of the ellipse encompassing 95% of the statokinesigram value is computed. This has been done for each repetition, those values being averaged to give a value for each subject and each movement.

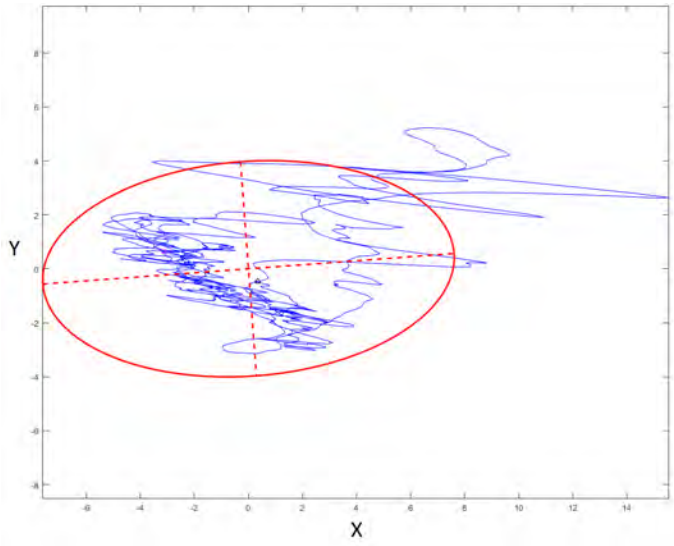

Figure 3.32: Visual example of a statokinesiogram. In blue the projection of the COP, and in red the elipse that encompass 95% of its values.

3.8.4.2 Ground force reaction ratio

The Ground Force Reaction (GRF) ratio has been computed using the following equation:

$$GRF_{ratio} = \frac{\sum_{n=1}^{N} \frac{leftGRF_n}{rightGRF_n}}{N} \tag{3.23}$$

With N being the number of sample, $leftGFR_n$ and $rightGFR_n$ the value for, respectively, the left and right GFR at the n^{th} sample.

The GFR ratio was added due to the fact that during data acquisition, it seemed that two distinct trends could be noted: subjects with relatively equal GFR ratio and subjects with unequal GFR ratio. We therefore put this variable to the test to see if there is any relevance to it

3.8.5 Metadata

As we discussed earlier, LBP is a multifactor symptom (Hartvigsen et al. 2018). In order to reflect this aspect, we used metadata. Age, Body Mass Index (BMI), weight and Height were used as metadata in the clustering analysis. Being only anthropometric data, they only yield direct or indirect information about the biophysical and genetic factor.

Chapter 4

Results

As we discussed earlier, one of the major problems of NSLBP at the time being, is that practitioner have no way to differentiate people afflicted by NSLBP between each other. This makes the creation of fine-tuned rehabilitation protocol difficult, or virtually impossible. This is the motivation for trying to find cluster among the NSLBP population.

Indeed, finding potential clusters inside the LBP population would help to define different sub-population, which would allow to analyze their characteristics in order to better understand them. Which in turn, would lead to more possibilities of designing personalized treatments for these subgroups, and also to develop clinical test to categorize them easily and at lower cost in clinical setup.

But the clustering task, especially on continuous variables, is not an easy one and this is why we start this work by an exploratory analysis, using DNN and FA. This exploratory work will help us better understand the importance of the relation of domains, and their variables, with the NSLBP symptom, as well as help us with our clustering attempt. Following this exploratory work, we will use different unsupervised clustering algorithms, and the insights gained from the exploratory work, to attempt to discriminate clusters in our population sample.

4.1 Exploratory analysis

The following exploratory work was peer reviewed and published as the work of Robinault and collaborators (Robinault et al., in press, 2023). Nonetheless, we invite the reader to focus on the present manuscript, as it yields additional details that will help understand the exploratory work done.

4.1.1 Deep Neural Network

4.1.1.1 Implementation

4.1.1.1.1 Classic DNN

To categorize people as Healthy, and LBP we used a linear supervised DNN, with the following architecture:

- Dense input layer of 11 neurons, with a sigmoid activation function
- Dense layer of 128 neurons, with a sigmoid activation function
- Dropout layer with a 50% rate of connection
- Dense layer of 36 neurons, with a sigmoid activation function
- Dense layer of 3 neurons, with a sigmoid activation function
- Output layer of 1 neurons

We used the python package `keras` (François Chollet et al. 2015) to build a `Sequential()` DNN with `Dense()` and `Dropout()` layers and then train it on the chosen data sets. The optimizer used here is the `adam` optimizer (Bock and Weiß 2019), and the loss function is the `categorical_crossentropy` (Charniak 2021). The validation data set was set to be 30% of the total data set. The training set was split using the default value of 75% training data, 25% test data. Batch size was set to 10. It was also made sure the training, testing and validation sets did not had any common subject, in order to avoid information leakage into the model.

We started with a model trained on the full data set, without the spine data in order to maximize the amount of data point at our disposal. This model was created as a *null model* to assess our supposed maximum classification accuracy. After that model, this model was trimmed by domain:

- Anthropometric
- Biomechanics
- Neuromuscular control
- Balance and proprioception

This was done in order to assess the potential of information of each domain. Some domains were further divided in order to get a more detailed look into them.

The Table 4.1 details the data used in the different models. For more details about each variables, we refer the reader to the section Variables used.

Variables	Models
Age	Full, Anthropometric (Full, Trimmed)
Area of the normalized statokinesigram	Full, Balance
BMI	Full, Anthropometric (Full, Trimmed)
Centroid of the EMG activity	Full, Neuromuscular(Full, Centroid)
EMG entropy	Full, Neuromuscular(Full, Entropy)
Entropy of the movement	Full, Biomechanical (Full)
Foot barycentre trajectory	Full, Biomechanical (Full, Trimmed)
Ground force reaction ratio	Full, Balance
High Density EMG	CNN
Height	Full, Anthropometric (Full)
Maximum amplitude of the movement	Full, Biomechanical (Full, Trimmed)
Maximum angle to maximum angle	Full, Biomechanical (Full)
Sex	Full, Anthropometric (Full, Trimmed)
Time to maximum amplitude	Full, Biomechanical (Full, Trimmed)
Time to maximum angle	Full, Biomechanical (Full)
Variability inter-subject	Full, Biomechanical (Full)
Variability intra-subject	Full, Biomechanical (Full)
Weight	Full, Anthropometric (Full)

Table 4.1: Variables used in each models.

4.1.1.1.2 Convolutional Neural Network

The Convolutional Neural Network was fed HD EMG data previously cleaned, and divided by repetitions. Due to time constraints, only the data from the movement **Back Flexion Preferred Speed** were used.

The Convolutional Neural Network architecture is displayed in Table 4.2.

Layer (type)	Output Shape	Nb of parameters
input_1 (InputLayer)	(None, 26, 10, 6000, 1)	0
conv3d (Conv3D)	(None, 26, 10, 6000, 8)	1448
conv3d_1 (Conv3D)	(None, 26, 10, 6000, 8)	11528
max_pooling3d (MaxPooling3D)	(None, 13, 5, 599, 8)	0
batch_normalization (BatchNormalization)	(None, 13, 5, 599, 8)	32
conv3d_2 (Conv3D)	(None, 13, 5, 599, 16)	23056
conv3d_3 (Conv3D)	(None, 13, 5, 599, 16)	46096
max_pooling3d_1 (MaxPooling3D)	(None, 6, 2, 58, 16)	0
batch_normalization_1 (BatchNormalization)	(None, 6, 2, 58, 16)	64
conv3d_4 (Conv3D)	(None, 6, 2, 58, 32)	92192
conv3d_5 (Conv3D)	(None, 6, 2, 58, 32)	184352
max_pooling3d_2 (MaxPooling3D)	(None, 3, 1, 4, 32)	0
batch_normalization_2 (BatchNormalization)	(None, 3, 1, 4, 32)	128
flatten (Flatten)	(None, 384)	0
dense (Dense)	(None, 64)	24640
dropout (Dropout)	(None, 64)	0
dense_1 (Dense)	(None, 64)	4160
dropout_1 (Dropout)	(None, 64)	0
dense_2 (Dense)	(None, 1)	520

Table 4.2: Convolutional neural network architecture.

4.1.1.2 Results

4.1.1.2.1 Full model

This model was trained on the whole set of variables, except for the spine data as to maximize the number of data points available. This full model was done to have some sort of a null model, in order to see if it was already possible to categorize healthy and NSLBP subjects from our data set.

After 100 epochs, the model reached an accuracy of 99.88% on the test set and 93.30% on the validation set, showing signs of significant, but not dramatic, over fitting. This model attests that the data acquired contains valuable information about the NSLBP symptom. Details of the training performance can be seen in Figure 4.1a and 4.1b.

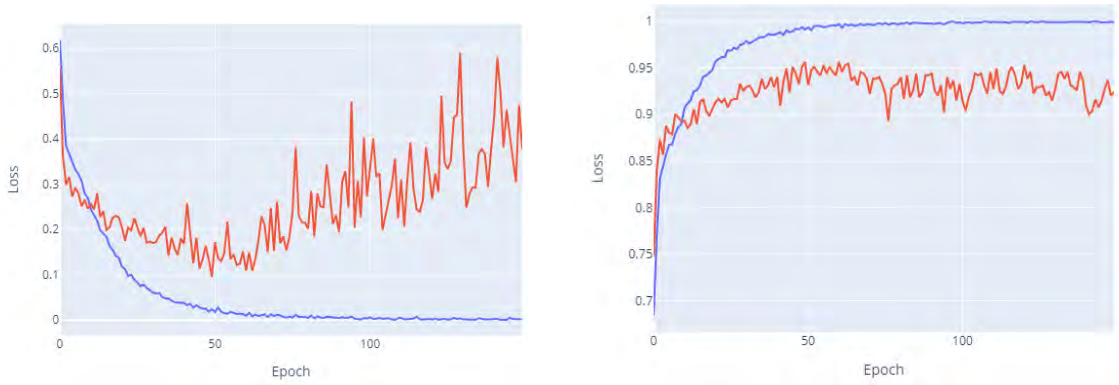

(a) Loss (b) Accuracy

Figure 4.1: Full model performance. In blue, performance on the test set. In red, performance on the validation set.

4.1.1.2.2 Anthropometric model

This model focused on the anthropometric data of the subjects and was trained for 300 epochs with the following variables:

- Age
- BMI
- Height
- Weight
- Sex

This model was trained to show how important the impact of only the anthropometric variables was on the capacity to classify these people, and therefore, the strength of their link to NSLBP. Indeed, the model after training, reached a precision score of 92.84% on the test set, and 94.40% on the validation set.

Below is the history of the model training, with the Figure 4.2a showing the loss score of the model, and the Figure 4.2b showing the accuracy of the model.

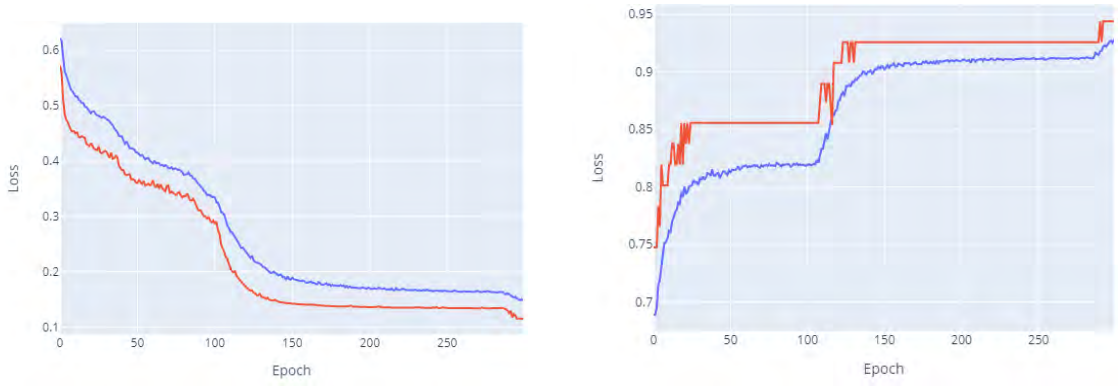

(a) Loss (b) Accuracy

Figure 4.2: Anthropometric model performance. In blue, performance on the test set. In red, performance on the validation set.

A trimmed version of this model, without the weight and the height variables, was also trained and reached a precision score of 94.40% on the test set, and 98.19% on the validation set. Below is the history of the model training, with the Figure 4.3a showing the loss score of the model, and the Figure 4.3b showing the accuracy of the model.

While training these models, we got a very high accuracy result despite the fact that we solely fed them with basic anthropometric data. These results were obtained whilst not displaying any obvious sign of over fitting.

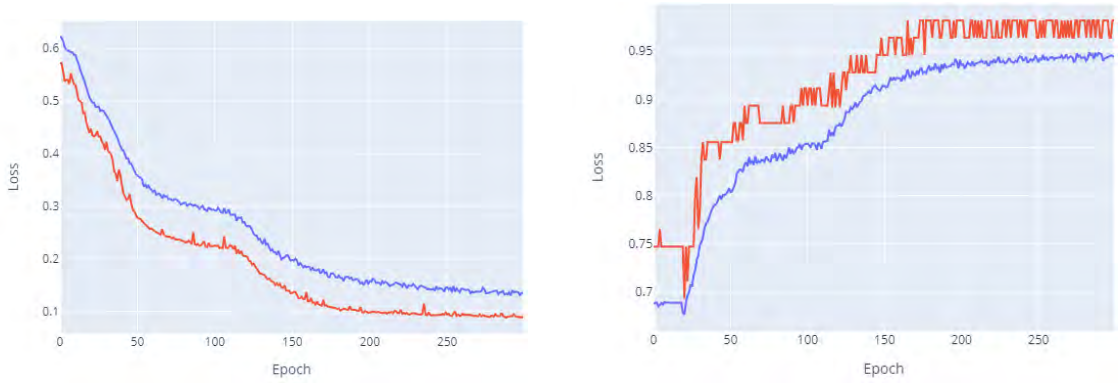

(a) Loss (b) Accuracy

Figure 4.3: Trimmed anthropometric model performance. In blue, performance on the test set. In red, performance on the validation set.

Training these models, we got a very high accuracy result while we solely fed them with basic anthropometric data. It is to be noted that, no data linked to the movement or giving an indication of the performance of the subject were fed to the models, attesting of the tremendous information power of those variables and therefore that domain. And these results were obtained while not displaying any obvious sign of over fitting.

4.1.1.2.3 Biomechanical model

This model was built with the biomechanics data, and trained for 400 epochs, using the following variables:

- Maximum amplitude of the left shoulder trajectory in the X, Y and Z axis
- Time to maximum amplitude of the left shoulder trajectory in the X, Y and Z axis
- Entropy of the movement of the left shoulder in the X, Y and Z axis
- Variability intra-subject of the movement of the left shoulder in the X, Y and Z axis
- Variability inter-subject of the movement of the left shoulder in the X, Y and Z axis
- Position of the barycentre of the feet in the X, Y and Z axis
- Movement performed
- Speed of the movement

After training, we ended up with a precision of 83.05% for the test set and 84.47% for the validation set after 90 epochs but start over fitting right after. Details of the loss of the model can be seen in Figure 4.4a.

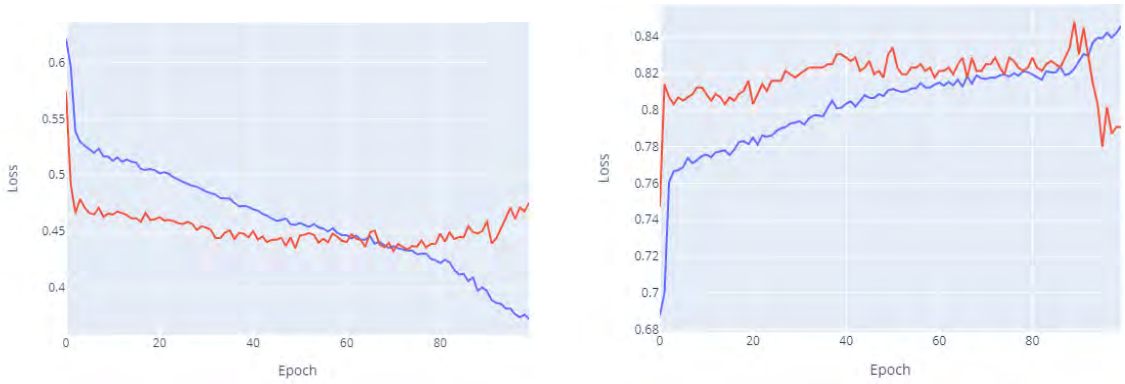

(a) Loss

(b) Accuracy

Figure 4.4: Biomechanical model performance. In blue, performance on the test set. In red, performance on the validation set.

The same model was trimmed down, and trained with only very basic information this time:

- Maximum amplitude of the left shoulder trajectory in the X, Y and Z axis
- Time to maximum amplitude of the left shoulder trajectory in the X, Y and Z axis
- Position of the barycentre of the feet in the X, Y and Z axis
- Movement performed
- Speed of the movement

After being trained for 398 epochs, the model reaches an accuracy of 88.29% on the test set and 88.45% on the validation set, before over fitting. Details about model accuracy and loss can be found, respectively, in Figure 4.5b and 4.5a.

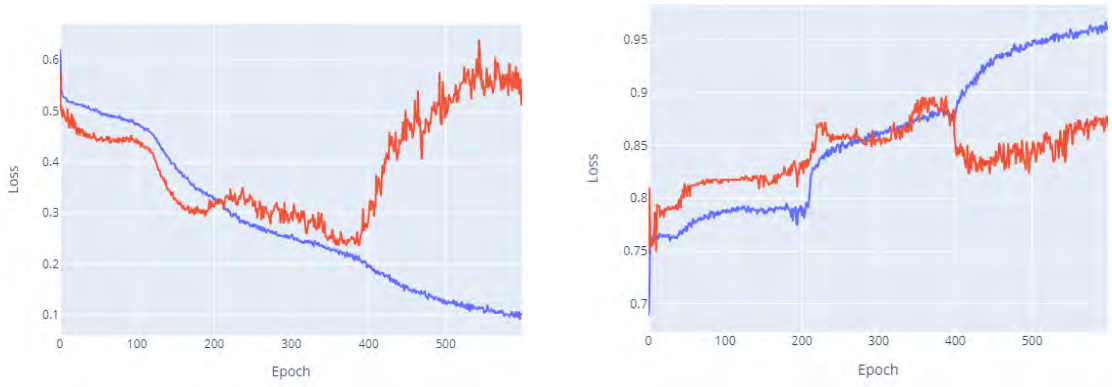

(a) Loss (b) Accuracy

Figure 4.5: Trimmed biomechanical model performance. In blue, performance on the test set. In red, performance on the validation set.

That same model was trained, anew, this time with the variable normalized by height of the subject. Indeed, as the shoulder displacement in space is correlated to the height of the subject, chances are that the height of subject is interfering with the relative displacement and tempering our results in a negative way. Normalizing by the height of the subject would allow us to focus on the actual relative movement of the subject in space, which we think would yield more accurate information and therefore better results. This time, after 194 epochs, we reached a maximum accuracy of 87.40% on the test set and 92.96% on the validation set, before the performance deteriorated before over fitting. Details about the training loss and accuracy can be found, respectively, in Figure 4.6a and 4.6b.

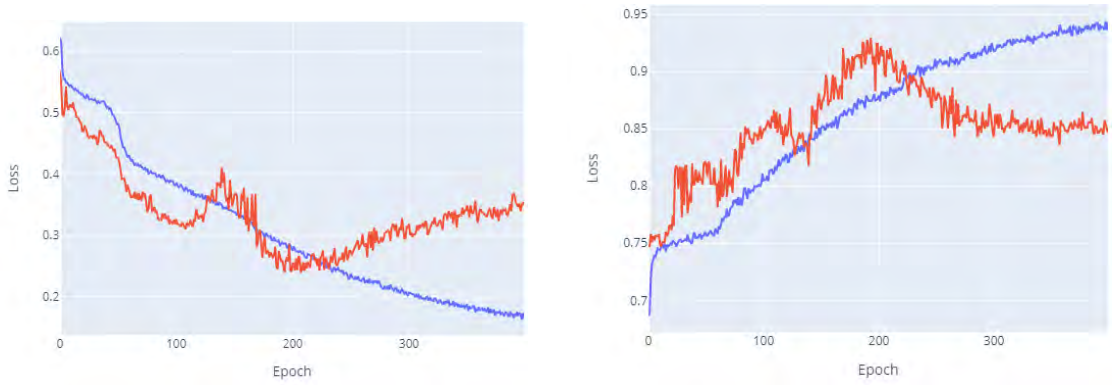

(a) Loss (b) Accuracy

Figure 4.6: Trimmed and normalized biomechanical model performance. In blue, performance on the test set. In red, performance on the validation set.

These results show us that we can gain a lot of information from just people's motion information. Indeed, while feeding the model with only limited and basic information about the movement of the subjects we still ended up with a categorization reaching very high accuracy score.

4.1.1.2.4 Neuromuscular model

This model was trained using all the variables related to the neuromuscular aspect of the subject:

- Centroid of the EMG activity of each of the 4 patches of electrodes
- Global centroid of the EMG activity of the 4 patches of electrodes
- EMG entropy of each of the 4 patches of electrodes
- Movement performed
- Speed of the movement

After being trained for 15 epochs, the model reaches a maximum accuracy of 83.27% on the test set and 88.07% on the validation set, before performance deteriorate, and then over fit. Details about model accuracy and loss can be found, respectively, in Figure 4.7b and 4.7a. Those results are relatively high, so we tried to go deeper by trimming down the model.

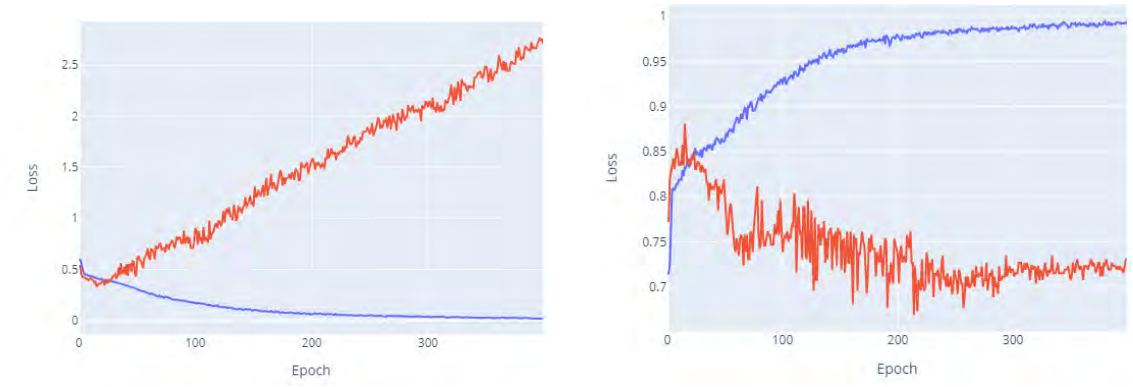

(a) Loss (b) Accuracy

Figure 4.7: Neuromuscular model performance. In blue, performance on the test set. In red, performance on the validation set.

A model accounting only for the entropy of the 4 patch was trained. This model reached a maximum accuracy of 76.21% on the test set and 87.30% on the validation set after 104 epochs, after which performance stays stable for around 80 epochs before performance degrade and over fit, indeed, clear signs of over fitting start to appear around 375 epochs. Details about model accuracy and loss can be found, respectively, in Figure 4.8b and 4.8a. Clear signs of over fitting start to appear around 375 epochs, as seen in the loss, Figure 4.8a and accuracy, Figure 4.8b training history.

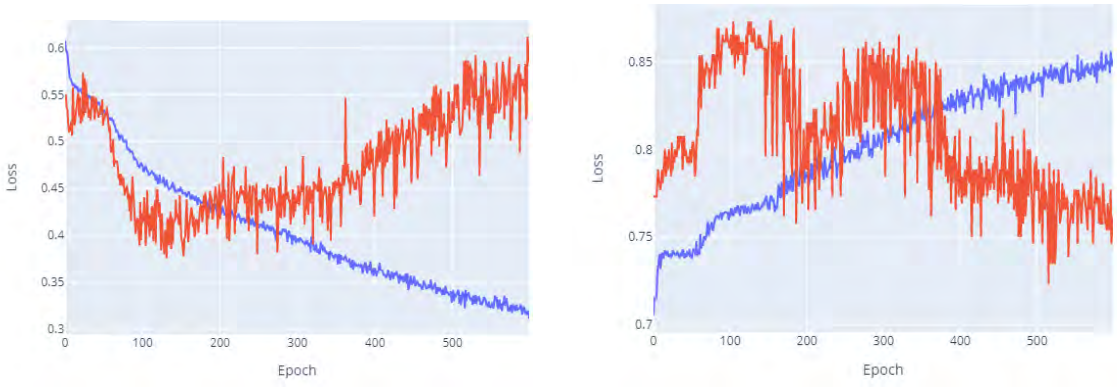

(a) Loss (b) Accuracy

Figure 4.8: Entropy neuromuscular model performance. In blue, performance on the test set. In red, performance on the validation set.

Another model accounting for the centroid of the 4 patches was trained. This model reached a maximum accuracy of 71.13% on the test set and 82.69% on the validation set in 285 epochs. Details about model accuracy and loss can be found. The valuable data seems to be the centroid of the EMG, or at least, less susceptible to the noise that couldn't be filtered out of the EMG. The behaviour of the loss seems relatively unexceptional. The behaviour of the accuracy can let us think of potential local minima trap, which will ponder our expectation concerning the extrapolation capacity of the model on other data set. Indeed, the accuracy starts off with a very high value and stays extremely stable, exhibiting a non-typical "stuck" like behaviour, but tends to lower quickly after more epochs. Details about model accuracy and loss can be found, respectively, in Figure 4.9b and 4.9a.

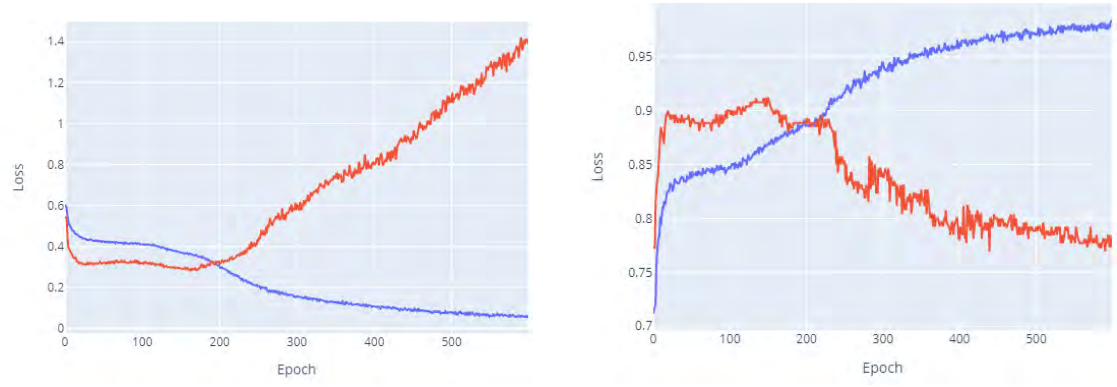

(a) Loss (b) Accuracy

Figure 4.9: Centroid neuromuscular model performance. In blue, performance on the test set. In red, performance on the validation set.

Those results show us that we can gain a lot of information just from people's basic neuromuscular information. Indeed, while feeding the model solely with limited and basic information about the neuromuscular control of the subjects, we still ended up with a categorization reaching a decent accuracy score, even if some over fitting issues started to show up. As this does not happen on the full neuromuscular data set, this might indicate that the variables, from the neuromuscular domain, that we used could be complementary, the variables being affected in synergy to each other by NSLBP.

Following this, we trained the CNN model using the pre-processed HD EMG data. The accuracy and loss of the model are found, respectively. The model reached a maximum accuracy of 100% on the test set in only a couple of epochs but only reached a low and unstable accuracy score. Details of the accuracy and loss of the model are found, respectively, in the Figure 4.10b and 4.10a.

A result to put in perspective to the lack of training sample. The fact that the model could learn to such a high accuracy on the test set is encouraging as it means that there is something to learn from in the data, but the low validation accuracy results remind us that we cannot infer if the pattern learned by the model is correlated to NSLBP or not.

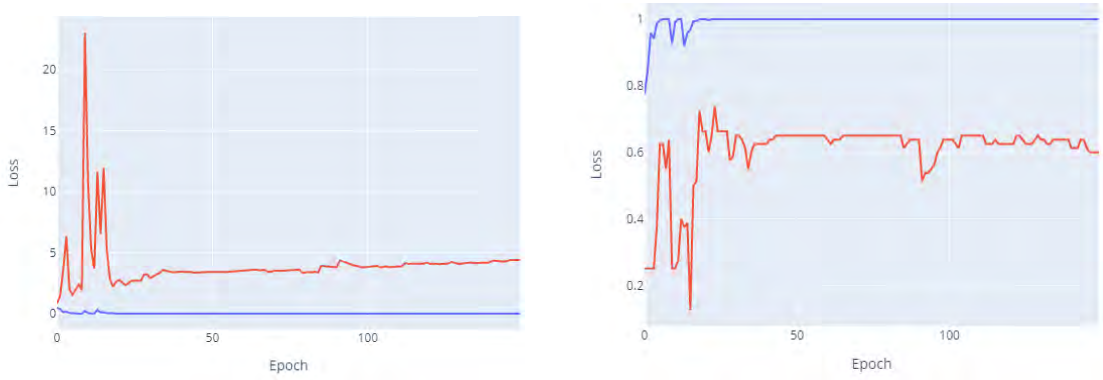

(a) Loss (b) Accuracy

Figure 4.10: HD EMG CNN model performance. In blue, performance on the test set. In red, performance on the validation set.

4.1.1.2.5 Balance model

This model used the variable related to the balance and proprioception of the subject:

- Area of the normalized statokinesigram
- GFR ratio
- Movement performed
- Speed of the movement

After being trained for 68 epochs, the model reached a maximum accuracy of 68.90% on the test set and 74.76% on the validation set, after which the model over fitted and performance deteriorated significantly. Details about model accuracy and loss can be found. The model shows the same "stuck" like behaviour on its accuracy metrics as the centroid model. This added to the over fitting behaviour acknowledged by the loss value, warning us not to draw strong conclusions from that model's results, which might be due to lack of sample and lucky local minima. Details about model accuracy and loss can be found, respectively, in Figure 4.11b and 4.11a.

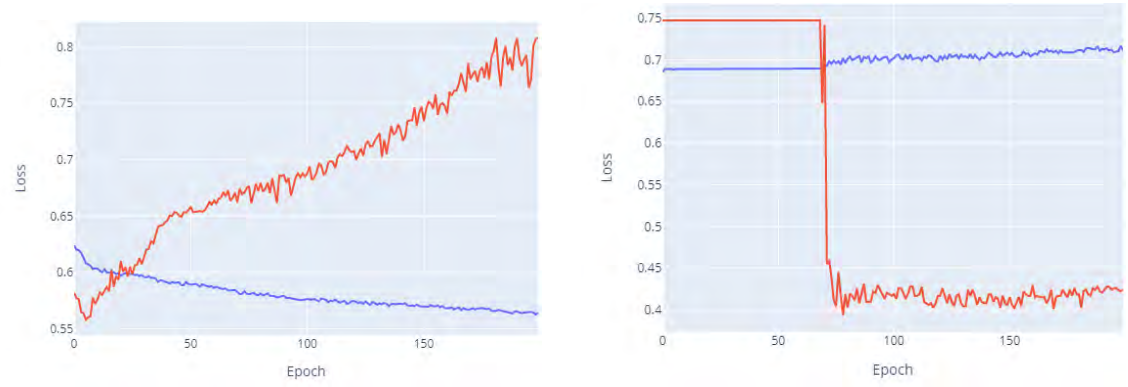

(a) Loss (b) Accuracy

Figure 4.11: Balance model performance. In blue, performance on the test set. In red, performance on the validation set.

4.1.1.3 Summary

The Table 4.3 summarizes the maximum performance of the DNN trained.

Model \ Accuracy (%)	Test	Validation	Epochs
Full model	99.88	93.30	100
Anthropometric	92.84	94.40	300
Trimmed	94.40	98.19	300
Biomechanical	83.05	84.47	90
Trimmed	88.29	88.45	398
Trimmed normalized	87.40	92.96	194
Neuromuscular	83.27	88.07	15
Entropy	76.21	87.30	104
Centroid	85.37	90.00	50
3D Convolutional Neural Network	100.00	73.75	23
Balance	68.90	74.73	68

Table 4.3: DNN maximum performance.

4.1.2 Factor analysis

4.1.2.1 Implementation

The variables used for the FA were the following:

- Age
- Group
  - Healthy
  - NSLBP
- Sex
  - Male
  - Female
- BMI
- Maximum amplitude of the left shoulder trajectory
- Time to maximum amplitude of the left shoulder trajectory
- Entropy of the movement of the left shoulder trajectory
- Variability inter-subject of the left shoulder trajectory
- Variability intra-subject of the left shoulder trajectory
- Entropy of the EMG of the right low back
- Entropy of the EMG of the left low back
- Y position of the total back EMG centroid
- GFR distribution ratio (for readability of the result this variable was sightly changed, the GFR used for the FA is: $GFR_{FA} = |GFR| - 1$. This is done in order to have a balanced ratio on zero and changes are not side oriented, making results easier to read and to compare)

For the variables related to the left shoulder movement, only one axis was chosen in order to limit the number of variables used as to meet the factor analysis requirements for optimal behavior. The axis was chosen in regards to the movement performed, the axis where the most movement was happening being selected, as to stay as relevant as possible:

- Y axis for
  - Back extension Maximum and Preferred speed
  - Trunk rotation Left and Right, Maximum and Preferred speed
- Z axis for
  - Back flexion Maximum and Preferred speed
  - Lateral flexion Left and Right, Maximum and Preferred speed

If no factor was loading the Group component using the major axis of movement, secondary axes were used to run the factor analysis to assess if any factor would load the Group component this time. Indeed, we are making the assumption that the axis that see the most displacement is the one yielding the most information, but this might be a wrong assumption in some or all the case. So, if the axis showing the

largest displacement doesn't yield significant results, we will resort to the analysis of the secondary axis to assess for any valuable results.

For the rotation movements, the maximum angle on the Z axis and the time to maximum angle on the Z axis has been used instead of the maximum amplitude and time to maximum amplitude of the trajectory.

We used as little variable as could be, while still trying to tackle most of the aspect of the LBP symptom, in order to match factor analysis requirements. Optimally, FA are done on samples with a size of at least 100 occurrences, with a ratio of 20:1 subject per variables, but we were not able to meet these requirements, and therefore had to compromise. Only one axes was selected for every FA done, in order to limit the number of dimensions fed to the FA. The number of dimensions were limited, and only a couple of variables for each of the domain was kept. The number of components was selected via the function `nScree()` from the R package `nFactors`. The number of components being the rounded mean result of the different tests ran by the `nScree()` function:

- Eigenvalues
- Parallel Analysis
- Optimal Coordinates
- Acceleration Factor

In our analysis, the following categorical values have been simplified the following way:

- Group
  - Healthy: 0
  - NSLBP: 1
- Sex
  - Male: 0
  - Female: 1

The critical value of the correlation values was assessed using a Student's t-test (Soper et al. 1917; Barton 1976). With our sample size of 46, the critical values for the correlation are as follow:

- $p = 0.05 : c = 0.29$
- $p = 0.01 : c = 0.38$
- $p = 0.005 : c = 0.41$
- $p = 0.001 : c = 0.47$

4.1.2.2 Results R-type Analysis

4.1.2.2.1 Back extension Maximum

	Components			
Factors	3	1	4	2
Group			.370	
Age	.373	.783	.280	-.406
BMI	.477	.197	.196	
EMG centroid Y pos.		-.182	.338	
EMG entropy l. low back			.116	.376
EMG entropy r. low back		-.110		.284
GFR ratio	-.175			.466
Max. ROM, Y axis	-.145	.563	-.192	.788
Sex		-.476		
Time to max. ROM, Y axis	-.107	.296	.786	
Traj. entropy, Y axis	.192	-.251	-.645	
Traj. inter-var., Y axis	.957		-.102	
Traj. intra-var., Y axis	.584	-.347	-.151	-.287

Table 4.4: Back extension maximum factor analysis results, Y axis.

As shown in Table 4.4, using the Z axis as the axis of interest, the Group factor is the component 4 that load group at 0.370 ($p < 0.05$). The associated loadings with it are:

- Time to maximum amplitude of the left shoulder trajectory: 0.786 ($p < 0.001$)
- Entropy of the movement of the left shoulder trajectory: -0.645 ($p < 0.001$)
- Y position of the total back EMG centroid: 0.338 ($p < 0.05$)

Age is also close to being significant with a loading of 0.280 ($p > 0.05$). It seems that NSLBP move at a slower rate than their healthy counterpart, while having a movement which is less "noisy" movement. The latter could be interpreted either as a more efficient movement, or a more rigid movement. We will make the choice to interpret it as a more rigid movement due to the behaviour of the subjects afflicted by the symptom, which was much more cautious (Asgari et al. 2015;Madeleine 2010;J. H. van Dieën, Flor, and Hodges 2017). An interpretation corroborated by the longer time to complete the movement. This could also potentially be, in part, due to a lack of adaptability to the movement conditions. We can see that the EMG activity is distributed more cranially among NSLBP, just as seen by Sanderson and collaborator (Sanderson et al. 2019) during other task.

We can note the presence of large loading of age in the first factor, and significant loading of age in the other factor, which could indicate that age is of tremendous impact on the movement itself (Kienbacher et al. 2015;Kienbacher et al. 2016).

4.1.2.2.2 Back extension Preferred

	Components				
Factors	2	4	5	1	3
Group	.292		.112		
Age	.381	.282	-.351	.223	-.113
BMI	.183	.351		.310	.167
EMG centroid Y pos.			.244	.963	
EMG entropy l. low back				-.481	.149
EMG entropy r. low back	.138			-.198	.968
GFR ratio		-.400			
Max. ROM, Y axis		-.172	-.411		.246
Sex		-.112	.869	.111	.157
Time to max. ROM, Y axis	.958		-.252	-.104	
Traj. entropy, Y axis	-.736		.545		-.180
Traj. inter-var., Y axis	.104	.775			
Traj. intra-var., Y axis	-.194	.840	.270	-.187	-.128

Table 4.5: Back extension preferred factor analysis results, Y axis.

As shown in Table 4.5, using the Z axis as the axis of interest, the Group factor is the component 2 that load group at 0.292 ($p < 0.05$). The associated loadings associated with it are:

- Age: 0.381 ($p < 0.01$)
- Time to maximum amplitude of the left shoulder trajectory: 0.958 ($p < 0.001$)
- Entropy of the movement of the left shoulder trajectory: -0.736 ($p < 0.001$)
- Y position of the total back EMG centroid: 0.338 ($p < 0.01$)

We can draw the same conclusion than when the movement is performed at maximum speed, to the difference that age seems have even more correlated to the NSLBP component.

As the NSLBP factor is not loaded significantly, FA were run on the Y or X axis, but with no better results. Therefore, they were not dwell upon in this article.

4.1.2.2.3 Back flexion Maximum

Factors	Components 1	2	3
Group		.237	
Age	.977	.158	.127
BMI	.379		.124
EMG centroid Y pos.			.399
EMG entropy r. low back			.319
EMG entropy l. low back		.159	.538
GFR ratio	-.366	.131	
Max. ROM, X axis	-.118	.582	
Sex	-.355		
Time to max. ROM, Z axis	.186	.440	.579
Traj. entropy, Z axis	-.107		-.741
Traj. inter-var., Z axis	.398	-.324	
Traj. intra-var., Z axis	.375	-.923	

Table 4.6: Back flexion maximum factor analysis results, Z axis.

As shown in Table 4.6, using the Z axis the as axis of interest, the component 2 load Group at a non-significant level: 0.237 ($p > 0.05$), with the associated significant loadings:

- Maximum amplitude of the left shoulder trajectory: 0.582 ($p < 0.001$)
- Time to maximum amplitude of the left shoulder trajectory: 0.440 ($p < 0.005$)
- Variability inter-subject of the left shoulder trajectory: -0.324 ($p < 0.05$)
- Variability intra-subject of the left shoulder trajectory: -0.923 ($p < 0.001$)

These loadings seem to attest of the different movements strategy between Healthy and NSLBP subjects. While having a greater range of motion, the NSLBP subjects take longer to get there. Of course, the inter-subject component loading is a direct expression of the different movement strategy between healthy and NSLBP. At the same time, significant loading is seen on the intra-subject variability meaning that NSLBP do not adapt their movement much in regard to new starting conditions (Asgari et al. 2015). Nonetheless, the loading being non-significant for the Group component, those results are not to be taken as face value just as the associated discussion.

Factor analysis were run on the Y and X axis but did not yield any significant loading on the Group component and have therefore not been added here.

4.1.2.2.4 Back flexion Preferred

Factors	Components					
	1	3	2	6	4	5
Group		-.108	.986			
Age			.148	-.731	.211	.251
BMI		-.117	.240		.917	.253
EMG centroid Y pos.		-.357	.186	.153	.158	.228
EMG entropy l. low back		.986		.119		
EMG entropy r. low back		.224		.348	.201	
GFR ratio	.203		-.230	.361		
Max. ROM, Z axis	.975					.151
Sex				.390		
Time to max. ROM, Z axis			.270	-.142	.132	
Traj. entropy, Z axis		-.228		.389	-.209	.123
Traj. inter-var., Z axis				-.117	.108	.458
Traj. intra-var., Z axis	-.917			-.175		.349

Table 4.7: Back flexion preferred factor analysis results, Z axis.

As shown in Table 4.7, using the Z axis as axis of interest, the component 2 load Group at a significant level: 0.986 ($p < 0.001$). But no other loading are significantly loading on this component. We find age (0.148; $p > 0.05$), BMI (0.240; $p > 0.05$), time to maximum amplitude (0.270; $p > 0.05$), the position of the EMG centroid of activity on the Y axis (0.186; $p > 0.05$) and the GFR ratio (-0.230; $p > 0.05$), all loading at low and on significant level. A new factor analysis was run, this time using the Y axis as the axis of interest.

Factors	Components					
	5	6	1	2	4	3
Group	.143	.520	-.110		-.134	
Age	.776				-.199	-.151
BMI	.508	.405		-.166	.116	
GFR ratio	-.367		-.193			
Max. ROM, Y axis			-.110	.982		.106
EMG entropy l. low back		-.420			-.138	.888
EMG entropy r. low back	-.120	.143		.107	.159	.359
Sex	-.262	.103		-.207	.568	.149
Time to max. ROM, Y axis		.178	-.126	-.178		.238
Traj. entropy, Y axis	-.450	.553	.167		.167	
Traj. inter-var., Y axis	.275		.946	-.106		
Traj. intra-var., Y axis	.123		.465	.348	.786	-.140
EMG centroid Y pos.		.538				-.131

Table 4.8: Back flexion preferred factor analysis results, Y axis.

As shown in Table 4.8, using the Y axis as the axis of interest, the component 6 load Group at a significant level: 0.520 ($p < 0.001$), with the associated significant loadings:

- BMI: 0.405 ($p < 0.01$)
- Entropy of the movement of the left shoulder trajectory: 0.553 ($p < 0.001$)
- Entropy of the EMG of the left low back: -0.420 ($p < 0.005$)
- Y position of the total back EMG centroid: 0.538 ($p < 0.001$)

BMI seems to have a great influence on the component for this movement. A result which is not extremely surprising, as the NSLBP population tend to be associated with a higher BMI mean than their healthy counterpart (Koley et al. 2010;Uccar et al. 2021). Like the back extension movements, entropy of the movement of the left shoulder trajectory seems to indicate that the movement produced by the NSLBP people is correlated to a movement that is more rigid, with less fine-tuned adaptations. The entropy of the EMG of the left low back seems to indicate a muscle activity that is less localized, noisier. This is associated with a value of the general centroid position in Y that indicate a higher activation of the upper portion of the low back, something shown in other work (Sanderson et al. 2019). Surprisingly, the maximum amplitude variable is not loading on the Group component. A surprising finding regarding the literature.

4.1.2.2.5 Lateral flexion Left Maximum

	Components			
Factors	1	3	4	2
Group	.387			
Age	.157	.915	.257	-.260
BMI	.263	.378		
EMG centroid Y pos.	.169		.126	-.177
EMG entropy l. low back		.117	.401	
EMG entropy r. low back		-.101		.119
GFR ratio	-.481		-.249	
Max. ROM, X axis			.106	.985
Sex	.176	-.413		
Time to max. ROM, Z axis	.504		.654	
Traj. entropy, Z axis			-.772	
Traj. inter-var., Z axis	.872	.165		.452
Traj. intra-var., Z axis	.299	.452	-.148	-.204

Table 4.9: Lateral flexion left maximum factor analysis results, Z axis.

As shown in Table 4.9, using the Z axis the as axis of interest, the component 2 load Group at a significant level: 0.387 ($p < 0.01$), with the associated significant loadings:

- Time to maximum amplitude of the left shoulder trajectory: 0.504 ($p < 0.001$)
- Variation inter-subject of the left shoulder trajectory: 0.872 ($p < 0.001$)
- Variation intra-subject of the left shoulder trajectory: 0.299 ($p < 0.05$)
- GFR distribution ratio: -0.481 ($p < 0.001$)

These loadings can be interpreted as NSLBP subjects producing movements significantly different than their healthy counterpart. In addition, NSLBP subjects seems to distribute more equally their weight between each foot (Bourigua 2014). This could be seen as a lack of adaptation to the movement, limiting their performance, in order to maximize an instantaneous feeling of safety and control, for example by not working with the momentum of the movement. They also have a higher variation between repetition's trajectories, something that seems to go against the findings in other movements. Nonetheless, this does not go against the literature, which report a lot of variability intra-subject in the NSLBP population (Cholewicki et al. 2019). It could be hypothesized that the adaptations to NSLBP does not affects movements the same way, as the different results per movement in our analysis seems to indicate.

Again, the time to maximum amplitude seems significantly higher in people with NSLBP than their healthy counterpart.

4.1.2.2.6 Lateral flexion Left Preferred

	Components		
Factors	3	1	2
Group	.273		
Age	.856		
BMI	.447	-.123	.588
EMG centroid Y pos.	.198		.453
EMG entropy l. low back			.303
EMG entropy r. low back	-.237	.109	.904
GFR ratio	-.558	-.259	
Max. ROM, X axis	-.187	.534	
Sex	-.332		.200
Time to max. ROM, Z axis	.465	.780	
Traj. entropy, Z axis	-.411	-.745	-.170
Traj. inter-var., Z axis	.473	.422	
Traj. intra-var., Z axis	.525		.142

Table 4.10: Lateral flexion left preferred factor analysis results, Z axis.

As shown in Table 4.10, using the Z axis the as axis of interest, the component 3 load Group at a non-significant level: 0.273 ($p > 0.05$), with the associated significant loadings:

- Age: 0.856 ($p < 0.001$)
- Sex: -0.332 ($p < 0.01$)
- BMI: 0.447 ($p < 0.005$)
- Time to maximum amplitude of the left shoulder trajectory: 0.465 ($p < 0.005$)
- Entropy of the movement of the left shoulder trajectory: -0.411 ($p < 0.005$)
- Variation inter-subject of the left shoulder trajectory: 0.473 ($p < 0.001$)
- Variation intra-subject of the left shoulder trajectory: 0.525 ($p < 0.001$)
- GFR distribution ratio: -0.558 ($p < 0.001$)

The loading for the variable group is not significant, so no strong conclusions can be drawn from those results. A new factor analysis was run, but this time using the Y axis as the axis of interest.

Factors	Components 3	2	4	1
Group	.368		.154	
Age	.716			.109
BMI	.395	.574	.273	.194
EMG centroid Y pos.	.111	.418	.176	
EMG entropy l. low back		.290	-.147	
EMG entropy r. low back	-.218	.958	-.172	
GFR ratio	-.622		.166	
Max. ROM, Y axis			-.734	.205
Sex	-.403	.190		.164
Time to max. ROM, Y axis	.622	.111	-.299	
Traj. entropy, Y axis	-.380		.743	
Traj. inter-var., Y axis	.618			.546
Traj. intra-var., Y axis			-.230	.969

Table 4.11: Lateral flexion left preferred factor analysis results, Y axis.

As shown in Table 4.11, using the Y axis the as axis of interest, the component 3 load group at a significant level: 0.368 ($p < 0.05$), with the associated significant loadings:

- Age: 0.716 ($p < 0.001$)
- Sex: -0.403 ($p < 0.01$)
- BMI: 0.395 ($p < 0.01$)
- Time to maximum amplitude of the left shoulder trajectory: 0.622 ($p < 0.001$)
- Entropy of the movement of the left shoulder trajectory: -0.380 ($p < 0.01$)
- Variation inter-subject of the left shoulder trajectory: 0.618 ($p < 0.001$)
- GFR distribution ratio: -0.622 ($p < 0.001$)

We can see that NSLBP tend to perform their movement at a slower path, and more rigidly. This, while their movements trajectory tend to be different from their healthy counterpart. To be noted here, that like for the Lateral flexion Left Maximum, a higher variation between repetitions in NSLBP is to be seen. Again NSLBP people tend to be correlated with a more balanced distribution of the GFR. One interesting thing to note is the massive importance of the anthropometric variables on this movement: age, 0.856 ($p < 0.001$), sex, -0.332 ($p < 0.05$), and BMI, 0.447 ($p < 0.005$). This let us believe that anthropometric variable has a great impact on this movement, but also that male subjects or with higher BMI, or older, or a combination of this, tend to express more dramatically the adaptations from NSLBP compared to others.

4.1.2.2.7 Lateral flexion Right Maximum

Factors	Components 2	1	4	3
Group				.221
Age		.200	.483	.326
BMI	.354	.410		.199
EMG centroid Y pos.	.112	.786		.429
EMG entropy l. low back	-.251	.930	.220	-.138
EMG entropy r. low back	.200			-.585
GFR ratio	-.531		.252	
Max. ROM, X axis		-.107	.512	
Sex			-.489	
Time to max. ROM, Z axis	-.382	.252		.614
Traj. entropy, Z axis	-.119	-.170	-.785	-.418
Traj. inter-var., Z axis	.922		.154	-.162
Traj. intra-var., Z axis	.694		.350	

Table 4.12: Lateral flexion right maximum factor analysis results, Z axis.

As shown in Table 4.12, using the Z axis as axis of interest, the component 3 load Group at a non-significant level: 0.221 ($p > 0.05$), with the associated significant loadings:

- Age: 0.326 ($p < 0.05$)
- Time to maximum amplitude of the left shoulder trajectory: 0.614 ($p < 0.001$)
- Entropy of the movement of the left shoulder trajectory: -0.418 ($p < 0.005$)
- Entropy of the EMG of the right low back: -0.585 ($p < 0.001$)
- Y position of the total back EMG centroid: 0.429 ($p < 0.005$)

The loading for the variable Group is not significant, so no strong conclusions can be drawn from those results. A new factor analysis was run, this time using the Y or X axis as the axis of interest, but no component loaded the Group variable. Strangely, this problem did not arise when the same movement was performed at the same speed but to the other side. Nonetheless, we can see that the factors loading on the non-significant NSLBP component are still similar to results from other movements, but as the loading on the Group factor is never significant for any of the component we did not dwell upon those results.

4.1.2.2.8 Lateral flexion Right Preferred

Factors	Components 2	1	3
Group	.111		.154
Age	.656	-.143	
BMI	.200	.169	.284
EMG centroid Y pos.		-.450	
EMG entropy l. low back		.997	
EMG entropy r. low back		.642	.139
GFR ratio		-.126	-.484
Max. ROM, X axis	.622		.245
Sex	-.599	-.148	
Time to max. ROM, Z axis	.464	.140	-.404
Traj. entropy, Z axis	-.899		-.177
Traj. inter-var., Z axis		-.112	.917
Traj. intra-var., Z axis	.363	-.104	.508

Table 4.13: Lateral flexion right preferred factor analysis results, Z axis.

As shown in Table 4.13, using the Z axis as axis of interest, no component really load the Group variable. Component 2, 0.111 ($p > 0.05$) and 3, 0.154 ($p > 0.05$), do but at very low level. Due to the non-significant value of the correlation with the group variable, no conclusion can be drawn, and therefore, a new factor analysis was run, this time using the Y axis as the axis of interest.

Factors	Components 2	1	4	3
Group		.161	.281	
Age	-.220		.786	-.228
BMI	.140	.116	.464	
EMG centroid Y pos.		.196		-.519
EMG entropy l. low back		.214	.133	.965
EMG entropy r. low back	.136	.398		.573
GFR ratio	-.476	-.475	-.148	
Max. ROM, Y axis		.622	-.247	
Sex		.149	-.493	-.128
Time to max. ROM, Y axis	-.718	.214	.397	
Traj. entropy, Y axis	.254	-.930	-.253	
Traj. inter-var., Y axis	.861	-.166	.460	-.119
Traj. intra-var., Y axis	.795			

Table 4.14: Lateral flexion right preferred factor analysis results, Y axis.

As shown in Table 4.14, using the Y axis the as axis of interest, the component 4 load Group at a non-significant level: 0.281 ($p > 0.05$), with the associated significant loadings:

- Age: 0.786 ($p < 0.001$)
- Sex: -0.493 ($p < 0.001$)
- BMI: 0.464 ($p < 0.005$)
- Time to maximum amplitude of the left shoulder trajectory: 0.397 ($p < 0.01$)
- Variation inter-subject of the left shoulder trajectory: 0.460 ($p < 0.005$)

As no component loaded Group at a significant level, a new factor analysis was run, this time using the X axis as the axis of interest.

Factors	Components 1	2	4	3
Group	.135		.308	-.189
Age	.405	-.213	.442	
BMI		.145	.818	
EMG centroid Y pos.		-.468	.387	
EMG entropy l. low back	.133	.987		
EMG entropy r. low back		.634	.132	
GFR ratio		-.142	-.357	.321
Max. ROM, X axis	.348		-.220	.908
Sex	-.188	-.130		-.131
Time to max. ROM, X axis	.989			
Traj. inter-var., X axis	.378		-.214	
Traj. entropy, X axis	-.840	-.145	-.266	-.208
Traj. intra-var., X axis				.558

Table 4.15: Lateral flexion right preferred factor analysis results, X axis.

As shown in Table 4.15, using the X axis the as axis of interest, the component 4 loaded Group at a significant level: 0.308 ($p < 0.05$), with the associated significant loadings:

- Age: 0.442 ($p < 0.005$)
- BMI: 0.818 ($p < 0.001$)
- Y position of the total back EMG centroid: 0.387 ($p < 0.01$)
- GFR distribution ratio: -0.357 ($p < 0.05$)

We can see that mainly, it is the anthropometric variables that load on the NSLBP component. We again see that NSLBP people tend to be correlated with a more balanced distribution of the GFR, and that the muscle activity seems to be distributed more cranially.

4.1.2.2.9 Trunk rotation Left Maximum

Factors	Components 1	4	2	3	5
Group					.531
Age		.196	-.346	-.118	.319
Time to max. Angle, Z axis	-.332	.879	-.101		.229
Max. Angle, Z axis	-.346		-.204	.890	-.177
BMI	.249			-.102	.547
EMG centroid Y pos.		.262	.149	.181	.159
EMG entropy l. low back				.537	
EMG entropy r. low back	.369	-.209		.192	
GFR ratio	-.282		.240		-.300
Sex			.992		
Traj. entropy, Y axis		-.710	.101	.191	
Traj. inter-var., Y axis	.881		-.230	-.197	.356
Traj. intra-var., Y axis	.736		.148	-.105	-.123

Table 4.16: Trunk rotation left maximum factor analysis results, Y axis.

As shown in Table 4.16, using the Z axis the as axis of interest, the component 5 load Group at a significant level: 0.531 ($p < 0.001$), with the associated significant loadings:

- Age: 0.319 ($p < 0.05$)
- Maximum angle displacement on the Z axis for the left shoulder: 0.547 ($p < 0.001$)
- Variation inter-subject of the left shoulder trajectory: 0.356 ($p < 0.05$)
- GFR distribution ratio: -0.300 ($p < 0.05$)

Age seems to be a significant factor, which is not surprising at this point. Here a counter intuitive result comes up: the NSLBP group seems to be associated with an overall greater maximum angle of rotation than their healthy counterpart. As excepted, NSLBP subjects are associated with a different movement trajectory than the healthy subjects. We also see that they tend to distribute their weight more evenly between foot than the healthy population.

4.1.2.2.10 Trunk rotation Left Preferred

Factors	Components 1	2	5	3	4
Group			.266	-.378	
Age		-.291	.543		
Time to max. Angle, Z axis	-.229	-.708	.190		.193
Max. Angle, Z axis	-.465	.386	-.150	.222	.747
BMI	.259		.715	-.176	
EMG centroid Y pos.			.421		-.160
EMG entropy l. low back		-.214	-.115		.490
EMG entropy r. low back	.329	.163		-.265	
GFR ratio	-.242	.152	.149	.943	
Sex	.202	.151	-.163	.189	-.352
Traj. entropy, Y axis		.993			
Traj. inter-var., Y axis	.752		.305	-.212	-.182
Traj. intra-var., Y axis	.946	.122	-.231	.131	-.121

Table 4.17: Trunk rotation left preferred factor analysis results, Y axis.

As shown in Table 4.17, using the Z axis the as axis of interest, the component 3 load group at a significant level: -0.378 ($p < 0.05$), with the associated significant loadings:

- GFR distribution ratio: 0.943 ($p < 0.001$)

Here the only variable that load on the GFR distribution ratio, stating that healthy population seems to have an extremely uneven weight distribution between their feet.

The main peculiarity here, is that we have a second component loading the Group factor, close to a significant level, toward NSLBP rather than Healthy, like on component 3. We have therefore a “Healthy" component and a “NSLBP" component in the same movement analysis, which is quite interesting. For the curious reader, this NSLBP component load Age at 0.543 ($p < 0.001$) and a BMI at 0.715 ($p < 0.001$), which testifying again of the strong relation between the anthropometric variables and the NSLBP symptom. The trajectory of the movement produced by NSLBP is significantly different than the ones from the Healthy, with a loading of 0.305 ($p < 0.05$) of the inter-movement variablity factor. In addition, the centroid of the EMG activity seems to be more cranial for the NSLBP, with a loading of 0.421 ($p < 0.005$). Interestingly the “Healhty” component doesn’t load significantly on anthropometric data, in stark contrast with the NSLBP components found in the

other movements. Nonetheless, as the loading on the NSLBP componenent, does not reach significant level, no hard conclusion can be drawn.

4.1.2.2.11 Trunk rotation Right Maximum

	Components		
Factors	3	2	1
Group	.109	-.217	.138
Age	.455	-.390	
Time to max. Angle, Z axis		-.950	
Max. Angle, Z axis	-.413	.308	.272
BMI	.523	-.101	.249
EMG centroid Y pos.	.315	-.244	.281
EMG entropy r. low back		.519	.196
EMG entropy l. low back			.993
GFR ratio	-.390	.108	
Sex		.116	-.120
Traj. entropy, Y axis		.680	
Traj. inter-var., Y axis	.918	.131	.160
Traj. intra-var., Y axis	.693	.111	-.120

Table 4.18: Trunk rotation right maximum factor analysis results, Y axis.

As shown in Table 4.18, using the Z axis the as axis of interest, the component 2 load Group at a non-significant level: -0.217 ($p > 0.05$), with the associated significant loadings:

- Age: -0.390 ($p < 0.01$)
- Maximum angle displacement on the Z axis for the left shoulder: 0.308 ($p < 0.05$)
- Time to maximum angle displacement on the Z axis for the left shoulder: -0.950 ($p < 0.001$)
- Entropy of the movement of the left shoulder trajectory: 0.680 ($p < 0.001$)
- Entropy of the EMG of the right low back: 0.519 ($p < 0.001$)

Unusually, the component loading the Group factor does so toward the Healthy state. The healthy population is associated with a bigger amplitude of movement as well as a much faster movement speed. The higher entropy of the movement trajectory seems to testify of a movement that present more micro adaptations, which could be interpreted as a higher live correction of the movement (Asgari et al. 2015).

The higher EMG entropy associated to the component, seems to indicate a more diffuse muscular activity of the low back region (Sanderson et al. 2019). Unlike when performing the movement at maximum speed, the component is associated with lower average age this time. An interesting thing to point out, is that the component 1 and 3 also load the Group factor toward NSLBP, albeit to a non-significant level. Nonetheless, as the loading of the Group variable on the components is not significant, no conclusions can be drawn from those results. A new factor analysis was run, this time using the Y axis as the axis of interest.

	Components	
Factors	2	1
Group	.321	
Age	.532	.154
Time to max. Angle, Z axis	.746	
Max. Angle, Z axis	.117	.523
BMI	.349	.302
EMG centroid Y pos.	.405	
EMG entropy l. low back		.363
EMG entropy r. low back	-.597	.799
GFR ratio	-.200	
Sex	-.194	
Traj. entropy, X axis	-.594	-.223
Traj. inter-var., X axis		
Traj. intra-var., X axis	-.424	

Table 4.19: Trunk rotation right maximum factor analysis results, X axis.

As shown in Table 4.19, using the Y axis the as axis of interest, the component 1 load Group at a significant level: 0.321 ($p < 0.05$), with the associated significant loadings:

- Age: 0.532 ($p < 0.001$)
- BMI: 0.349 ($p < 0.05$)
- Time to maximum amplitude of the left shoulder trajectory: 0.746 ($p < 0.001$)
- Entropy of the movement of the left shoulder trajectory: -0.594 ($p < 0.001$)
- Variation intra-subject of the left shoulder trajectory: -0.424 ($p < 0.005$)
- Y position of the total back EMG centroid: 0.405 ($p < 0.01$)
- Entropy of the EMG of the right low back: -0.597 ($p < 0.001$)

From the factor's loadings, NSLBP subjecst seem to be associated with a slower movement, as the very high loading of the time to maximum amplitude of the left shoulder trajectory indicate, a lower entropy of the left shoulder trajectory, which could be due to a more rigid movement with less micro adjustments from the NSLBP subject. Interestingly NSLBP seems to be associated here, with a lower entropy of the EMG signal in this movement, which could indicate a muscular activation that is more localized than in healthy participant. At the same time, the variability intra-subject seems to be lower in NSLBP, possibly testifying of a lack of adaptation capability between repetitions. The NSLBP component is associated with higher BMI and older age.

4.1.2.2.12 Trunk rotation Right Preferred

	Components			
Factors	1	3	4	2
Group			.387	.190
Age	-.557	-.114	.494	
Time to max. Angle, Z axis	-.829			
Max. Angle, Z axis	-.137	-.419	-.345	.310
BMI	-.145	.188	.587	
EMG centroid Y pos.	.102		.412	-.135
EMG entropy l. low back		-.101		.986
EMG entropy r. low back	.171	.227		
GFR ratio	.226	-.189	-.218	.147
Sex	.408	.344		.122
Traj. entropy, Y axis	.984		.132	
Traj. inter-var., Y axis	-.199	.844	.373	-.121
Traj. intra-var., Y axis		.804	.101	-.128

Table 4.20: Trunk rotation right preferred factor analysis results, Y axis.

As shown in Table 4.20, using the Y axis the as axis of interest, the component 3 load Group at a significant level: 0.387 ($p < 0.01$), with the associated significant loadings:

- Age: 0.494 ($p < 0.001$)
- Maximum angle displacement on the Z axis for the left shoulder: 0.587 ($p < 0.001$)
- Time to maximum angle displacement on the Z axis for the left shoulder: -0.345 ($p < 0.05$)

- Variation inter-subject of the left shoulder trajectory: 0.373 ($p < 0.05$)
- Y position of the total back EMG centroid: 0.412 ($p < 0.005$)

Aside from the age variable loading, we see that NSLBP people tend to showcase larger amplitude of movement and faster speed of execution. The higher speed of execution and larger amplitude are a bit counter-intuitive. Maybe this could be a way to alleviate discomfort by performing the movement faster in order to be done with it. The larger amplitude being a side effect of the momentum created by the increased speed, which would be more difficult for NSLBP subjects to control without compromising on their feeling of spine integrity or pain level. Nontheless, this is still counter-intuitive looking back to the results from the same movement performed at maximum speed. In addition, a higher difference of the movement trajectory compared to their healthy counterpart. Also, the muscle activity is more cranially distributed.

4.1.2.3 Summary

The Table 4.21 summarize the results from the DNN training for the movements at preferred and maximum speed.

Movements \ Factors	Group	Age	BMI	Sex	max. ROM	Time to max. ROM	Traj. entropy	Traj. intra-var.	Traj. inter-var.	EMG centroid Y pos.	EMG entropy l. low back	EMG entropy r. low back	GFR ratio
Preferred speed													
Back ext.	.292*	.381**				.958‡	-.736‡			.338*			
Back flex.	.520‡		.405**				.553‡			.538‡	-.420†		
Lat. trunk flex. l.	.368*	.716‡	.395**	-.403**		.622‡	-.380**		.618‡				-.622‡
Lat. trunk flex. r.	.308*	.442†	.818‡							.387**			-.357*
Trunk rot. left	-.378*												.943‡
Trunk rot. right	.387**	.494			.587‡	-.345*			.373*	.412†			
Maximum speed													
Back ext.	.370*					.786‡	-.645‡			.338*			
Back flex.	.237				.582‡	.440†		-.923‡	-.324*				
Lat. trunk flex. l.	.387**					.504‡		.299*	.872				-.481‡
Lat. trunk flex. r.	.221	.326*				.614‡	-.418†			.429†		-.585‡	
Trunk rot. left	.531‡	.319*			.547‡				.356*				-.300*
Trunk rot. right	.321*	.532‡	.349*			.746‡	-.594‡	-.424†		.405†		-.597‡	

Table 4.21: Factor analysis results. *: $p < 0.05$. **: $p < 0.01$. †: $p < 0.005$. ‡: $p < 0.001$.

4.1.3 Exploratory analysis conclusion

Using the DNN, it was shown that the variables chosen yielded a substantial amount of information about the status of the subject, healthy or NSLBP. The subdivision into domains showed that information was not constrained to some domains only, but was distributed across them. It is to be noted that the information power was equally distributed, aside from the force plate data. In the context of clustering the NSLBP population, those results align with the consensus of looking at the NSLBP symptom as a multi factorial problem, and therefore, the clustering solution should itself rely on data that reliably represents the 5 main domains driving the NSLBP prognosis (Maher, Underwood, and Buchbinder 2017;Hartvigsen et al. 2018).

It is to be mentioned that, whilst most of the variables yielded relatively high accuracy results, it was not the case for the Balance model, and the CNN model. Stabilometry data are known to present significant differences between NSLBP and Healthy subjects (Ruhe, Fejer, and Walker 2011), but to present accurate and reliable results, stabilometry data should abide to certain standards, one of such being that data should be acquired on a sample of 90 seconds at least (Ruhe et al. 2010). A criteria that is hardly met when a subject is performing a dynamic movement, which spans for a few seconds only. But on the other side, using static standing recording to cluster the NSLBP population would overlook some of the neuromuscular and biomechanical differences that arise during dynamic tasks (Sanderson et al. 2019;Villafane et al. 2016;Laird et al. 2014;Asgari et al. 2015;J. Dieën, Reeves, and Kawchuk 2018). Looking at the counterperformance of the Balance model, especially in the light of the relatively high accuracy of the Biomechanical and Neuromuscular models, it seems that, when trying to cluster the NSLBP population, it is better to focus on dynamic movements.

Concerning the sub-part performance of the CNN, we suspect that the issue is a methodological one and not a data driven one. Beyond the problem of limited data points, studying the HD EMG signals from the subject performance as a "simple" image using CNN, might overlook some of the temporal relation present in those signals which cannot be grasped by a pure CNN. That temporal aspect might be of great importance for classification. Therefore, in order to use HD EMG signals without any feature extraction, we would recommend turning to solutions that also take into account the temporal resolution of those signals via the use of more complex models, such as support vector machine (SVM) for example, (Suthaharan et al. 2016), or a combination of CNN and SVM which could be more adapted for such complex data (Basly et al. 2020).

In addition, the fact that deep learning techniques are able to yield high performance, even with limited data, while clustering the population is still a hard and complex task, seems to be a testament to the complexity or subtleness of the relation between the variables and NSLBP. Just like the problem we encountered with the CNN,

those results might be a hint to push toward tools that can detect such complex relationships, or to find higher level variables that would encompass the NSLBP domains of interest while reducing the degree of freedom of the clustering problem in order to make it simpler for classic techniques.

The results from the FA show us that not all variables and domains of variables are equal in regards to different movements. Depending on the movement performed, the amount of information related to the NSLBP symptom vary across variables, and probably across domains of variables too. In the light of those results, we would recommend focusing on single movement based classification, and keeping the task/movement simple, as to prevent the complexification of the clustering task. Indeed, if different simple movements are strongly linked to different variables, it could be hypothesized that a complex movement, being a mix of simple movements, would see the number of variables strongly related add up, distributing the significant information across those variables, thus creating a more complex clustering problem. In addition to focusing on a single simple movement for acquiring data, the focus should be put on relevant associated variables. The benefit would be twofold: simpler study protocols, and if working solutions are found from them, easier clinical application.

From our results perspective, the trunk flexion could be a strong candidate for the movement of choice, as it is a well-studied movement (Laird et al. 2014). But also, this movement has the particularity to display the flexion relaxation phenomenon: the reduction of paraspinal muscle activity at maximum trunk flexion. A phenomenon known to present differences between the NSLBP and Healthy population (Gouteron et al. 2021). Another candidate would be the trunk rotation. Indeed, this movement had different components loading both on Healthy and NSLBP direction, which could means that this movement has an increased discriminatory capacity, compared to other.

Even using restricted data sets, the DNN models showed, most of the time, high accuracy results despite the complexity of the NSLBP symptom and the variability of its expression amongst afflicted subjects (Hartvigsen et al. 2018;Maher, Underwood, and Buchbinder 2017;Laird et al. 2014). In light of this, the case could be made that the tooling to study NSLBP and its clustering needs to be rethought, to fit the need to find complex and subtle relationships amongst the data, something that deep learning tools excel at (Najafabadi et al. 2015;Goodfellow, Bengio, and Courville 2016) and where classic cluster techniques might be facing difficulties, which can be harder to address (Ronan et al. 2016).

The exploratory analysis findings can be summarized in the following points:

- Higher level data, or "meta data" linked to the main domains influencing NSLBP prognosis should receive more attention when attempting to cluster and no domains should be discarded (a case could be made for the genetic domain due to the complexity of the task to study it).
- Dynamic conditions used to acquire data in order to study clustering of the NSLBP population should be kept as simple as possible in order to prevent the complexification of the clustering task.
- As the importance of relationships with NSLBP for each variables is dependent on the condition performed, care should be put into which variables are looked at, for each of the conditions studied. Exploratory work before attempting clustering of a population should be considered and the associated results shared along the clustering results.
- Back flexion and trunk rotation seems to be the movements to be privileged as the dynamic condition of choice for data acquisition.
- Tools that have the capacity to detect and model complex and subtle relationships should be privileged. Great importance should be placed into the choice of data analysis and tools framework used to process data from NSLBP when attempting to cluster it.

Concerning this last point, the focus on higher order variables linked to the domain influencing NSLBP prognosis should not be disregarded, as it could allow the researchers to study more fundamental and common adaptations from NSLBP and their expression, and for the clinicians to apply this knowledge straight away into their practice, to help develop personalized and more effective care protocols, in accord with the profile of his NSLBP patients, without the need for new or expensive equipment.

4.2 Clusters analysis

The following clustering algorithms were used:

- K-means clustering
- Spectral clustering
  - Affinity matrix construction technique: Nearest neighbors, Radial basis function (RBF)
  - Assign label strategy: K-means, discretize
- Hierarchical agglomerative clustering
  - Distance between instance metric: Euclidean, Manhattan, Cosine
  - Linkage criterion: Average, Complete, Single

This cluster analysis is divided in three parts. First we ran the clustering algorithms on the full data set, with and without using dimension reduction. The goal is to establish a baseline of the capacities of the unsupervised algorithms used. Following this, we will cluster our population using the insights gained from our exploratory analysis. Once this is done, we will analyze the valuable clusters found. Secondly we ran the clustering algorithms using the full data set, but only using the variables with significant correlation to NSLBP as shown in our FA results. Again, with and without dimension reduction being used. The goal is to assess if the results are better than with our null model using our newly acquired knowledge. Third, we ran the clustering algorithms on movement specific data set, again using the results from our exploratory analysis. Again, the goal is to see if our newly acquired knowledge will help us produce better results. More details about the variables used in the second and third part is given later on. We used the silhouette score (Rousseeuw 1987) to assess the potential quality of the clustering solutions. The silhouette score values are listed in the tables below. Only the combination yielding a silhouette score above 0.7 will be further investigated later. Once this three clustering attempts were done, we investigated the clustering models that yielded valuables results.

Due to time constraint, not all the spine cluster data could be processed for every subjects, therefore, we ran two analysis for each algorithms: one without data from the spine clusters, and one with a reduced set of the spine cluster data, as shown in Figure 3.10. This was done as to maximize the number of subjects aka data points used by our algorithms while still using spine cluster data.Here force plate data have been discarded, as the results from the DNN showed they were of low value when used in a movement agnostic context.

One of the problems encounter in this part was the very high number of dimensions of our data set, which could create what is called the curse of dimensionality (Bellman 1957): with the increase of dimension, the available data become sparse, due to the extremely fast growth of the spaces' volume in which the data evolve. To counter this problem, one of the best and most straight forward solution is to simply get more data. A solution that can quickly become inadequate. Indeed, recommendations state that at least 5 training samples by dimension should be acquired (Koutroumbas and Theodoridis 2008), which can bring the amount of data to acquire to an absurdly high amount. Another way to tackle this problem is to reduce the data dimensions. To do so, two things were implemented: Principal Component Analysis (PCA), and selection of variables. PCA was chosen as a way to objectively reduce the data set dimension. PCA is sensible to the scaling of the variable (Leznik and Tofallis 2005). To prevent this problem the data have been re-scaled using the method `sklearn.preprocessing.RobustScaler()` from the *Scikit Learn* Library (Pedregosa et al. 2011). In order to alleviate the obvious problem of subjectivity in choosing which variables to keep, we relied on the insights gained from our exploratory analysis, and this is what we explore in the second and third part of this cluster analysis. Due to the same concern of lowering data set dimension, anthropometric data were not included in our analysis as the clustering models yielded the same results without them. We also only used the left shoulder data, instead of both, again, as to limit the number of dimension of our data set.

We start the clustering of our population via two null models first: with and without dimension reductions via PCA.

4.2.1 Null model

4.2.1.1 No dimension reduction

4.2.1.1.1 No spine data

The silhouette scores for the null model, without spine data or dimension reduction, for the different clustering techniques, can be found in the table 4.22.

Clustering \ Cluster number	2	3	4	5	6	7	8	9
K-means								
	0.86	0.83	0.76	0.75	0.69	0.62	0.46	0.47
Spectral								
nearest neighbors								
kmeans	0.65	0.07	-0.03	-0.11	-0.11	-0.12	-0.13	-0.13
discretize	0.54	-0.02	-0.12	-0.16	-0.16	-0.16	-0.14	-0.15
rbf								
kmeans	-0.57	-0.57	-0.56	-0.55	-0.55	-0.55	-0.55	-0.55
discretize	0.0	-0.51	-0.4	-0.37	-0.52	-0.46	-0.53	-0.55
Agglomerative								
euclidean								
average	0.87	0.83	0.81	0.75	0.69	0.62	0.59	0.45
single	0.87	0.83	0.81	0.75	0.69	0.62	0.59	0.45
complete	0.87	0.83	0.81	0.75	0.69	0.62	0.46	0.47
manhattan								
average	0.87	0.83	0.81	0.61	0.52	0.62	0.48	0.42
single	0.87	0.82	0.81	0.61	0.52	0.62	0.59	0.45
complete	0.87	0.83	0.81	0.72	0.69	0.62	0.45	0.05
cosine								
average	0.06	-0.28	-0.15	-0.11	-0.11	-0.09	-0.08	-0.06
single	-0.58	-0.58	-0.59	-0.57	-0.42	-0.42	-0.41	-0.39
complete	-0.07	-0.32	-0.31	-0.25	-0.13	-0.13	-0.12	-0.11

Table 4.22: Silhouette scores for the null model, without spine data or dimension reduction.

4.2.1.1.2 Spine data

The silhouette scores for the null model, with spine data but without dimension reduction, for the different clustering techniques, can be found in the table 4.23.

Clustering \ Cluster number	2	3	4	5	6	7	8	9
K-means								
	0.67	0.62	0.65	0.46	0.43	0.39	0.29	0.31
Spectral								
nearest neighbors								
kmeans	0.18	0.31	0.15	0.17	0.12	0.19	0.17	0.19
discretize	0.18	0.25	0.12	0.17	0.12	-0.05	-0.11	-0.17
rbf								
kmeans	-0.02	-0.03	-0.16	-0.39	-0.33	-0.36	-0.38	-0.4
discretize	-0.01	-0.12	-0.17	-0.21	-0.31	-0.29	-0.32	-0.31
Agglomerative								
euclidean								
average	0.67	0.57	0.65	0.46	0.43	0.39	0.32	0.25
single	0.67	0.57	0.65	0.46	0.38	0.39	0.33	0.25
complete	0.67	0.57	0.65	0.46	0.43	0.39	0.32	0.31
manhattan								
average	0.67	0.57	0.65	0.46	0.43	0.22	0.25	0.19
single	0.67	0.57	0.27	0.46	0.39	0.36	0.15	0.16
complete	0.53	0.57	0.65	0.46	0.34	0.35	0.25	0.06
cosine								
average	0.01	-0.23	-0.23	-0.34	-0.32	-0.29	-0.23	-0.21
single	-0.06	-0.45	-0.42	-0.4	-0.37	-0.34	-0.28	-0.28
complete	0.01	-0.35	-0.33	-0.33	-0.3	-0.27	-0.23	-0.2

Table 4.23: Silhouette scores for the null model, with spine data but without dimension reduction.

4.2.1.2 Dimension reduction

4.2.1.2.1 No spine data

The silhouette scores for the null model, without spine data but with dimension reduction, for the different clustering techniques, can be found in the table 4.24.

Clustering \ Cluster number	2	3	4	5	6	7	8	9
K-means								
	0.94	0.94	0.91	0.86	0.85	0.65	0.62	0.64
Spectral								
nearest neighbors								
kmeans	0.01	-0.01	0.13	0.37	0.31	0.49	0.33	0.29
discretize	0.01	-0.01	0.16	0.37	0.31	0.18	0.41	0.39
rbf								
kmeans	0.94	0.94	0.91	0.86	-0.0	-0.07	-0.18	-0.18
discretize	0.94	0.94	0.94	-0.5	-0.52	-0.55	-0.54	-0.54
Agglomerative								
euclidean								
average	0.91	0.94	0.91	0.86	0.85	0.81	0.62	0.63
single	0.91	0.94	0.91	0.82	0.85	0.81	0.62	0.52
complete	0.91	0.94	0.91	0.86	0.85	0.63	0.61	0.63
manhattan								
average	0.91	0.94	0.91	0.86	0.85	0.81	0.62	0.63
single	0.91	0.94	0.91	0.82	0.85	0.81	0.62	0.52
complete	0.91	0.94	0.91	0.86	0.85	0.63	0.61	0.63
cosine								
average	0.86	-0.54	-0.43	-0.54	-0.54	-0.61	-0.62	-0.61
single	0.86	0.82	0.79	0.81	0.8	-0.53	-0.4	-0.51
complete	0.86	-0.54	-0.43	-0.54	-0.54	-0.61	-0.62	-0.61

Table 4.24: Silhouette scores for the null model, without spine data but with dimension reduction.

4.2.1.2.2 Spine data

The silhouette score for the null model, using the spine data and dimension reduction, for the different clustering techniques, can be found in the table 4.25.

Clustering \ Cluster number	2	3	4	5	6	7	8	9
K-means								
	0.72	0.77	0.83	0.69	0.77	0.69	0.45	0.49
Spectral								
nearest neighbors								
kmeans	0.43	0.33	0.31	0.46	0.23	-0.01	0.12	0.28
discretize	0.05	-0.14	0.31	0.46	0.05	-0.11	-0.03	0.01
rbf								
kmeans	0.72	0.74	0.83	0.69	0.77	0.5	0.18	0.19
discretize	0.72	0.77	0.83	0.83	0.83	0.83	-0.28	-0.24
Agglomerative								
euclidean								
average	0.72	0.74	0.83	0.69	0.61	0.69	0.48	0.46
single	0.72	0.74	0.83	0.69	0.61	0.69	0.48	0.4
complete	0.72	0.74	0.83	0.69	0.77	0.69	0.48	0.46
manhattan								
average	0.71	0.74	0.83	0.69	0.61	0.69	0.48	0.46
single	0.71	0.74	0.83	0.69	0.61	0.69	0.48	0.4
complete	0.72	0.74	0.83	0.69	0.77	0.69	0.48	0.46
cosine								
average	0.72	0.77	0.67	0.69	0.77	0.51	0.4	0.32
single	0.72	0.77	0.67	0.69	0.77	0.51	0.4	0.32
complete	0.58	0.6	0.67	0.62	0.77	0.51	0.57	0.52

Table 4.25: The silhouette scores for the null model, using the spine data and dimension reduction.

4.2.2 Model using exploratory insights

The variables used for each movements comes from the finding from the exploratory FA done earlier. The factors loadings significantly on the Group component were selected. We did not discard the use of the force plate data. Indeed, from the DNN analysis, it seems that they are of no use. But it is to be said, that the DNN were movement agnostic, and that it may have been why the force plate data didn't yield interesting results. As the FA found the force plate data valuable in some cases, we added them in our clustering model when it came to movement specific tasks. As the data from the spine cluster were not investigated through the FA, we did not use them in this specific part, and also with the aim of maximizing the number of data point available to us as they were not available to every subjects. Again, as the clustering models yielded the same, or marginally better, results by not using the anthropometric data, they were not included in our analysis in order to reduce the number of dimension of the data sets.

Variables used for *back extension preferred*:

- Time to maximum amplitude of the left shoulder trajectory, Y axis
- Entropy of the movement of the left shoulder trajectory, Y axis
- Y position of the total back EMG centroid
- Entropy of the EMG of the left low back

Variables used for *back extension maximum*:

- Time to maximum amplitude of the left shoulder trajectory, Y axis
- Entropy of the movement of the left shoulder trajectory, Y axis
- Y position of the total back EMG centroid

Variables used for *back flexion preferred*:

- Entropy of the movement of the left shoulder trajectory, Z axis
- Y position of the total back EMG centroid

Variables used for *back flexion maximum*:

- Maximum amplitude of the left shoulder trajectory, Z axis
- Time to maximum amplitude of the left shoulder trajectory, Z axis
- Variability intra-subject of the left shoulder trajectory, Z axis
- Variability inter-subject of the left shoulder trajectory, Z axis

Variables used for *lateral flexion left preferred*:

- Time to maximum amplitude of the left shoulder trajectory, Z axis
- Entropy of the movement of the left shoulder trajectory, Z axis
- Variability inter-subject of the left shoulder trajectory, Z axis
- GFR distribution ratio

Variables used for *lateral flexion left maximum*:

- Time to maximum amplitude of the left shoulder trajectory, Z axis
- Variability intra-subject of the left shoulder trajectory, Z axis
- Variability inter-subject of the left shoulder trajectory, Z axis
- GFR distribution ratio

Variables used for *lateral flexion right preferred*:

- Y position of the total back EMG centroid
- GFR distribution ratio

Variables used for *lateral flexion right maximum*:

- Time to maximum amplitude of the left shoulder trajectory, Z axis
- Entropy of the movement of the left shoulder trajectory, Z axis
- Y position of the total back EMG centroid
- Entropy of the EMG of the right low back

Variables used for *trunk rotation left preferred*:

- GFR distribution ratio

Variables used for *trunk rotation left maximum*:

- Maximum amplitude of the left shoulder trajectory, Y axis
- Variability inter-subject of the left shoulder trajectory, Y axis
- GFR distribution ratio

Variables used for *trunk rotation right preferred*:

- Maximum amplitude of the left shoulder trajectory, Y axis
- Time to maximum amplitude of the left shoulder trajectory, Y axis
- Variability inter-subject of the left shoulder trajectory, Y axis
- Y position of the total back EMG centroid

Variables used for *trunk rotation right maximum*:

- Time to maximum amplitude of the left shoulder trajectory, Y axis
- Entropy of the movement of the left shoulder trajectory, Y axis
- Variability inter-subject of the left shoulder trajectory, Y axis
- Y position of the total back EMG centroid
- Entropy of the EMG of the right low back

As the back extension at maximum speed, the back flexion at preferred and maximum speed, the lateral flexion left and right at preferred speed, the trunk rotation left at maximum speed and the trunk rotation right at preferred speed clustering didn't yield any valuable results, their results were not displayed in this part, as to not clutter this chapter more than necessary.

4.2.2.1 Full model with anthropometric data

4.2.2.1.1 No dimension reduction

The silhouette scores for the full model from exploratory insight, without dimension reduction, for the different clustering techniques, can be found in the table 4.26.

Clustering \ Cluster number	2	3	4	5	6	7	8	9
K-means								
	0.84	0.79	0.67	0.41	0.12	0.1	0.09	0.07
Spectral								
nearest neighbors								
kmeans	0.05	-0.08	-0.1	-0.08	-0.02	-0.02	-0.05	-0.02
discretize	0.05	-0.06	-0.15	-0.09	-0.04	-0.17	-0.05	-0.06
rbf								
kmeans	0.29	0.29	0.17	0.03	0.03	0.03	0.11	0.03
discretize	0.5	0.06	-0.11	-0.11	-0.09	-0.08	-0.25	-0.14
Agglomerative								
euclidean								
average	0.84	0.79	0.67	0.47	0.39	0.3	0.26	0.23
single	0.84	0.79	0.67	0.47	0.39	0.3	0.25	0.23
complete	0.84	0.79	0.67	0.41	0.38	0.09	0.08	0.07
manhattan								
average	0.76	0.79	0.35	0.36	0.39	0.19	0.2	0.2
single	0.76	0.79	0.67	0.47	0.39	0.3	0.19	0.17
complete	0.84	0.79	0.05	0.05	0.04	0.07	0.05	0.03
cosine								
average	0.07	0.06	0.04	0.02	-0.0	0.01	-0.0	-0.01
single	-0.38	-0.38	-0.33	-0.33	-0.35	-0.34	-0.3	-0.31
complete	0.12	-0.02	-0.21	-0.12	-0.11	-0.07	-0.05	-0.08

Table 4.26: Silhouette scores for the full model from exploratory insight, without dimension reduction.

4.2.2.1.2 Dimension reduction

The silhouette scores for the full model from exploratory insight, with dimension reduction, for the different clustering techniques, can be found in the table 4.27.

Clustering \ Cluster number	2	3	4	5	6	7	8	9
K-means								
	0.89	0.89	0.82	0.78	0.71	0.5	0.52	0.41
Spectral								
nearest neighbors								
kmeans	0.17	-0.3	-0.2	-0.08	0.09	0.17	0.17	0.16
discretize	0.16	-0.27	-0.2	-0.08	-0.04	0.01	0.04	0.06
rbf								
kmeans	0.89	0.89	0.82	0.8	0.71	0.46	-0.24	-0.19
discretize	0.89	0.89	0.89	0.89	0.89	0.89	-0.54	-0.53
Agglomerative								
euclidean								
average	0.89	0.89	0.82	0.8	0.71	0.5	0.52	0.51
single	0.89	0.89	0.82	0.8	0.71	0.51	0.44	0.49
complete	0.89	0.89	0.82	0.78	0.71	0.5	0.52	0.41
manhattan								
average	0.89	0.89	0.82	0.8	0.71	0.5	0.52	0.51
single	0.89	0.89	0.82	0.8	0.71	0.51	0.44	0.49
complete	0.88	0.89	0.82	0.78	0.71	0.5	0.52	0.32
cosine								
average	0.77	0.78	0.44	0.44	0.21	0.24	0.25	0.23
single	0.78	0.78	0.49	0.42	0.43	0.44	0.19	0.16
complete	0.77	0.78	0.2	0.23	0.24	0.23	0.19	0.2

Table 4.27: Silhouette scores for the full model from exploratory insight, with dimension reduction.

4.2.2.2 Movement specific models

Only the movements that seemed to showcase potentially valuable cluster models were inserted in this part, as to nut clutter the chapter. Potentially valuable cluster models were evaluated via the silhouette score (Rousseeuw 1987) and had to reach at least a score of 0.7. The movements who failed to reach such a score in every cluster algorithms were not included below.

4.2.2.2.1 Back extension preferred

The silhouette score for back extension preferred regarding the different clustering techniques used can be found in the table 4.28.

Clustering \ Cluster number		2	3	4	5	6	7	8	9
K-means									
		0.93	0.87	0.64	0.53	0.25	0.27	0.3	0.23
Spectral									
	nearest neighbors								
	kmeans	0.03	-0.14	-0.06	0.16	0.15	0.13	0.12	0.08
	discretize	0.03	-0.07	-0.06	0.15	0.14	0.07	0.1	0.06
	rbf								
	kmeans	0.8	0.8	0.8	0.8	0.8	0.8	0.8	0.8
	discretize	0.71	0.21	0.61	-0.23	-0.04	-0.01	-0.18	0.16
Agglomerative									
	euclidean								
	average	0.93	0.87	0.72	0.53	0.38	0.35	0.32	0.27
	single	0.93	0.87	0.72	0.57	0.44	0.34	0.3	0.28
	complete	0.93	0.87	0.61	0.53	0.27	0.27	0.27	0.24
	manhattan								
	average	0.93	0.87	0.72	0.53	0.4	0.33	0.31	0.28
	single	0.93	0.87	0.72	0.57	0.42	0.31	0.3	0.28
	complete	0.93	0.87	0.72	0.53	0.22	0.26	0.26	0.21
	cosine								
	average	0.31	-0.03	0.09	0.12	0.04	0.03	0.02	0.02
	single	0.59	-0.31	-0.27	-0.25	-0.22	-0.15	-0.15	-0.13
	complete	-0.18	-0.03	-0.03	0.1	0.03	0.01	-0.0	0.02

Table 4.28: Silhouette score for back extension preferred.

It can be noted the strange silhouette scores for the Spectral clustering using the RBF kernel and assigning label using K-means, where the score for all the number of cluster is 0.80. It might be due to the inability of the Spectral algorithm to converge, but will still be investigate for good measure.

4.2.2.2.2 Lateral flexion left maximum

The silhouette score for lateral flexion left maximum regarding the different clustering techniques used can be found in the table 4.29.

Clustering \ Cluster number	2	3	4	5	6	7	8	9
K-means								
	0.71	0.69	0.2	0.21	0.22	0.22	0.25	0.2
Spectral								
nearest neighbors								
kmeans	0.18	0.13	0.03	0.01	-0.02	0.07	0.02	0.05
discretize	0.18	0.12	0.05	0.03	-0.03	-0.1	0.02	-0.02
rbf								
kmeans	0.4	0.49	0.37	0.31	0.26	0.22	0.22	0.18
discretize	0.36	0.14	0.34	0.17	0.17	0.34	0.16	0.12
Agglomerative								
euclidean								
average	0.71	0.69	0.5	0.38	0.38	0.34	0.27	0.28
single	0.71	0.69	0.5	0.38	0.37	0.3	0.26	0.19
complete	0.71	0.69	0.26	0.29	0.25	0.27	0.28	0.23
manhattan								
average	0.68	0.69	0.42	0.37	0.36	0.32	0.24	0.21
single	0.71	0.69	0.5	0.38	0.37	0.3	0.21	0.15
complete	0.68	0.69	0.42	0.33	0.32	0.25	0.21	0.22
cosine								
average	0.21	0.19	-0.02	-0.04	-0.08	-0.04	-0.03	0.01
single	-0.32	-0.33	-0.27	-0.26	-0.32	-0.32	-0.28	-0.22
complete	0.21	0.19	0.02	-0.01	-0.01	0.01	-0.02	-0.01

Table 4.29: Silhouette score for lateral flexion left maximum.

4.2.2.2.3 Lateral flexion right maximum

The silhouette score for lateral flexion right maximum regarding the different clustering techniques used can be found in the table 4.30.

Clustering \ Cluster number		2	3	4	5	6	7	8	9
K-means									
		0.92	0.79	0.39	0.36	0.27	0.27	0.23	0.23
Spectral									
	nearest neighbors								
	kmeans	0.02	-0.1	-0.03	-0.0	0.02	0.04	0.1	0.05
	discretize	0.02	-0.09	-0.03	-0.02	0.0	0.04	0.07	0.09
	rbf								
	kmeans	0.71	0.09	0.05	-0.11	-0.18	-0.2	-0.18	-0.15
	discretize	0.28	0.28	0.03	0.1	0.2	0.13	0.11	0.2
Agglomerative									
	euclidean								
	average	0.92	0.79	0.63	0.35	0.3	0.28	0.27	0.26
	single	0.92	0.79	0.63	0.28	0.27	0.24	0.19	0.18
	complete	0.92	0.79	0.63	0.36	0.26	0.27	0.26	0.27
	manhattan								
	average	0.92	0.79	0.63	0.36	0.31	0.29	0.28	0.25
	single	0.92	0.79	0.63	0.28	0.18	0.24	0.2	0.19
	complete	0.92	0.79	0.63	0.36	0.2	0.19	0.2	0.2
	cosine								
	average	0.14	-0.09	-0.16	0.01	0.03	-0.02	-0.01	-0.01
	single	-0.31	-0.26	-0.26	-0.3	-0.36	-0.28	-0.34	-0.24
	complete	0.32	-0.04	-0.11	-0.1	-0.09	-0.01	-0.01	-0.01

Table 4.30: Silhouette score for lateral flexion right maximum.

4.2.2.2.4 Trunk rotation left preferred

The silhouette score for trunk rotation left preferred regarding the different clustering techniques used can be found in the table 4.31.

Clustering \ Cluster number	2	3	4	5	6	7	8	9
K-means								
	0.82	0.55	0.58	0.48	0.55	0.57	0.58	0.57
Spectral								
nearest neighbors								
kmeans	0.52	0.29	0.32	0.3	0.3	0.31	0.36	0.51
discretize	0.52	0.29	0.28	0.25	0.29	0.21	0.31	0.51
rbf								
kmeans	0.53	0.55	0.45	0.33	0.56	0.53	0.29	0.29
discretize	0.55	0.55	0.58	0.58	0.58	0.58	0.14	0.06
Agglomerative								
euclidean								
average	0.82	0.61	0.59	0.55	0.56	0.53	0.57	0.55
single	0.82	0.61	0.42	0.36	0.32	0.2	0.33	0.33
complete	0.82	0.5	0.53	0.48	0.46	0.44	0.58	0.58
manhattan								
average	0.82	0.61	0.59	0.55	0.56	0.53	0.57	0.55
single	0.82	0.61	0.42	0.36	0.32	0.2	0.33	0.33
complete	0.82	0.5	0.53	0.48	0.46	0.44	0.58	0.58
cosine								
average	0.45	-0.17	-0.21	-0.25	-0.32	-0.56	-0.55	-0.54
single	0.45	-0.17	-0.21	-0.25	-0.24	-0.23	-0.31	-0.31
complete	0.45	-0.17	-0.21	-0.25	-0.32	-0.56	-0.55	-0.54

Table 4.31: Silhouette score for trunk rotation left preferred.

4.2.2.2.5 Trunk rotation right maximum

The silhouette score for trunk rotation right maximum regarding the different clustering techniques used can be found in the table 4.32.

Clustering \ Cluster number		2	3	4	5	6	7	8	9
K-means									
		0.89	0.75	0.25	0.26	0.25	0.25	0.25	0.23
Spectral									
	nearest neighbors								
	kmeans	0.05	0.01	0.03	0.08	0.09	0.17	0.2	0.2
	discretize	0.05	0.04	0.06	0.08	0.05	0.01	0.12	0.16
	rbf								
	kmeans	0.89	0.89	0.89	0.89	0.89	0.89	0.89	0.89
	discretize	0.89	0.69	-0.02	-0.08	-0.07	0.38	0.24	0.01
Agglomerative									
	euclidean								
	average	0.89	0.75	0.48	0.43	0.4	0.24	0.22	0.15
	single	0.89	0.75	0.7	0.45	0.4	0.37	0.19	0.15
	complete	0.89	0.75	0.47	0.43	0.2	0.2	0.19	0.21
	manhattan								
	average	0.89	0.75	0.48	0.43	0.4	0.23	0.15	0.13
	single	0.89	0.75	0.7	0.45	0.4	0.37	0.2	0.15
	complete	0.89	0.75	0.19	0.24	0.21	0.21	0.21	0.18
	cosine								
	average	0.06	0.09	0.07	0.1	-0.05	-0.01	0.01	-0.0
	single	-0.31	-0.46	-0.42	-0.42	-0.42	-0.38	-0.38	-0.31
	complete	0.05	0.11	0.05	0.09	0.04	-0.07	-0.04	-0.04

Table 4.32: Silhouette score for trunk rotation right maximum.

It can be noted the strange silhouette scores for the Spectral clustering using the RBF kernel and assigning label using K-means, where the score for all the number of cluster is 0.89. It might be due to the inability of the Spectral algorithm to converge, but will still be investigate for good measure.

4.2.3 Analysis of the cluster models of interest

Unfortunately only one combination gave us a valuable cluster model. This happened using Spectral algorithm with RBF kernel, alongside the discretize algorithm for label assignment on the full data set with spine data, while using dimension reduction. No other combination gave valuable results.

The Figure 4.12 give us a more detailed look at the cluster distribution which seem to showcase an interesting distribution. Nonetheless, even we have to remember that we are working on a relatively small subset here, which could be biasing our results towards artificially a valuable, or abnormal, cluster distribution. This could explain the distribution close to 50% of healthy and LBP into some clusters which can seem strange. To be noted that in his work from 2018, Laird found subgroups with the following distribution (Laird, Keating, and Kent 2018):

- Subgroup 1: 26.3% LBP
- Subgroup 2: 71.2% LBP
- Subgroup 3: 82.9% LBP
- Subgroup 4: 100.0% LBP

In Laird and collaborator work, it is to be remembered that there was a substantial proportion of LBP subjects in each group that incorporated a large proportion of Healthy subjects. Laird and collaborators managed to run their study on a cohort of 266 participants, which was much larger, and therefore, yielded stronger conclusion. Our data set is only 10% of the size of the one from this study. Our results can't be interpreted with the same confidence than his. But those results don't seem to be too far off, which is encouraging.

Figure 4.12: Cluster distribution for Spectral clustering after dimension reduction via PCA and with Spine data using different methods. In red, NSLBP. In green healthy.

4.2.4 Cluster analysis conclusion

Unsupervised clustering algorithms have been used on our data set. In most cases, the results showed poor clustering capabilities and no valuable cluster models could be found but on one occasion. One thing to note was that, we were often facing outliers that would artificially improve the results, or at least the metric used to assess the quality of the results. The problem of the high number of dimensionality was dealt using dimension reduction either through PCA, or through educated guess from our exploratory work. Unfortunately, it wasn't sufficient, and a more important data set would be needed to alleviate that issue, but due to time constraints, we couldn't afford to collect on more participants.

The dimension reduction proved to be valuable, substantially improving the performance of some of the clustering algorithms, namely the spectral analysis algorithms which managed to discriminate 4 subgroups using the reduced data set with spine cluster data. The results are close to the one seen in previous work from Laird and collaborators (Laird, Keating, and Kent 2018), with one cluster that mostly encompasses NSLBP subjects and another cluster that encompasses a mix of healthy and NSLBP, presenting NSLBP as a spectrum. This is encouraging in regards to the size of our data set compared to the one of Laird and collaborators. The results for less clusters seem to go according to the results from Laird and collaborators. Due to its better performance, spectral algorithm using the RBF kernel might be the cluster technique to favor in future work.

An interesting fact to mention, is that discarding anthropometric data didn't yield much changes to the clustering result. It could be interpreted by saying that they in fact yield no valuable information, but our exploratory work proved that it was the total opposite. The results from the DNN and FA showed us that the anthropometric data had a tremendous information power and correlation not only to the NSLBP symptom but also to the biophysical data in general. The other possibility, which we can hypothesize, is that anthropometric data might be redundant with the other variables. Indeed, we can see the anthropometric data as the high levels variables of the biophysical domain (Hartvigsen et al. 2018), and the other variables as lower level variables. It might be that that anthropometric variables, the high level variables, drove some adaptations from NSLBP in the biophysical domain. We can hypothesize that the higher level variables are the ones driving the adaptation of NSLBP, so that those adaptations express itself into the lower level variables in a certain way. For this reason, leveraging the use of high level variables as a source of data for clustering should be investigated. It is to be noted that using high level variables would probably allow us to integrate a significant amount of information in our data set, while at the same time limiting the number of variables needed, making the task of clustering population sample much easier at the same time. Also let us remember that NSLBP is a multi-factorial symptom (Hartvigsen et al. 2018), and maybe what we see and hypothesize with the anthropometric domain, is consistent across the

other main domains influencing LBP prognosis (Hartvigsen et al. 2018).

Discussion

NSLBP is extremely prevalent in the population (Hoy et al. 2012; Hartvigsen et al. 2018), and is a growing health problem worldwide (Hoy et al. 2014). As of today, NSLBP is a major and costly issue both materially and socially, for society and the affected people (Hoy et al. 2014). The major obstacle to solving the NSLBP equation comes from the symptom main characteristic: its idiopathic nature. The absence of clues about the underlying causes in addition to the fact that the symptom encompasses a very large and diverse population make it relatively hard to study the NSLBP population and the associated consequences, or to design effective treatments and rehabilitation protocols, for researcher and clinicians alike (Hodges, Cholewicki, and Van Dieën 2013; Haskins, Osmotherly, and Rivett 2015b, 2015a).

In order to circumvent this problem, one solution that is emerging is to cluster the NSLBP population into more homogeneous subgroups in order to facilitate the development of more targeted and patient specific care which should be more effective than the currently available tools (Hodges, Cholewicki, and Van Dieën 2013; Haskins, Osmotherly, and Rivett 2015b, 2015a; Hartvigsen et al. 2018). Regrettably, no reliable and, or, clinically meaningful subgrouping solution of the NSLBP population has been found so far (Maher, Underwood, and Buchbinder 2017).

Today, most attempts made at subgrouping the NSLBP population rely on the use of categorical data. One major issue of categorical data, is that their categories are set through subjective measures, such as the educated guess of an experimenter. This might limit the extrapolation and usefulness of the cluster models found through the use of categorical variables as they therefore depend on subjective ruling. Being able to design classification models based on more objective data would ground the subgrouping models using them into a more solid foundation. But to define valuable cluster models using continuous variables there is first, a need to better understand continuous variables in relation to NSLBP. Exploratory work in different conditions on NSLBP population is required in order to acquire valuable knowledge and to facilitate the development of clinically relevant clusters among this population.

In light of the present problem of NSLBP, our approach for this work lied in the following objectives:

1. First objective: Provide an exploratory work to better understand the influence and importance of the selected variables in regards to NSLBP and our sample population, and gather information to prepare subgrouping
2. Second objective: Provide an attempt at clustering our population sample in order to discriminate valuables subgroups

To accomplish those objectives, we defined a protocol relying on the patient's performance on range of simple movements at different speed as to cover a broad spectrum of conditions for our exploratory analysis. HD EMG and MOCAP data were acquired during these tasks in order to capture as much data as possible on different aspects of the movement through continuous variables, be it biomechanical or neuromscular. Following this and after pre-processing the acquired data, we dived into the core of our research work.

We started with an exploratory analysis. Using DNN and FA, we managed to gather valuable information about the variables of interest and the NSLBP symptom. The main findings from our exploratory analysis were:

- Higher level data, or "meta data" linked to the main domains influencing NSLBP prognosis should receive more attention when attempting to cluster and no domains should be discarded (a case could be made for the genetic domain due to the complexity of the task to study it).
- Dynamic conditions used to acquire data in order to study clustering of the NSLBP population should be kept as simple as possible in order to prevent the complexification of the clustering task.
- As the importance of relationships with NSLBP for each variables is dependent on the condition performed, care should be put into which variables are looked at, for each of the conditions studied. Exploratory work before attempting clustering of a population should be considered and the associated results shared along the clustering results.
- Back flexion and trunk rotation seems to be the movements to be privileged as the dynamic condition of choice for data acquisition.
- Tools that have the capacity to detect and model complex and subtle relationships should be privileged. Great importance should be placed into the choice of data analysis and tools framework used to process data from NSLBP when attempting to cluster it.

This answered our first objective.

Once the exploratory work was done, we went on to the clustering attempts. First we created null clustering models using our whole data set, with and without dimension reduction, and with and without the spine data. Indeed, due to constraints outside of our control, it wasn't possible to get the spine data of all participants ready in time. We used two solutions for dimension reduction, making sure to avoid subjective ones. Our first solution for dimension reduction was to use PCA, as this technique rely very little, to say the least, on human decisions, making it extremely objective. Using PCA and the whole data set with spine data, we managed to extract a relatively interesting cluster model using the spectral algorithm, with the RBF kernel and the discretize label assignment's algorithm. After this null clustering models, we moved to the next step in our clustering attempt: using our newly acquired insights from our previous exploratory analysis. For each movements, we selected variables that were deemed of high value from our exploratory analysis' results. We then went on to try to find valuable cluster models on a this reduced data set using all the movements, with and without PCA to further narrow down the number of dimension as to maximize our algorithms clustering capability. Then we tried our clustering algorithms on each movement specific data set. Unfortunately, no other valuable clustering models were found, and we weren't able to provide a definite answer to our second objective. Nonetheless, we still managed to produce a cluster model close to the one from the work from Laird and collaborator (Laird, Keating, and Kent 2018), using a data set 4 to 5 times smaller than in their work. Even if our data set was relatively small and unbalanced compared to theirs, it still provided an encouraging result, and some valuable insights could still be extracted from this. First, spectral clustering using the RBF kernel seems to be the clustering solution to prefer. Second, it seems like anthropometric data can be discarded as they appeared to be redundant even if they seemed to be of great importance in our exploratory analysis, an ambivalent fact to which we will come back to a bit later in this discussion. Third, spine cluster data should be given the highest priority when studying biomechanic of NSLBP subjects. Even if they require much more pre-processing work and usually the creation of personalized cluster of maker solution, as the market doesn't provide a wide variety of them. Due to the higher demand during pre-processing, a compromise might have to be found, and the MOCAP model used might need to be simplified to accomodate for the workload related to spinal clusters of markers.

Our project focused on continuous variables as we think that clustering models using them will yield results closer to the clinical reality. Learning more about continuous variables, their relationships to NSLBP and their use in clustering models is of great value, but it is also more complex, and more data points and population diversity are required. Thus, care should be taken concerning the extrapolation to our findings to the full NSLBP population, and be used only as guidance and not hard-set rules to be followed by the book. The lack of data point was most problematic for the FA as the number of variables that could be investigated was dramatically limited by our sample size (Paul Kline 2014). Nonetheless, the FA and DNN results present,

respectively, strong significance, and strong accuracy. Our clustering attempts wasn't as fruitful as expected, but showed us that our intuition was valid, and more work needs to be put in this direction. As categorical clustering models have not yet proven effective on the field (Koppenaal et al. 2023; McCarthy et al. 2004; Alrwaily et al. 2016) there is a need to try new solutions. Therefore, the use of continuous variables should not be discarded when investigating the clustering of NSLBP population for clinical purposes.

To continue on a tangent regarding our results, a case can be made for the possibility of a reliable "meta data clustering" for NSLBP population. By meta data, we refer to high level variables relating to the 5 main domains driving the NSLBP prognosis: biophysical, comorbidities, social, psychological and genetic. Indeed, regarding meta data, in the present exploratory work constrained to the biophysical domain via the anthropometric data, two points can be made:

- Concerning their use in DNN, the models were able to classify with extreme accuracy between NSLBP and Healthy subjects.
- Concerning their use in the FA, they consistently loaded for each movement, even though via different variables, on the Group factor.

In the light of such results, a case could be made for the search of a "meta clustering model", relying on high level data from the main domains of interest in order to subgroup the NSLBP population. This could provide, for little cost and complexity, a framework easily usable clinically. Something already attempted, for example by the Quebec task force (Loisel et al. 2002) but which failed, maybe because some domains were overlooked, or the data being too categorical. This thoughts are further backed up by what happened when we attempted clustering our population sample: anthropometric data appeared redundant. It could have been supposed that those variables did not carry useful information, but our exploratory results explicitly showed the tremendous information power of those variables in regards to NSLBP, just like the earlier works cited in this manuscript.

Therefore, meta data, or higher level variables, should not be discarded as they might provide us with a framework allowing to "summarize" the complex relationships between domains linked to NSLBP and ease off the complexity of the task of subgrouping NSLBP. This could prevent the need for more complex modeling tools or solutions in general, as long as all the main domains influencing the NSLBP prognosis are represented (Heitz et al. 2009; Uccar et al. 2021); Rolli et al. 2013), and the probable dose/response effect of the time under NSLBP on related adaptations is taken into account (Miki et al. 2021). Indeed, some studies have shown that higher motor variability was observed in the upper limb or in the trunk in the presence of acute pain, whereas the variability was lower under chronic pain conditions (Madeleine 2010; J. H. van Dieën, Flor, and Hodges 2017), which tends to suggest adaptations specific to the chronicity of NSLBP in the affected subjects. It is therefore not

unbelievable to think that NSLBP carry some sort of a dose/response relation with its related adaptations and their expression in afflicted subjects. But if there is one, it might not be a simple and straight forward answer, which might be also under the influence of meta data, as other work showed that pain intensity and disability from NSLBP seemed to be all uncorrelated to the observed changes in coordination. This could suggest that the observed changes in trunk coordination and ES activity, which seem to be direct consequence of NSLBP would be correlated more strongly to the duration under the symptom's affliction, and not as much as the pain intensity of it (Lamoth et al. 2006).

We would like to end this discussion by sharing with the reader a daring thought. In addition to being relatively non costly and easy to test, this hypothesis push us to ask ourselves: Could NSLBP be a generic symptom that is driven to express itself differently in every individuals due to their unique profile in the main domains? While still being in accordance with the consensus about what influence the prognosis of NSLBP, this is a daring question, but which could lead to extremely interesting perspectives in research, as well as directly in clinic (Maher, Underwood, and Buchbinder 2017; Hartvigsen et al. 2018). Even if daring, this hypothesis is not ungrounded: Biological factor are known to be directly linked to NSLBP (Koley et al. 2010), as well as genetic factors (Aroke et al. 2020; Balague et al. 2012; El-Metwally et al. 2008). In addition, it has been shown that health is significantly impacted by the socioeconomic status of an individual (Adler et al. 1999; Mc Ewen et al. 2010; Chan et al. 2018; Cutler et al. 2008). While psychological factors have been shown to hinder recovery of LBP (Kendall et al. 1999). These are all the main domains known to impact the NSLBP prognosis.

This hypothesis can be summarized in a simple metaphore: NSLBP drives common adaptation to every patient afflicted, just like the "genotype" of the symptom. But due to differences in the subject and its environment, both of which being the environment in which the NSLBP symptom evolves, those common adaptations are expressed differently in each and every subjects, just like the "phenotype" of the symptom. To put it simply, LBP induce changes in a consistent and relatively similar manner across subjects, but those changes are expressed in an individual manner in every subjects due the specificity of their biophysical, social, psychological, comorbidities and genetic state or background, and the time under the influence of the symptom. These is summarized in the simple scheme from figure 4.13.

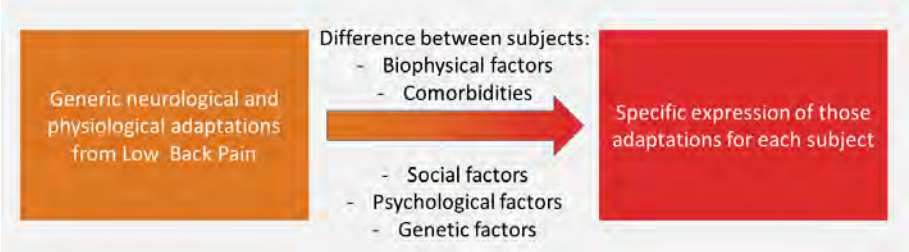

Figure 4.13: Hypothesis diagram.

If factually proven, this hypothesis could provide a useful and simple framework to answer diversity issue of the NSLBP population. Indeed, it is extremely hard to recruit population samples that all showcase the same profile on the 5 main domains and we can rightfully suppose that NSLBP samples studied so far most likely differed in other domains as the domains are rarely all controlled for. The heterogeneity of the main factors in the population samples would drive the expression of the NSLBP in different directions, accordingly to the different subject's profiles, explaining the extreme variability of this population and the vastly different reactions to rehabilitation protocols.

Conclusion

This study led to interesting results concerning NSLBP and its major problem to date, its population extreme diversity in profile and responses to treatment, and the unsolved task of subgrouping that same population. The present work attempted the exploratory analysis and clustering on a NSLBP population sample through the framework of continuous variables instead of categorical variables, usually favored. Its results provided insights on where to go and how to look at NSLBP.

The direct findings from this work can gathered into the following points:

- Higher level data, or "meta data" linked to the main domains influencing NSLBP prognosis should receive more attention when attempting to cluster and no domains should be discarded (a case could be made for the genetic domain due to the complexity of the task to study it).
- Dynamic conditions used to acquire data in order to study clustering of the NSLBP population should be kept as simple as possible in order to prevent the complexification of the clustering task.
- As the importance of relationships with NSLBP for each variables is dependent on the condition performed, care should be put into which variables are looked at, for each of the conditions studied. Exploratory work before attempting clustering of a population should be considered and the associated results shared along the clustering results.
- Back flexion and trunk rotation seems to be the movements to be privileged as the dynamic condition of choice for data acquisition.
- Tools that have the capacity to detect and model complex and subtle relationships should be privileged. Great importance should be placed into the choice of data analysis and tools framework used to process data from NSLBP when attempting to cluster it.
- Spectral clustering algorithm using RBF kernel seems to be the choice to favor if using classic clustering algorithm.
- Objective dimension reduction is to be used, whether through the use of unsupervised algorithm, via PCA for example, or through the use of objective exploratory analysis which would yield objective guideline on the variables to focus on.

Beyond these recommendations directly deduced from the findings from our work, we went further and hypothesized, through the combination of the findings from our work and the ones from others, the following new NSLBP paradigm Hypothesis:

> Non specific low back pain yields common adaptations in every subject, but due to inter-subject differences in the 5 domains known to have a major influence on LBP prognosis, these adaptations are expressed in a very unique way in each subject.

This new paradigm hypothesis if proven true through subsequent works, would allow for the researchers to study the fundamental and common adaptations from NSLBP and their expressions; and for the clinicians to apply this new paradigm straight away into their practice to manage NSLBP patients through personalized and more effective therapeutic protocols, without the need for new or expensive equipment and or complex new techniques. This new paradigm would of course not solve instantly the NSLBP question and associated problems. But rather open a door to finally understand the symptom itself, instead of trying to put up with its complexity. Allowing researchers, clinicians and patients to move forward, towards a solution to non specific low back pain.

Appendix

Compute the cluster Local Coordinate System: `LCScluster()`

```
function [measured_origin, measured_X, measured_Y,
↪  measured_Z,rotMat2systems] = LCScluster(measured_left,
↪  measured_right, measured_mid, control_left, control_right,
↪  control_mid, control_origin)
%% This function compute the LCS of the cluster in regards to its
↪  control data
% By this we mean the data when the cluster is set to be in a
↪  neutral
% position, his Local Coordinate System being equivalent to the
% Global Coordinate System.
%
% Sources:
% Wikipedia contributors. (2021, February 8). Rotation matrix. In
↪  Wikipedia, The Free Encyclopedia. Retrieved 22:44, February 8,
↪  2021, from
↪  https://en.wikipedia.org/w/index.php?title=Rotation_matrix&oldid=1005511626
%
% Contact: lucien.robinault@protonmail.com

%% 1. COMPUTE THE MEASURED LCS FOR THE CLUSTER
% Compute the centroid of the cluster of marker
measured_centroid = centrdTri3D(measured_left, measured_right,
↪  measured_mid);

% Create the cluster LCS
% Y axis
measured_LCSy = measured_right - measured_left;
```

```
19
20  % X axis
21  measured_midPos = measured_left+(measured_LCSy/2);
22  measured_midVec = measured_mid-measured_midPos;
23  measured_LCSx = cross(measured_LCSy,measured_midVec);
24
25  % Z axes
26  measured_LCSz = cross(measured_LCSy, measured_LCSx);
27
28  % X axes
29  measured_LCSx = cross(measured_LCSz,measured_LCSy);
30
31
32  % Normalizing vectors
33  if numel(measured_LCSx)>3
34      for i = 1:1:length(measured_LCSz)
35          measured_LCSx(:,i) =
             ↪  measured_LCSx(:,i)/norm(measured_LCSx(:,i));
36          measured_LCSy(:,i) =
             ↪  measured_LCSy(:,i)/norm(measured_LCSy(:,i));
37          measured_LCSz(:,i) =
             ↪  measured_LCSz(:,i)/norm(measured_LCSz(:,i));
38      end
39  else
40      measured_LCSx = measured_LCSx/norm(measured_LCSx);
41      measured_LCSy = measured_LCSy/norm(measured_LCSy);
42      measured_LCSz = measured_LCSz/norm(measured_LCSz);
43  end
44
45  %% 2. COMPUTE THE CONTROL LCS FOR THE CLUSTER
46  % Compute the centroid of the cluster of marker
47  control_centroid = centrdTri3D(control_left, control_right,
     ↪  control_mid);
48
49  % Create the cluster LCS
50  % Y axis
51  control_LCSy = control_right - control_left;
52
53  % X axis
54  control_midPos = control_left+(control_LCSy/2);
55  control_midVec = control_mid-control_midPos;
56  control_LCSx = cross(control_LCSy,control_midVec);
```

```
57
58  % Z axes
59  control_LCSz = cross(control_LCSy, control_LCSx);
60
61  % X axes
62  control_LCSx = cross(control_LCSz,control_LCSy);
63
64
65  % Normalizing vectors
66
67  control_LCSx =  control_LCSx/norm(control_LCSx);
68  control_LCSy =  control_LCSy/norm(control_LCSy);
69  control_LCSz =  control_LCSz/norm(control_LCSz);
70
71  %% 3. COMPUTE THE ROTATION BETWEEN MEASURED_LCS AND CONTROL_LCS
72  % Rotation matrix control
73  rotMatControl = [control_LCSx,control_LCSy,control_LCSz];
74
75  % Rotation matrix measured
76  if numel(measured_LCSx)>3
77      rotMatMeasured(1,1,:) = measured_LCSx(1,:);
78      rotMatMeasured(2,1,:) = measured_LCSx(2,:);
79      rotMatMeasured(3,1,:) = measured_LCSx(3,:);
80
81      rotMatMeasured(1,2,:) = measured_LCSy(1,:);
82      rotMatMeasured(2,2,:) = measured_LCSy(2,:);
83      rotMatMeasured(3,2,:) = measured_LCSy(3,:);
84
85      rotMatMeasured(1,3,:) = measured_LCSz(1,:);
86      rotMatMeasured(2,3,:) = measured_LCSz(2,:);
87      rotMatMeasured(3,3,:) = measured_LCSz(3,:);
88  else
89      rotMatMeasured(1,1) = measured_LCSx(1);
90      rotMatMeasured(2,1) = measured_LCSx(2);
91      rotMatMeasured(3,1) = measured_LCSx(3);
92
93      rotMatMeasured(1,2) = measured_LCSy(1);
94      rotMatMeasured(2,2) = measured_LCSy(2);
95      rotMatMeasured(3,2) = measured_LCSy(3);
96
97      rotMatMeasured(1,3) = measured_LCSz(1);
98      rotMatMeasured(2,3) = measured_LCSz(2);
```

```
    rotMatMeasured(3,3) = measured_LCSz(3);
end

%% 4. ROTATE THE TRANSLATION VECTOR AND APPLY THE TRANSLATION OF THIS NEW
%     FOUND VECTOR TO GET THE ORIGIN OF THE DEFINITIVE CLUSTER'S LCS
control_translation = (control_origin-control_centroid);
if numel(measured_LCSx)>3
    for i = 1:1:length(measured_LCSz)
        rotMat2systems(:,:,i) = rotMatControl*rotMatMeasured(:,:,i)';
        translationRotated(:,i) = control_translation'*rotMat2systems(:,:,i);
    end
else
    rotMat2systems(:,:) = rotMatControl*rotMatMeasured(:,:)';
    translationRotated(:) = control_translation'*rotMat2systems(:,:);
end
measured_origin = measured_centroid+translationRotated;

measured_X = {measured_LCSx, control_LCSx,measured_centroid};
measured_Y = {measured_LCSy, control_LCSy,control_centroid};
measured_Z = {measured_LCSz, control_LCSz};
end
```

Find the section of interest boundaries: `trigBound()`

```
function [start, stop] = trigBound(signal)
    % Find the trigger boundary of the HD EMG files
    % Signal acquisition frequency
    fqAcq = 2048;

    % Offset frames (231)
    offsetBound = 241; % A margin of has been added to deal with
    ↪  eventual misshap

    % Values used as limit for the detection
    limValue = 9;

    % Filter out two major noise band
    filtSig = bandstop(bandstop(signal, [48 52],fqAcq),[148 152],
    ↪  fqAcq);

    % Find the limits
    trigSup = find(filtSig>limValue);

    trigInf = find(filtSig(trigSup(1):end)<limValue);
    diffInf = diff(trigInf);

    start = trigInf(1)+trigSup(1)-offsetBound;
    if(sum(diffInf)==length(diffInf))
        stop = trigInf(end)+offsetBound+1;
    else
        stop = trigInf(diffInf>1)+trigSup(1)+offsetBound+1;
    end
end
```

Baseline Wander filter: `BWfilt()`

```
function EMG_proper = BWfilt(sigToFilt, varargin)
%% Based on Fasano, A., & Villani, V. (2014). Baseline wander removal for bioelectrical signals by quadratic variation reduction. Signal Processing, 99, 48-57.
% This function filter out baseline wander also called baseline fluctation
% from classic EMG signal
% Contact: lucien.robinault@protonmail.com

%%%%%%%%%%%%%%%%%%%%%%%%%%%%%%%%%%%%%%%%%%%%%%%%%%%%%%%%%%%%%%%%%%%%%%%%%%%%%%%
% INPUTS
%%%%%%%%%%%%%%%%%%%%%%%%%%%%%%%%%%%%%%%%%%%%%%%%%%%%%%%%%%%%%%%%%%%%%%%%%%%%%%%
%   sigToFilt --> Signals to filter (must be of a shape N*1
%       setpL --> The step used in the gradient descent function to find the
%                 optimal lambda. The early test showed good result with
%                 lambda around the [600:700] mark.
%                 default value = 25;
% formulaUsed --> Formula used for the gradient descent (more details
%                 below)
%                 1 = s^x
%                 2 = tanh(a*s^b)
%                 3 = -log10(1+s)
%                 default value = 3;
%           x --> parameter from the sparsity formula 1
%                 default value = 2;
%           a --> parameter from the sparsity formula 2
%                 default value = 1;
%           b --> parameter from the sparsity formula 2
%                 default value = 2;

%%%%%%%%%%%%%%%%%%%%%%%%%%%%%%%%%%%%%%%%%%%%%%%%%%%%%%%%%%%%%%%%%%%%%%%%%%%%%%%
% OUTPUTS
%%%%%%%%%%%%%%%%%%%%%%%%%%%%%%%%%%%%%%%%%%%%%%%%%%%%%%%%%%%%%%%%%%%%%%%%%%%%%%%
% EMG_proper --> EMG signals filtered

%% DISCLAIMERS
% CALCUL OPTIMIZATION:
```

```
%     This filter uses a matrix inversion of a matrix of the size N*N, thus
%     being extremely costly memory and computationally wise. Because the
%     matrix is a tridiagonal, symmetric, positive-definite system it is
%     possible to "linearize" the calculus. To do so the equation (16) have
%     been developed,and the linear system solver "\" has been used to "get rid of"
%     the standard inverse calculation. This is possible due to the
%     aforementioned specific properties of the system.
%     More details and explanation can be found in the books from Golub on
%     matrix computation.
%     Nonetheless, clear optimization process not being detailed in
%     Fasano et al, 2014, the optimization process implemented here might not be
%     the one used by the author of the article

% GRADIENT DESCENT:
%     The process to find the optimal lambda for the filter is not detailed
%     in Fasano et al., 2014. Therefore, the process implemented here is of
%     my own design.
%     The logic behind it is, we are facing a signal away from the baseline
%     it should be on, which is 0. The filter is trying to get the signal
%     back on this baseline. As the signal get filtered closer and closer to
%     the baseline, the number of 0 value increase.
%     We therefore can formulate the problem as a sparsity problem.
%     The gradient descent work on the following logic:
%     if sparsity of sFilt(n-1) - sparsity of sFilt(n) < 0 then stop
%     we found the optimal lambda.
%     The formula used have been chosen from Hurley, N., & Rickard, S. (2009). Comparing measures of sparsity. IEEE Transactions on Information Theory, 55(10), 4723-4741, and selected for their behavior that seemed to get close to the optimal lambda found experimentally.
```

```
61  %     The default formula (3) seems to be the best.
62  %     Customization of the parameters of the formula (1) and (2)
    ↪  have been
63  %     made possible but is not recommended.
64  %     Multiple formula had been chosen in the first place due to
    ↪  them being
65  %     used on an unoptimized algorithm and therefore were showing
    ↪  different
66  %     computation time. This is not relevant anymore and formula
    ↪  (1) and (2)
67  %     might be deleted if extensive testing show that formula (3)
    ↪  does the job.
68
69  %% INITIALIZATION
70  % Default value for the parameters
71  defaultStepL = 25;
72  defaultFormulaUsed = 3;
73  expectedFormula = [1, 2 ,3];
74  defaulta = 1;
75  defaultb = 2;
76  defaultx = 2;
77
78  % To prevent the need to to that for the user (I am too lazy to go
    ↪  back
79  % into the math formula of the filter to correct that directly)
80  sigToFilt = sigToFilt';
81
82  % Function handle for the testing if parameter value is numeric
83  validNumericParameter = @(x) isnumeric(x);
84
85  % Create the input parser (IP) object
86  inParser = inputParser;
87
88  % Requiered input
89  addRequired(inParser,'sigToFilt');
90
91  % Main parameters
92  addParameter(inParser,'stepL',defaultStepL,validNumericParameter);
93  addParameter(inParser,'formulaUsed',defaultFormulaUsed,@(formulaChoice)
    ↪  (ismember(formulaChoice,expectedFormula)));
94
95  % Formula 1 parameter
```

```
addParameter(inParser,'x',defaultx,validNumericParameter);

% Formula 2 parameters
addParameter(inParser,'a',defaulta,validNumericParameter);
addParameter(inParser,'b',defaultb,validNumericParameter);

% Parse the argument into the IP object
parse(inParser,sigToFilt,varargin{:});

lengthSignal = length(inParser.Results.sigToFilt);


switch inParser.Results.formulaUsed
    %% FORMULA 1
    case 1
       % First step of the filter
        lambda = 0.1;
        for stepInit = 1:1:3
            % Creating the compressed matrix I+L*D'D from (16)
    systemD = spdiags([-lambda*ones(1,lengthSignal);,...
    [lambda+1, 2*lambda*ones(1,lengthSignal-2)+1, lambda+1];,...
    -lambda*ones(1,lengthSignal)]',-1:1,lengthSignal,lengthSignal);
            % Eq (16) developped and optimized from Fasano et al.,
            ↪ 2014
            % This is the actual filtering process
            EMG_proper = inParser.Results.sigToFilt-systemD\,...
            inParser.Results.sigToFilt;

            % Compute the sparsity value of the filtered signal
            sparsity(stepInit) =
            ↪ sqrt(sum(EMG_proper.^inParser.Results.x));

            % Increase lambda by stepL
            lambda = lambda + inParser.Results.stepL;
        end

        % Filtering
        while (diff([(diff([sparsity(1) sparsity(2)]).*sparsity(1))
        ↪ (diff([sparsity(2) sparsity(3)]).*sparsity(2))])>0)
            % Increase lambda by stepL
            lambda = lambda+inParser.Results.stepL;

```

```
135             % Creating the compressed matrix I+L*D'D from (16)
136         systemD = spdiags([-lambda*ones(1,lengthSignal);,...
137         [lambda+1, 2*lambda*ones(1,lengthSignal-2)+1, lambda+1];,...
138         -lambda*ones(1,lengthSignal)]',-1:1,lengthSignal,lengthSignal);
139             % Eq (16) developped and optimized from Fasano et al.,
                ↪ 2014
140             % This is the actual filtering process
141             EMG_proper = inParser.Results.sigToFilt-systemD\,...
142             inParser.Results.sigToFilt;
143
144             % Refresh the sparsity values to n-2, n-1, n
145             sparsity(1) = sparsity(2);
146             sparsity(2) = sparsity(3);
147             sparsity(3) = sqrt(sum(EMG_proper.^inParser.Results.x));
148         end
149
150     %% FORMULA 2
151     case 2
152         % First step of the filter
153         lambda = 0.1;
154         for stepInit = 1:1:3
155             % Creating the compressed matrix I+L*D'D from (16)
156         systemD = spdiags([-lambda*ones(1,lengthSignal);,...
157         [lambda+1, 2*lambda*ones(1,lengthSignal-2)+1, lambda+1];,...
158         -lambda*ones(1,lengthSignal)]',-1:1,lengthSignal,lengthSignal);
159             % Eq (16) developped and optimized from Fasano et al.,
                ↪ 2014
160             % This is the actual filtering process
161             EMG_proper = inParser.Results.sigToFilt-systemD\,...
162             inParser.Results.sigToFilt;
163
164             % Compute the sparsity value of the filtered signal
165             sparsity(stepInit) =,...
166
                ↪ -sum(tanh((inParser.Results.a*EMG_proper).^inParser.Results.b));
167
168             % Increase lambda by stepL
169             lambda = lambda + inParser.Results.stepL;
170         end
171         % Filtering
172         while (diff([(diff([sparsity(1) sparsity(2)]).*sparsity(1))
            ↪ (diff([sparsity(2) sparsity(3)]).*sparsity(2))])>0)
```

```
173             % Increase lambda by stepL
174             lambda = lambda+inParser.Results.stepL;
175 
176             % Creating the compressed matrix I+L*D'D from (16)
177         systemD = spdiags([-lambda*ones(1,lengthSignal);,...
178         [lambda+1, 2*lambda*ones(1,lengthSignal-2)+1, lambda+1];,...
179         -lambda*ones(1,lengthSignal)]',-1:1,lengthSignal,lengthSignal);
180             % Eq (16) developped and optimized from Fasano et al.,
                ↪  2014
181             % This is the actual filtering process
182             EMG_proper = inParser.Results.sigToFilt-systemD\,...
183             inParser.Results.sigToFilt;
184 
185             % Refresh the sparsity values to n-2, n-1, n
186             sparsity(1) = sparsity(2);
187             sparsity(2) = sparsity(3);
188             sparsity(3) =,...
189 
                  ↪  -sum(tanh((inParser.Results.a*EMG_proper).^inParser.Results.b));
190         end
191 
192         %% FORMULA 3
193         case 3
194             % First step of the filter
195             lambda = 0.1;
196             for stepInit = 1:1:3
197             % Creating the compressed matrix I+L*D'D from (16)
198         systemD = spdiags([-lambda*ones(1,lengthSignal);,...
199         [lambda+1, 2*lambda*ones(1,lengthSignal-2)+1, lambda+1];,...
200         -lambda*ones(1,lengthSignal)]',-1:1,lengthSignal,lengthSignal);
201             % Eq (16) developped and optimized from Fasano et al.,
                ↪  2014
202             % This is the actual filtering process
203             EMG_proper = inParser.Results.sigToFilt-systemD\,...
204             inParser.Results.sigToFilt;
205 
206             % Compute the sparsity value of the filtered signal
207             sparsity(stepInit) = sum(-log(1+EMG_proper));
208 
209             % Increase lambda by stepL
210             lambda = lambda + inParser.Results.stepL;
211         end
```

```
212
213         % Filtering
214         while (diff([(diff([sparsity(1) sparsity(2)]).*sparsity(1))
            ↪  (diff([sparsity(2) sparsity(3)]).*sparsity(2))])>0)
215             % Increase lambda by stepL
216             lambda = lambda+inParser.Results.stepL;
217
218             % Creating the compressed matrix I+L*D'D from (16)
219     systemD = spdiags([-lambda*ones(1,lengthSignal);,...
220     [lambda+1, 2*lambda*ones(1,lengthSignal-2)+1, lambda+1];,...
221     -lambda*ones(1,lengthSignal)]',-1:1,lengthSignal,lengthSignal);
222             % Eq (16) developped and optimized from Fasano et al.,
                ↪  2014
223             % This is the actual filtering process
224             EMG_proper = inParser.Results.sigToFilt-systemD\,...
225             inParser.Results.sigToFilt;
226
227             % Refresh the sparsity values to n-2, n-1, n
228             sparsity(1) = sparsity(2);
229             sparsity(2) = sparsity(3);
230             sparsity(3) = sum(-log(1+EMG_proper));
231         end
232 end
233
234 % Same as for sigToFilt
235 EMG_proper = EMG_proper';
236 end
```

Electrocardiogram artifacts filter: `ACGartRm()`

```
function [EMG_proper, ECG_proper] = ECGartRm(sigToFilt, fqAcq)
%% Based on Mak, J. N., Hu, Y., & Luk, K. D. (2010). An automated ECG-artifact removal method for trunk muscle surface EMG recordings. Medical engineering & physics, 32(8), 840-848.
% This function filter out ECG componant from High Density EMG signal
% Contact: lucien.robinault@protonmail.com
%%%%%%%%%%%%%%%%%%%%%%%%%%%%%%%%%%%%%%%%%%%%%%%%%%%%%%%%%%%%%%%%%%%
% INPUTS
%%%%%%%%%%%%%%%%%%%%%%%%%%%%%%%%%%%%%%%%%%%%%%%%%%%%%%%%%%%%%%%%%%%
% sigToFilt --> Signals to filter, with COLUMNS = Samples & ROWS = Sources
% fqAcq     --> Acquisition frequency of the EMG signals

%%%%%%%%%%%%%%%%%%%%%%%%%%%%%%%%%%%%%%%%%%%%%%%%%%%%%%%%%%%%%%%%%%%
% OUTPUTS
%%%%%%%%%%%%%%%%%%%%%%%%%%%%%%%%%%%%%%%%%%%%%%%%%%%%%%%%%%%%%%%%%%%
% EMG_proper --> EMG signals filtered, with COLUMNS = Samples & ROWS = Sources
% ECG_Proper --> ECG signals taken out, with COLUMNS = Samples & ROWS = Sources

%%%%%%%%%%%%%%%%%%%%%%%%%%%%%%%%%%%%%%%%%%%%%%%%%%%%%%%%%%%%%%%%%%%
% PART 1: Signal pre-processing and fastICA
%%%%%%%%%%%%%%%%%%%%%%%%%%%%%%%%%%%%%%%%%%%%%%%%%%%%%%%%%%%%%%%%%%%
% fastICA
[ICAsig, sepMat, mixMat] = fastica(sigToFilt);
[rowIcaSig, colIcaSig] = size(ICAsig);
EMGvsECG = zeros(rowIcaSig, 1);

% Pre processing based on
% Myers, L. ., Lowery, M., O'Malley, M., Vaughan, C. ., Heneghan, C., St Clair Gibson, A., ... Sreenivasan, R. (2003). Rectification and non-linear pre-processing of EMG signals for cortico-muscular analysis. Journal of Neuroscience Methods, 124(2), 157-165. doi:10.1016/s0165-0270(03)00004-9
% as seen in Mak et al., 2010
for i=1:1:rowIcaSig
    % Hilbert transform
    sigToFiltH(i,:) = hilbert(ICAsig(i,:)./max(ICAsig(i,:)));
```

```
31
32      % get the a value of the complex number
33      sigToFiltH(i,:) = abs(sigToFiltH(i,:));
34
35      % Median filter order 50
36      sigToFiltH(i,:) = medfilt1(sigToFiltH(i,:),50);
37
38      % THIS PART HAS BEEN ADDED BY EMPIRICAL EVIDENCE
39      % IN ORDER FOR THE FILTER TO WORK IN THE FIELD
40      % Moving average filter to smooth potential artifact on the ECG
        ↪ signal
41      % (multiple crests) that can appear in field conditions
42      windowWidth = round(fqAcq*0.05);
43      kernel = ones(windowWidth,1) / windowWidth;
44      sigToFiltH(i,:) = filter(kernel, 1, sigToFiltH(i,:));
45  end
46
47  S1 = sigToFiltH;
48
49  for i = 1:1:rowIcaSig
50      %%%%%%%%%%%%%%%%%%%%%%%%%%%%%%%%%%%%%%%%%%%%%%%%%%%%%%%%%%%%%%%%%%%%
51      % PART 2: Peak detection
52      %%%%%%%%%%%%%%%%%%%%%%%%%%%%%%%%%%%%%%%%%%%%%%%%%%%%%%%%%%%%%%%%%%%%
53      % Searching for peaks in a source component
        ↪ signals(n)was
54      % accomplished by a simple peak detection algorithm as follows:
55
56      % 1. Scan the signals(n) which may be expected to contain a
        ↪ series
57      %   of peaks and determine the maximum value Smax.
58      Smax = max(sigToFiltH(i,:));
59
60      % 2.Define a threshold as a fraction of the maximum,Th = 0.6
        ↪ Smax
61      threshold = 0.6*Smax;
62
63      % 3. Convert the signal into binary format:
64      %       if S1(n)>= Th, S(n)=1
65      %       if S1(n)< Th, S(n)=0
66      S1(i,sigToFiltH(i,:)>=threshold) = 1;
67      S1(i,sigToFiltH(i,:)<threshold) = 0;
68
```

```
69      % 4. Calculate the rate of change of signal S1(n),
70      %   i.e. the first derivativeof S(n), which is approximated as:
71      %   s2(n)=s1(n)-s1(n-1),n=2,3, ..., N
72      %   where N is the number of samples
73      S2(i,1) = 0;
74      for j = 2:1:colIcaSig
75          S2(i,j) = S1(i,j) - S1(i,j-1);
76      end
77
78      % 5. Select those samples for which the corresponding S2(n)
        ↪  value is equal
79      %   to one, that is, having a positive rate of change:
80      %   P={n|s2(n)=1}
81      %   The setPdefine as above contains the indices of the peaks
        ↪  ins(n).
82      P{i} = find(S2(i,:) == 1);
83
84      %%%%%%%%%%%%%%%%%%%%%%%%%%%%%%%%%%%%%%%%%%%%%%%%%%%%%%%%%%%%
85      % PART 3: Identification of ECG source components
86      %%%%%%%%%%%%%%%%%%%%%%%%%%%%%%%%%%%%%%%%%%%%%%%%%%%%%%%%%%%%
87      % 1. Number of peaks:
88      %   (200 BPM/60 s)·d>=|P|>=(40 BPM/60 s)*d
89      %   where |P| indicates the number of elements in the set P,
        ↪  that is
90      %   the number of peaks detected,
91      %   and d represents the length of source component signal (in
        ↪  second).
92      limPeaksLow = (40/60)*(colIcaSig/fqAcq);
93      limPeaksHigh = (200/60)*(colIcaSig/fqAcq);
94
95      % 2. RR interval:
96      %   1.5 s>=P(n+1)-P(n)>=0.3s, n=1,2,...,N
97      %   where P(n) represents the time information of thenth
        ↪  detected peak.
98      %   Nis the number of peaks detected. 1.5 s is the averaged RR
        ↪  interval
99      %   value with a heart rate of 40 BPM and 0.3 s is
100     %   the averaged RR interval value with a heart rate of 200
        ↪  BPM.
101     limRRlow = 0.3*fqAcq;
102     limRRhigh = 1.5*fqAcq;
103
```

```
    % 3. Variance of RR intervals:
    %   [P(n+2)-P(n+1)]-[P(n+1)-P(n)]<=R*(1.5s),n=1,2,..., N
    %   where 1.5 s is the upper limit of the RR interval value.
    %   A scaling factor R of 0.5 was adopted in this study.
    R = 0.5;
    limVarRR = 0.5*1.5*fqAcq;

    % Is the ICA signal a ECG component?
    check1 = false;
    check2 = false;
    check3 = false;

    % Check Number of peaks
    if (length(P{i})<=limPeaksHigh)&&(length(P{i})>=limPeaksLow)
        check1 = true;
    end

    % Check RR interval
    intervalCheck = zeros(length(P{i})-1,1);
    for j = 1:1:length(P{i})-1
        test2 = P{i}(j+1)- P{i}(j);
        if (test2<=limRRhigh)&&(test2>=limRRlow)
            intervalCheck(j) = 1;
        end
    end

    % THE 10% ERROR ALLOWED HAS BEEN ADDED BY EMPIRICAL EVIDENCE
    % IN ORDER FOR THE FILTER TO WORK IN THE FIELD
    % It might be optional though
    if sum(intervalCheck)>=(floor((length(P{i})-1)*0.90))
        check2 = true;
    end

    % Check Variance of RR intervals
    varianceCheck = zeros(length(P{i})-2,1);
    for j = 1:1:length(P{i})-2
        test3 = (P{i}(j+2)-P{i}(j+1)) - (P{i}(j+1)-P{i}(1));
        if test3 <= (R*1.5*fqAcq)
            varianceCheck(j) = 1;
        end
    end

```

```
146     if sum(varianceCheck)==(length(P{i})-2)
147         check3 = true;
148     end
149 
150     % Check all the conditions
151     % EMGvsECG = 1 --> ECG component
152     % EMGvsECG = 0 --> EMG component
153     if check1 && check2 && check3
154         EMGvsECG(i) = 1;
155     end
156 
157 end
158 
159 %%%%%%%%%%%%%%%%%%%%%%%%%%%%%%%%%%%%%%%%%%%%%%%%%%%%%%%%%%%%%%%%%%%%%%%
160 % PART 4: Reconstruct EMG
161 %%%%%%%%%%%%%%%%%%%%%%%%%%%%%%%%%%%%%%%%%%%%%%%%%%%%%%%%%%%%%%%%%%%%%%%
162 
163 EMG_proper = sepMat(:,~EMGvsECG)*ICAsig(~EMGvsECG,:);
164 
165 
166 %%%%%%%%%%%%%%%%%%%%%%%%%%%%%%%%%%%%%%%%%%%%%%%%%%%%%%%%%%%%%%%%%%%%%%%
167 % PART 3: Reconstruct ECG
168 %%%%%%%%%%%%%%%%%%%%%%%%%%%%%%%%%%%%%%%%%%%%%%%%%%%%%%%%%%%%%%%%%%%%%%%
169 
170 ECG_proper =
    ↪  sepMat(:,logical(EMGvsECG))*ICAsig(logical(EMGvsECG),:);
171 
172 end
```

Extreme artifacts filter: `ACGartRm()`

```
function [filtered]=distriFilter(rawSignal, upperLim, lowerLim)
% Filter EMG values on the edges of the distribution below lowerLim and
% above upperLim value

% rawSignal must be in the form rawSignal(X,:)

% Get the distribution of the values
dataHist = histogram(rawSignal);


distribEdges = cumsum(dataHist.BinCounts);
prctDistri = distribEdges/distribEdges(end);

lowerValue = find(prctDistri<lowerLim);
upperValue = find(prctDistri>upperLim);
lowerValue = dataHist.BinEdges(lowerValue(end)+1);
upperValue = dataHist.BinEdges(upperValue(1));

filtered = rawSignal;

filtered(filtered<lowerValue) = median(rawSignal);
filtered(filtered>upperValue) = median(rawSignal);

end
```

PLI, WGN and MA filtering: `EMGccaFilt()`

```
function EMG_proper = EMGccaFilt(sigToFilter, fqAcq)
%% Based on Al Harrach, M., Boudaoud, S., Hassan, M., Ayachi, F. S., Gamet, D., Grosset, J. F., & Marin, F. (2017). Denoising of HD-EMG signals using canonical correlation analysis. Medical & biological engineering & computing, 55(3), 375-388.
% This function remove movement artifact, white noise (WGN) and power line inference (PLI)
% Contact: lucien.robinault@protonmail.com
%%%%%%%%%%%%%%%%%%%%%%%%%%%%%%%%%%%%%%%%%%%%%%%%%%%%%%%%%%%%%%%%%%%%%%%%%%%%
%%%%%%%%%%%%%%%%%%%%%%%%%%/!\IMPORTANT/!\%%%%%%%%%%%%%%%%%%%%%%%%%%%%%%%%%%%

% The function need the first 0.5 seconds of signals to contain no muscle
% activity.
% ECG contamination prevent successful use most of the time, it is vividly
% recommended to filter them out before. A function serving this purpose is
% available in this repository
%%%%%%%%%%%%%%%%%%%%%%%%%%%%%%%%%%%%%%%%%%%%%%%%%%%%%%%%%%%%%%%%%%%%%%%%%%%%

% Power line interference (PLI) from HD EMG signals
%%%%%%%%%%%%%%%%%%%%%%%%%%%%%%%%%%%%%%%%%%%%%%%%%%%%%%%%%%%%%%%%%%%%%%%%%%%%
% INPUTS
%%%%%%%%%%%%%%%%%%%%%%%%%%%%%%%%%%%%%%%%%%%%%%%%%%%%%%%%%%%%%%%%%%%%%%%%%%%%
% sigToFilter --> Signals to filter, with COLUMNS = Samples & ROWS = Sources
% fqAcq      --> Acquisition frequency of the EMG signals

%%%%%%%%%%%%%%%%%%%%%%%%%%%%%%%%%%%%%%%%%%%%%%%%%%%%%%%%%%%%%%%%%%%%%%%%%%%%
% OUTPUTS
%%%%%%%%%%%%%%%%%%%%%%%%%%%%%%%%%%%%%%%%%%%%%%%%%%%%%%%%%%%%%%%%%%%%%%%%%%%%
% EMG_proper --> EMG signals filtered, with COLUMNS = Samples & ROWS = Sources


%%%%%%%%%%%%%%%%%%%%%%%%%%%%%%%%%%%%%%%%%%%%%%%%%%%%%%%%%%%%%%%%%%%%%%%%%%%%
%% PART I: CANONICAL CORRELATION ANALSYS
%%%%%%%%%%%%%%%%%%%%%%%%%%%%%%%%%%%%%%%%%%%%%%%%%%%%%%%%%%%%%%%%%%%%%%%%%%%%
[rowSig, colSig] = size(sigToFilter);
```

```
32
33  % Create a lagged signal to improve quality of the CCA result
34  laggedSigToFilter = [sigToFilter(:, end) sigToFilter(:, 1:(end-1))];
35
36  % CCA operation
37  [A, B, r, U, V] = canoncorr(sigToFilter', laggedSigToFilter');
38  [lenU, compU] = size(U);
39
40
41
42  %%%%%%%%%%%%%%%%%%%%%%%%%%%%%%%%%%%%%%%%%%%%%%%%%%%%%%%%%%%%%%%%%%%%%%%%
43  %% PART II: CCA COMPONENT THRESHOLDING
44  %%%%%%%%%%%%%%%%%%%%%%%%%%%%%%%%%%%%%%%%%%%%%%%%%%%%%%%%%%%%%%%%%%%%%%%%
45  intensityRatio = zeros(1,compU);
46
47  %% Calculus of the Intensity Ratio (IR)
48  for i = 1:1:compU
49      % Equation (6) from Al Harrach et al., 2016
50      intensityRatio(i) =  (sum(abs(U(:,i)))/length(U))*...
51          ((fqAcq*0.5)/sum(abs(U(1:round(fqAcq*0.5),i))));
52
53  end
54
55  % Check which ratio threshold is the best suited, from 1 to 4
56  for threshold = 10:1:40
57      % Check which CCA components are below or equal to the IR
58      compBelowRatio{threshold} = intensityRatio<=threshold/10;
59
60      % Put the CCA components who are <= threshold to zero
61      tempU = U;
62      tempU(:,compBelowRatio{threshold}) = 0;
63      % reconstruction of the EMG signals (temporary) to test the
        ↪  correlation
64      % of these new signals to the non filtered ones
65      cleanSignalTest = tempU / A;
66
67      % Test the correlation between these filtered signals and the
68      % unfiltered ones.
69      corrSignals{threshold} = corrcoef(cleanSignalTest,sigToFilter');
70      % If correlation is < 0.8 the CCA filtering stop and we take
        ↪  the last
71      % CCA filtering setup that had a correlation of >= 0.8.
```

```
72      % If we go up to a threshold of 4 we keep the threshold 4
        ↪  (therefore
73      % the last.
74      if ~(corrSignals{threshold}(1,2)>=0.8)
75          finalThreshold = threshold-1;
76
77          break
78      else
79          finalThreshold = threshold;
80      end
81  end
82
83  % Filtering the HD EMG signals by removing the selected components
84  tempU = U;
85  tempU(:,compBelowRatio{finalThreshold}) = 0;
86  cleanSignal = (tempU / A)';
87
88  %%%%%%%%%%%%%%%%%%%%%%%%%%%%%%%%%%%%%%%%%%%%%%%%%%%%%%%%%%%%%%%%%%%%%%%%
89  %% PART III: SELECTIVE CCA
90  %%%%%%%%%%%%%%%%%%%%%%%%%%%%%%%%%%%%%%%%%%%%%%%%%%%%%%%%%%%%%%%%%%%%%%%%
91
92  % Check if filtered signals got better PNR than the non filtered
    ↪  ones, in
93  % order to prevent noise contamination during reconstruction of the
94  % signals.
95  % This is done channel/electrode by channel/electrode
96  for i = 1:1:rowSig
97      % Calculus of the non filtered channel PNR
98      dirtySNR = 20*log10(((sum(abs(sigToFilter(i,:))))/colSig)*...
99
    ↪  ((0.5*fqAcq)/(sum(abs(sigToFilter(i,1:round(fqAcq*0.5)))))));
100
101     % Calculus of the filtered channel PNR
102     cleanSNR = 20*log10(((sum(abs(cleanSignal(i,:))))/colSig)*...
103
    ↪  ((0.5*fqAcq)/(sum(abs(cleanSignal(i,1:round(fqAcq*0.5)))))));
104
105     % Compare PNR between those two and add the highest one to the
106     % definitive filtered HD EMG matrix (EMG_proper)
107     if dirtySNR>=cleanSNR
108         EMG_proper(i,:) = sigToFilter(i,:);
109
```

```
110     else
111         EMG_proper(i,:) = cleanSignal(i,:);
112     end
113 
114 end
```

References

Abdi, Hervé, and Lynne J Williams. 2010. "Principal Component Analysis." *Wiley Interdisciplinary Reviews: Computational Statistics* 2 (4): 433–59.

Abraham, Ajith. 2005. "Artificial Neural Networks." *Handbook of Measuring System Design*.

Adler, Nancy E and Ostrove, Joan M. 1999. "Socioeconomic status and health: what we know and what we don't." *Annals of the New York academy of Sciences* 896(1): 3–15.

Al Harrach, Mariam, Sofiane Boudaoud, Mahmoud Hassan, Fouaz Sofiane Ayachi, D Gamet, Jean-François Grosset, and Frédéric Marin. 2017. "Denoising of HD-sEMG Signals Using Canonical Correlation Analysis." *Medical & Biological Engineering & Computing* 55 (3): 375–88.

Alrwaily, Muhammad and Timko, Michael and Schneider, Michael and Stevans, Joel and Bise, Christopher and Hariharan, Karthik and Delitto, Anthony. 2016. "Treatment-based classification system for low back pain: revision and update." *Physical therapy*. Oxford University Press. 96 (7) : 1057–1066

Aroke, Edwin N and Overstreet, Demario S and Penn, Terence M and Crossman, David K and Jackson, Pamela and Tollefsbol, Trygve O and Quinn, Tammie L and Yi, Nengjun and Goodin, Burel R. 2020. "Identification of DNA methylation associated enrichment pathways in adults with non-specific chronic low back pain." *Molecular Pain*. SAGE Publications Sage CA: Los Angeles, CA. 16 : 1744806920972889.

Asgari, Morteza, Mohammad Ali Sanjari, Hamid Reza Mokhtarinia, Samaneh Moeini Sedeh, Kinda Khalaf, and Mohamad Parnianpour. 2015. "The Effects of Movement Speed on Kinematic Variability and Dynamic Stability of the Trunk in Healthy Individuals and Low Back Pain Patients." *Clinical Biomechanics* 30 (7): 682–88.

Avilov, Oleksii, Sébastien Rimbert, Anton Popov, and Laurent Bougrain. 2020. "Deep Learning Techniques to Improve Intraoperative Awareness Detection from Electroencephalographic Signals." In *2020 42nd Annual International Conference of the IEEE Engineering in Medicine & Biology Society (EMBC)*, 142–45. IEEE.

Balagué, Federico and Mannion, Anne F and Pellisé, Ferran and Cedraschi, Christine. 2012. "Non-specific low back pain." *The lancet*. Elsevier. 379 (9814) : 482–491

Barbero, Marco, Roberto Merletti, and Alberto Rainoldi. 2012. *Atlas of Muscle Innervation Zones: Understanding Surface Electromyography and Its Applications*. Springer Science & Business Media.

Bartlett, Peter, Fernando Pereira, Christopher Burges, Leon Bottou, and Kilian Weinberger. 2012. "Advances in Neural Information Processing Systems 25 (NIPS 2012): 26th Annual Conference on Neural Information Processing Systems 2012."

Barton, DE. 1976. "The Advanced Theory of Statistics; Vol. II, Inference and Relationship." JSTOR.

Basly, Hend and Ouarda, Wael and Sayadi, Fatma Ezahra and Ouni, Bouraoui and Alimi, Adel M. 2020. "CNN-SVM learning approach based human activity recognition." *Image and Signal Processing: 9th International Conference, ICISP 2020, Marrakesh, Morocco, June 4–6, 2020, Proceedings 9*. Springer. 271–281.

Battié, Michele Crites, Daniel C Cherkin, Roxanne Dunn, Marcia A Ciol, and Kimberly J Wheeler. 1994. "Managing Low Back Pain: Attitudes and Treatment Preferences of Physical Therapists." *Physical Therapy* 74 (3): 219–26.

Bellman, RJNJ. 1957. "Dynamic Programming Princeton University Press Princeton." *New Jersey Google Scholar*.

Bengio, Yoshua, Yann LeCun, et al. 2007. "Scaling Learning Algorithms Towards AI." *Large-Scale Kernel Machines* 34 (5): 1–41.

Bernell, Stephanie, and Steven W Howard. 2016. "Use Your Words Carefully: What Is a Chronic Disease?" *Frontiers in Public Health* 4: 159.

Black, Paul E. 2005. "Greedy Algorithm." *Dictionary of Algorithms and Data Structures*. https://www.nist.gov/dads/HTML/greedyalgo.html; National Institute of Standards; Technology.

Black, Paul E. 2019. "Manhattan Distance." *Dictionary of Algorithms and Data Structures*. https://xlinux.nist.gov/dads/HTML/manhattanDistance.html; National Institute of Standards; Technology.

Blei, David M, and John D Lafferty. 2009. "Topic Models." In *Text Mining*, 101–24. Chapman; Hall/CRC.

Bock, Sebastian, and Martin Weiß. 2019. "A Proof of Local Convergence for the Adam Optimizer." In *2019 International Joint Conference on Neural Networks (IJCNN)*, 1–8. IEEE.

Bourigua, Imen. 2014. "Évaluation Biomécanique Des Mouvements Du Tronc Et de l'initiation de La Marche Chez Les Patients Lombalgiques Chroniques: Mise En évidence d'un déconditionnement Moteur Avant Et Après Un Programme de Restauration Fonctionnelle Du Rachis." PhD thesis, Université de Valenciennes et du Hainaut-Cambresis.

Bouter, Lex M, Maurits W van Tulder, and Bart W Koes. 1998. "Methodologic Issues in Low Back Pain Research in Primary Care." *Spine* 23 (18): 2014–20.

Bro, Rasmus, and Age K Smilde. 2014. "Principal Component Analysis." *Analytical Methods* 6 (9): 2812–31.

Brumagne, Simon, Paul Cordo, and Sabine Verschueren. 2004. "Proprioceptive

Weighting Changes in Persons with Low Back Pain and Elderly Persons During Upright Standing." *Neuroscience Letters* 366 (1): 63–66.

Brumagne, Simon, Lotte Janssens, Evelien Janssens, and Lieselotte Goddyn. 2008. "Altered Postural Control in Anticipation of Postural Instability in Persons with Recurrent Low Back Pain." *Gait & Posture* 28 (4): 657–62.

Brumagne, Simon, Roeland Lysens, and Arthur Spaepen. 1999. "Lumbosacral Position Sense During Pelvic Tilting in Men and Women Without Low Back Pain: Test Development and Reliability Assessment." *Journal of Orthopaedic & Sports Physical Therapy* 29 (6): 345–51.

Buchbinder, Rachelle and van Tulder, Maurits and Öberg, Birgitta and Costa, Lucíola Menezes and Woolf, Anthony and Schoene, Mark and Croft, Peter and Hartvigsen, Jan and Cherkin, Dan and Foster, Nadine E and others. 2018. "The Lancet." *The Neuroscientist* 391(10137): 2384–2388.

Byl, Nancy Nies, and Patricial Sinnott. 1991. "Variations in Balance and Body Sway in Middle-Aged Adults: Subjects with Healthy Backs Compared with Subjects with Low-Back Dysfunction." *Spine* 16 (3): 325–30.

Byrne, Karol, Catherine Doody, and Deirdre A Hurley. 2006. "Exercise Therapy for Low Back Pain: A Small-Scale Exploratory Survey of Current Physiotherapy Practice in the Republic of Ireland Acute Hospital Setting." *Manual Therapy* 11 (4): 272–78.

Cao, Zheng, Benjamin Lu Davis, Wanchaloem Wunkaew, and Xinyu Chang. 2022. "Elevator Optimization: Application of Spatial Process and Gibbs Random Field Approaches for Dumbwaiter Modeling and Multi-Dumbwaiter Systems." *arXiv Preprint arXiv:2209.12401*.

Cappozzo, Aurelio, Fabio Catani, Ugo Della Croce, and Alberto Leardini. 1995. "Position and Orientation in Space of Bones During Movement: Anatomical Frame Definition and Determination." *Clinical Biomechanics* 10 (4): 171–78.

Cattell, Raymond. 2012. *The Scientific Use of Factor Analysis in Behavioral and Life Sciences*. Springer Science & Business Media.

Cauchy, Augustin-Louis. 2009. "Sur l'équation à l'aide de Laquelle on Détermine Les Inégalités Séculaires Des Mouvements Des Planètes." In *Oeuvres Complètes: Series 2*, 9:174–95. Cambridge Library Collection - Mathematics. Cambridge University Press. https://doi.org/10.1017/CBO9780511702686.009.

Chan, Catherine Qiu Hua and Lee, Kheng Hock and Low, Lian Leng. 2018. "A systematic review of health status, health seeking behaviour and healthcare utilisation of low socioeconomic status populations in urban Singapore." *International journal for equity in health* 17(1): 1–21.

Charniak, Eugene. 2021. *Introduction Au Deep Learning*. Dunod.

Chiari, Lorenzo, Laura Rocchi, and Angelo Cappello. 2002. "Stabilometric Parameters Are Affected by Anthropometry and Foot Placement." *Clinical Biomechanics* 17 (9-10): 666–77.

Cholewicki, Jacek, Alan Breen, John M Popovich Jr, N Peter Reeves, Shirley A

Sahrmann, Linda R Van Dillen, Andry Vleeming, and Paul W Hodges. 2019. "Can Biomechanics Research Lead to More Effective Treatment of Low Back Pain? A Point-Counterpoint Debate." *Journal of Orthopaedic & Sports Physical Therapy* 49 (6): 425–36.

Chollet, Francois. 2021. *Deep Learning with Python*. Simon; Schuster.

Chollet, François et al. 2015. "Keras." https://github.com/fchollet/keras; GitHub.

Collobert, Ronan, and Jason Weston. 2008. "A Unified Architecture for Natural Language Processing: Deep Neural Networks with Multitask Learning." In *Proceedings of the 25th International Conference on Machine Learning*, 160–67.

Colloca, Christopher J, and Richard N Hinrichs. 2005. "The Biomechanical and Clinical Significance of the Lumbar Erector Spinae Flexion-Relaxation Phenomenon: A Review of Literature." *Journal of Manipulative and Physiological Therapeutics* 28 (8): 623–31.

Comrey, Andrew L. 1962. "The Minimum Residual Method of Factor Analysis." *Psychological Reports* 11 (1): 15–18.

Corbeil, Philippe, Jean-Sébastien Blouin, and Normand Teasdale. 2004. "Effects of Intensity and Locus of Painful Stimulation on Postural Stability." *Pain* 108 (1-2): 43–50.

Costa, Luciola da C Menezes, Christopher G Maher, James H McAuley, Mark J Hancock, Robert D Herbert, Kathryn M Refshauge, and Nicholas Henschke. 2009. "Prognosis for Patients with Chronic Low Back Pain: Inception Cohort Study." *Bmj* 339.

Cutler, David M and Lleras-Muney, Adriana and Vogl, Tom. 2018. "Socioeconomic status and health: dimensions and mechanisms." *National Bureau of Economic Research*.

Dagenais, Simon, Jaime Caro, and Scott Haldeman. 2008. "A Systematic Review of Low Back Pain Cost of Illness Studies in the United States and Internationally." *The Spine Journal* 8 (1): 8–20.

DALYs, GBD2015, Hale Collaborators, NJ Kassebaum, M Arora, RM Barber, J Brown, A Carter, et al. 2016. "Global, Regional, and National Disability-Adjusted Life-Years (DALYs) for 315 Diseases and Injuries and Healthy Life Expectancy (HALE), 1990â 2015: A Systematic Analysis for the Global Burden of Disease Study 2015." *The Lancet* 388 (10053): 1603–58.

Della Volpe, Raimondo, T Popa, F Ginanneschi, R Spidalieri, R Mazzocchio, and A Rossi. 2006. "Changes in Coordination of Postural Control During Dynamic Stance in Chronic Low Back Pain Patients." *Gait & Posture* 24 (3): 349–55.

Deng, Dong, Li. 2014. "Deep Learning: Methods and Applications. Foundations and Trends r in Signal Processing" 7 (3-4): 197–387.

Denker, John, W Gardner, Hans Graf, Donnie Henderson, R Howard, W Hubbard, Lawrence D Jackel, Henry Baird, and Isabelle Guyon. 1988. "Neural Network Recognizer for Hand-Written Zip Code Digits." *Advances in Neural Information Processing Systems* 1.

Descarreaux, Martin, Jean-Sébastien Blouin, and Normand Teasdale. 2005. "Repositioning Accuracy and Movement Parameters in Low Back Pain Subjects and Healthy Control Subjects." *European Spine Journal* 14 (2): 185–91.

Deyo, Richard A, Daniel Cherkin, Douglas Conrad, and Ernest Volinn. 1991. "Cost, Controversy, Crisis: Low Back Pain and the Health of the Public." *Annual Review of Public Health* 12 (1): 141–56.

Deyo, Richard A, and Weinstein. 2001. "Low Back Pain." *The New England Journal of Medicine* 344 (5): 363–70.

Diday, Edwin, and JC Simon. 1976. "Clustering Analysis." In *Digital Pattern Recognition*, 47–94. Springer.

Dieën, Jaap H van, Herta Flor, and Paul W Hodges. 2017. "Low-Back Pain Patients Learn to Adapt Motor Behavior with Adverse Secondary Consequences." *Exercise and Sport Sciences Reviews* 45 (4): 223–29.

Dieën, J, NP Reeves, and G Kawchuk. 2018. "Analysis of Motor Control in Low-Back Pain Patients: A Key to Personalized Care." *J Orthop Sport Phys Ther*, 1–24.

Dimitriadou, Evgenia, Sara Dolničar, and Andreas Weingessel. 2002. "An Examination of Indexes for Determining the Number of Clusters in Binary Data Sets." *Psychometrika* 67 (1): 137–59.

Dimitrov, George V, and Nonna A Dimitrova. 1998. "Fundamentals of Power Spectra of Extracellular Potentials Produced by a Skeletal Muscle Fibre of Finite Length: Part i: Effect of Fibre Anatomy." *Medical Engineering & Physics* 20 (8): 580–87.

Ding, Shifei, Hongjie Jia, Liwen Zhang, and Fengxiang Jin. 2014. "Research of Semi-Supervised Spectral Clustering Algorithm Based on Pairwise Constraints." *Neural Computing and Applications* 24 (1): 211–19.

Dionne, Clermont E, Kate M Dunn, Peter R Croft, Alf L Nachemson, Rachelle Buchbinder, Bruce F Walker, Mary Wyatt, et al. 2008. "A Consensus Approach Toward the Standardization of Back Pain Definitions for Use in Prevalence Studies." *Spine* 33 (1): 95–103.

Directions, IO. 1983. "Standardization in Platform Stabilometry Being a Part of Posturography." *Agressologie* 24 (7): 321–26.

Downie, Aron, Christopher M Williams, Nicholas Henschke, Mark J Hancock, Raymond WJG Ostelo, Henrica CW De Vet, Petra Macaskill, et al. 2013. "Red Flags to Screen for Malignancy and Fracture in Patients with Low Back Pain: Systematic Review." *Bmj* 347.

Dubois, Jean-Daniel and Abboud, Jacques and St-Pierre, Charles and Piché, Mathieu and Descarreaux, Martin. 2014. "Neuromuscular adaptations predict functional disability independently of clinical pain and psychological factors in patients with chronic non-specific low back pain." *Journal of Electromyography and Kinesiology* 24(4): 550–557.

El-Metwally, Ashraf and Mikkelsson, Marja and Ståhl, Minna and Macfarlane, Gary J and Jones, Gareth T and Pulkkinen, Lea and Rose, Richard J and Kaprio, Jaakko. 2008. "Genetic and environmental influences on non-specific low back

pain in children: a twin study." *European Spine Journal*. Springer. 17 : 502–508.
Enthoven, Wendy TM, Judith Geuze, Jantine Scheele, Sita MA Bierma-Zeinstra, Herman J Bueving, Arthur M Bohnen, Wilco C Peul, et al. 2016. "Prevalence and 'Red Flags' Regarding Specified Causes of Back Pain in Older Adults Presenting in General Practice." *Physical Therapy* 96 (3): 305–12.
Falla, Deborah, Leonardo Gizzi, Marika Tschapek, Joachim Erlenwein, and Frank Petzke. 2014. "Reduced Task-Induced Variations in the Distribution of Activity Across Back Muscle Regions in Individuals with Low Back Pain." *PAIN®* 155 (5): 944–53.
Farina, Dario, Corrado Cescon, and Roberto Merletti. 2002. "Influence of Anatomical, Physical, and Detection-System Parameters on Surface EMG." *Biological Cybernetics* 86 (6): 445–56.
Farina, Dario, and Aleš Holobar. 2016. "Characterization of Human Motor Units from Surface EMG Decomposition." *Proceedings of the IEEE* 104 (2): 353–73.
Farina, Dario, Frédéric Leclerc, Lars Arendt-Nielsen, Olivier Buttelli, and Pascal Madeleine. 2008. "The Change in Spatial Distribution of Upper Trapezius Muscle Activity Is Correlated to Contraction Duration." *Journal of Electromyography and Kinesiology* 18 (1): 16–25.
Fasano, Antonio, and Valeria Villani. 2014. "Baseline Wander Removal for Bioelectrical Signals by Quadratic Variation Reduction." *Signal Processing* 99: 48–57.
Florek, K, L Lukaszewiez, L Perkal, H Steinhaus, and S Zubrzchi. 1951. "Sur La Liaison Et La Division Des Points d'un Ensemble Fini, Colloquium Mathematicum."
Foster, Nadine E, Kate A Thompson, G David Baxter, and James M Allen. 1999. "Management of Nonspecific Low Back Pain by Physiotherapists in Britain and Ireland: A Descriptive Questionnaire of Current Clinical Practice." *Spine* 24 (13): 1332.
Fukushima, Kunihiko. 1980. "A Self-Organizing Neural Network Model for a Mechanism of Pattern Recognition Unaffected by Shift in Position." *Biol, Cybern* 36: 193–202.
Fukushima, Kunihiko, Sei Miyake, and Takayuki Ito. 1983. "Neocognitron: A Neural Network Model for a Mechanism of Visual Pattern Recognition." *IEEE Transactions on Systems, Man, and Cybernetics*, no. 5: 826–34.
Fukushima, Kunihiko. 2007. "Neocognitron." *Scholarpedia* 2 (1): 1717.
Galar, D, and U Kumar. 2017. "Chapter 3-Preprocessing and Features." *eMaintenance*, 129–77.
Gill, Karl P, and Michael J Callaghan. 1998. "The Measurement of Lumbar Proprioception in Individuals with and Without Low Back Pain." *Spine* 23 (3): 371–77.
Gombatto, Sara P, Tricia Brock, Anthony DeLork, Glynis Jones, Erin Madden, and Chelsea Rinere. 2015. "Lumbar Spine Kinematics During Walking in People with and People Without Low Back Pain." *Gait & Posture* 42 (4): 539–44.
Gombatto, Sara P, Barbara J Norton, Shirley A Sahrmann, Michael J Strube, and

Linda R Van Dillen. 2013. "Factors Contributing to Lumbar Region Passive Tissue Characteristics in People with and People Without Low Back Pain." *Clinical Biomechanics* 28 (3): 255–61.

Goodfellow, Ian, Yoshua Bengio, and Aaron Courville. 2016. "Deep Learning, ISBN 978-0262035613." The MIT Press.

Goossens, Nina, Sofie Rummens, Lotte Janssens, Karen Caeyenberghs, and Simon Brumagne. 2018. "Association Between Sensorimotor Impairments and Functional Brain Changes in Patients with Low Back Pain: A Critical Review." *American Journal of Physical Medicine & Rehabilitation* 97 (3): 200–211.

Gouteron, Anaïs and Tabard-Fougere, Anne and Bourredjem, Abderrahmane and Casillas, Jean-Marie and Armand, Stéphane and Genevay, Stéphane. 2021. "The flexion relaxation phenomenon in nonspecific chronic low back pain: prevalence, reproducibility and flexion–extension ratios. A systematic review and meta-analysis." *European Spine Journal*. Springer. 1–16.

Gracey, Jacqueline H, Suzanne M McDonough, and G David Baxter. 2002. "Physiotherapy Management of Low Back Pain: A Survey of Current Practice in Northern Ireland." *Spine* 27 (4): 406–11.

Hamill, Joseph, Christopher Palmer, and Richard EA Van Emmerik. 2012. "Coordinative Variability and Overuse Injury." *Sports Medicine, Arthroscopy, Rehabilitation, Therapy & Technology* 4 (1): 1–9.

Hamm, Lena, Birger Mikkelsen, Johnny Kuhr, Henrik Støvring, Anders Munck, and Jakob Kragstrup. 2003. "Danish Physiotherapists' Management of Low Back Pain." *Advances in Physiotherapy* 5 (3): 109–13.

Harman, Harry H. 1976. *Modern Factor Analysis*. University of Chicago press.

Hartigan, John A, and Manchek A Wong. 1979. "Algorithm AS 136: A k-Means Clustering Algorithm." *Journal of the Royal Statistical Society. Series c (Applied Statistics)* 28 (1): 100–108.

Hartvigsen, Jan, Mark J Hancock, Alice Kongsted, Quinette Louw, Manuela L Ferreira, Stéphane Genevay, Damian Hoy, et al. 2018. "What Low Back Pain Is and Why We Need to Pay Attention." *The Lancet* 391 (10137): 2356–67.

Hasegawa, Tetsuya, Junji Katsuhira, Hiroyuki Oka, Tomoko Fujii, and Ko Matsudaira. 2018. "Association of Low Back Load with Low Back Pain During Static Standing." *PLoS One* 13 (12): e0208877.

Haskins, Robin, Peter G Osmotherly, and Darren A Rivett. 2015a. "Diagnostic Clinical Prediction Rules for Specific Subtypes of Low Back Pain: A Systematic Review." *Journal of Orthopaedic & Sports Physical Therapy* 45 (2): 61–76.

Haskins, Robin, Peter G Osmotherly, and Darren A Rivett. 2015b. "Validation and Impact Analysis of Prognostic Clinical Prediction Rules for Low Back Pain Is Needed: A Systematic Review." *Journal of Clinical Epidemiology* 68 (7): 821–32.

Hassan, Mahmoud, Sofiane Boudaoud, Jeremy Terrien, Brynjar Karlsson, and Catherine Marque. 2011. "Combination of Canonical Correlation Analysis and Empirical Mode Decomposition Applied to Denoising the Labor Electrohysterogram." *IEEE*

Transactions on Biomedical Engineering 58 (9): 2441–47.

Hawker, Gillian A, Samra Mian, Tetyana Kendzerska, and Melissa French. 2011. "Measures of Adult Pain: Visual Analog Scale for Pain (Vas Pain), Numeric Rating Scale for Pain (Nrs Pain), Mcgill Pain Questionnaire (Mpq), Short-Form Mcgill Pain Questionnaire (Sf-Mpq), Chronic Pain Grade Scale (Cpgs), Short Form-36 Bodily Pain Scale (Sf-36 Bps), and Measure of Intermittent and Constant Osteoarthritis Pain (Icoap)." *Arthritis Care & Research* 63 (S11): S240–52.

Rolli Salathé, Cornelia and Elfering, Achim. 2013. "A health-and resource-oriented perspective on NSLBP." *International Scholarly Research Notices*. Hindawi.

Hennig, Christian. 2015. "What are the true clusters?." *Pattern Recognition Letters* 64: 53–62.

Henschke, Nicholas, Christopher G Maher, Kathryn M Refshauge, Robert D Herbert, Robert G Cumming, Jane Bleasel, John York, Anurina Das, and James H McAuley. 2008. "Prognosis in Patients with Recent Onset Low Back Pain in Australian Primary Care: Inception Cohort Study." *Bmj* 337.

Henschke, Nicholas, Christopher G Maher, Kathryn M Refshauge, Robert D Herbert, Robert G Cumming, Jane Bleasel, John York, Anurina Das, and James H McAuley. 2009a. "Characteristics of Patients with Acute Low Back Pain Presenting to Primary Care in Australia." *The Clinical Journal of Pain* 25 (1): 5–11.

Henschke, Nicholas, Christopher G Maher, Kathryn M Refshauge, Robert D Herbert, Robert G Cumming, Jane Bleasel, John York, Anurina Das, and James H McAuley. 2009b. "Prevalence of and Screening for Serious Spinal Pathology in Patients Presenting to Primary Care Settings with Acute Low Back Pain." *Arthritis & Rheumatism: Official Journal of the American College of Rheumatology* 60 (10): 3072–80.

Hodges, Paul W, Jacek Cholewicki, and Jaap H Van Dieën. 2013. "Spinal Control: The Rehabilitation of Back Pain: State of the Art and Science."

Hodges, Paul W, and G Lorimer Moseley. 2003. "Pain and Motor Control of the Lumbopelvic Region: Effect and Possible Mechanisms." *Journal of Electromyography and Kinesiology* 13 (4): 361–70.

Hodges, Paul W, and Carolyn A Richardson. 1996. "Inefficient Muscular Stabilization of the Lumbar Spine Associated with Low Back Pain: A Motor Control Evaluation of Transversus Abdominis." *Spine* 21 (22): 2640–50.

Hodges, Paul W, and Carolyn A Richardson. 1999. "Altered Trunk Muscle Recruitment in People with Low Back Pain with Upper Limb Movement at Different Speeds." *Archives of Physical Medicine and Rehabilitation* 80 (9): 1005–12.

Hotelling, Harold. 1933. "Analysis of a Complex of Statistical Variables into Principal Components." *Journal of Educational Psychology* 24 (6): 417.

Hoy, Damian, Christopher Bain, Gail Williams, Lyn March, Peter Brooks, Fiona Blyth, Anthony Woolf, Theo Vos, and Rachelle Buchbinder. 2012. "A Systematic Review of the Global Prevalence of Low Back Pain." *Arthritis & Rheumatism* 64 (6): 2028–37.

Hoy, Damian, Lyn March, Peter Brooks, Fiona Blyth, Anthony Woolf, Christopher Bain, Gail Williams, et al. 2014. "The Global Burden of Low Back Pain: Estimates from the Global Burden of Disease 2010 Study." *Annals of the Rheumatic Diseases* 73 (6): 968–74.

Hubel, DH. n.d. "Wiesel. TN (1968),'receptive Fields and Functional Architecture of Monkey Striate Cortex'." *Journal of Physiology* 195 (215243): 1703–19.

Ippersiel, Patrick, Shawn Robbins, and Richard Preuss. 2018. "Movement Variability in Adults with Low Back Pain During Sit-to-Stand-to-Sit." *Clinical Biomechanics* 58: 90–95.

Ivakhnenko, Alekse Grigorevich, A G Ivakhnenko, Valentin Grigorevich Lapa, and Valentin Grigorevich Lapa. 1967. *Cybernetics and Forecasting Techniques*. Vol. 8. American Elsevier Publishing Company.

Jackson, David A. 2001. "How Is Low Back Pain Managed?: Retrospective Study of the First 200 Patients with Low Back Pain Referred to a Newly Established Community-Based Physiotherapy Department." *Physiotherapy* 87 (11): 573–81.

Jia, Hongjie, Shifei Ding, Xinzheng Xu, and Ru Nie. 2014. "The Latest Research Progress on Spectral Clustering." *Neural Computing and Applications* 24 (7): 1477–86.

Jöreskog, Karl G. 1970. "A General Method for Estimating a Linear Structural Equation System." *ETS Research Bulletin Series* 1970 (2): i–41.

Karayannis, Nicholas V, Gwendolen A Jull, and Paul W Hodges. 2012. "Physiotherapy Movement Based Classification Approaches to Low Back Pain: Comparison of Subgroups Through Review and Developer/Expert Survey." *BMC Musculoskeletal Disorders* 13 (1): 1–15.

Kendall, Nicholas AS. 1999. "Psychosocial approaches to the prevention of chronic pain: the low back paradigm." *Best Practice & Research Clinical Rheumatology* 13(3): 545–554.

Kienbacher, Thomas and Paul, Birgit and Habenicht, Richard and Starek, Christian and Wolf, Markus and Kollmitzer, Josef and Mair, Patrick and Ebenbichler, Gerold. 2015. "Age and gender related neuromuscular changes in trunk flexion-extension." *Journal of neuroengineering and rehabilitation*. Springer. 12:1–10.

Kienbacher, Thomas and Fehrmann, Elisabeth and Habenicht, Richard and Koller, Daniela and Oeffel, Christian and Kollmitzer, Josef and Mair, Patrick and Ebenbichler, Gerold. 2016. "Age and gender related neuromuscular pattern during trunk flexion-extension in chronic low back pain patients." *Journal of neuroengineering and rehabilitation*. BioMed Central. 13(1):1–13.

Kiers, Henri, Jaap H van Dieën, Simon Brumagne, and Luc Vanhees. 2015. "Postural Sway and Integration of Proprioceptive Signals in Subjects with LBP." *Human Movement Science* 39: 109–20.

Kim, Min-hee, Chung-hwi Yi, Oh-yun Kwon, Sang-hyun Cho, Heon-seock Cynn, Young-ho Kim, Seon-hong Hwang, Bo-ram Choi, Ji-a Hong, and Doh-heon Jung. 2013. "Comparison of Lumbopelvic Rhythm and Flexion-Relaxation Response

Between 2 Different Low Back Pain Subtypes." *Spine* 38 (15): 1260–67.
Kline, P. 1992. "The Handbook of Psych the Handbook of Psych the Handbook of Psychological Testing Ological Testing Ological Testing." London, New York: Routledge.
Kline, Paul. 2014. *An Easy Guide to Factor Analysis*. Routledge.
Koch, Cathrin and Hänsel, Frank. 2019. "Non-specific low back pain and postural control during quiet standing—a systematic review." *Frontiers in psychology*. Frontiers Media SA. 10 : 586.
Koes, Bart W, MWm Van Tulder, and Siep Thomas. 2006. "Diagnosis and Treatment of Low Back Pain." *Bmj* 332 (7555): 1430–34.
Koley, Shyamal and Kaur, Jaswinder and Sandhu, JS. 2010. "Biological risk indicators for non-specific low back pain in young adults of Amritsar, Punjab, India." *Journal of Life Sciences*. Taylor & Francis. 2(1):43–48.
Kosko, Bart, and Sanya Mitaim. 2003. "Stochastic Resonance in Noisy Threshold Neurons." *Neural Networks* 16 (5-6): 755–61.
Koppenaal, Tjarco and Pisters, Martijn F and Kloek, Corelien JJ and Arensman, Remco M and Ostelo, Raymond WJG and Veenhof, Cindy. 2022. "The 3-month effectiveness of a stratified blended physiotherapy intervention in patients with nonspecific low back pain: cluster randomized controlled trial." *Clinical Biomechanics* 24 (2): e31675.
Koutroumbas, Konstantinos, and Sergios Theodoridis. 2008. *Pattern Recognition*. Academic Press.
Laird, Robert A, Jayce Gilbert, Peter Kent, and Jennifer L Keating. 2014. "Comparing Lumbo-Pelvic Kinematics in People with and Without Back Pain: A Systematic Review and Meta-Analysis." *BMC Musculoskeletal Disorders* 15 (1): 1–13.
Laird, Robert A, Jennifer L Keating, and Peter Kent. 2018. "Subgroups of Lumbo-Pelvic Flexion Kinematics Are Present in People with and Without Persistent Low Back Pain." *BMC Musculoskeletal Disorders* 19 (1): 1–13.
Lamoth, Claudine JC, Onno G Meijer, Andreas Daffertshofer, Paul IJM Wuisman, and Peter J Beek. 2006. "Effects of Chronic Low Back Pain on Trunk Coordination and Back Muscle Activity During Walking: Changes in Motor Control." *European Spine Journal* 15 (1): 23–40.
Lamoth, Claudine JC, Onno G Meijer, Paul IJM Wuisman, Jaap H van Dieën, Mindy F Levin, and Peter J Beek. 2002. "Pelvis-Thorax Coordination in the Transverse Plane During Walking in Persons with Nonspecific Low Back Pain." *Spine* 27 (4): E92–99.
Landau, Sabine, Morven Leese, Daniel Stahl, and Brian S Everitt. 2011. *Cluster Analysis*. John Wiley & Sons.
Le, Quoc V et al. 2015. "A Tutorial on Deep Learning Part 1: Nonlinear Classifiers and the Backpropagation Algorithm." *Mountain View, CA*.
LeCun, Yann, Bernhard Boser, John S Denker, Donnie Henderson, Richard E Howard,

Wayne Hubbard, and Lawrence D Jackel. 1989. "Backpropagation Applied to Handwritten Zip Code Recognition." *Neural Computation* 1 (4): 541–51.

Lee, Kijoon. 2022. "Sample Entropy." *MATLAB Central File Exchange*. https://www.mathworks.com/matlabcentral/fileexchange/35784-sample-entropy.

Leitner, Christoph, P Mair, B Paul, F Wick, C Mittermaier, T Sycha, and G Ebenbichler. 2009. "Reliability of Posturographic Measurements in the Assessment of Impaired Sensorimotor Function in Chronic Low Back Pain." *Journal of Electromyography and Kinesiology* 19 (3): 380–90.

Leznik, Michael, and Chris Tofallis. 2005. "Estimating Invariant Principal Components Using Diagonal Regression."

Loisel, Patrick and Vachon, Brigitte and Lemaire, Jacques and Durand, Marie-José and Poitras, Stéphane and Stock, Susan and Tremblay, Claude. 2002. "Discriminative and predictive validity assessment of the quebec task force classification." *Spine*. LWW. 27 (8) : 851–857.

MacDonald, David, G Lorimer Moseley, and Paul W Hodges. 2009. "Why Do Some Patients Keep Hurting Their Back? Evidence of Ongoing Back Muscle Dysfunction During Remission from Recurrent Back Pain." *PAIN®* 142 (3): 183–88.

MacQueen, J. 1967. "Classification and Analysis of Multivariate Observations." In *5th Berkeley Symp. Math. Statist. Probability*, 281–97.

Madeleine, Pascal. 2010. "On Functional Motor Adaptations: From the Quantification of Motor Strategies to the Prevention of Musculoskeletal Disorders in the Neck–Shoulder Region." *Acta Physiologica* 199: 1–46.

Maher, Chris, Martin Underwood, and Rachelle Buchbinder. 2017. "Non-Specific Low Back Pain." *The Lancet* 389 (10070): 736–47.

Mak, Joseph NF, Yong Hu, and Keith DK Luk. 2010. "An Automated ECG-Artifact Removal Method for Trunk Muscle Surface EMG Recordings." *Medical Engineering & Physics* 32 (8): 840–48.

Marras, William S, Sue A Ferguson, Purnendu Gupta, Smarajit Bose, Mohamad Parnianpour, Jung-Yong Kim, and Robert R Crowell. 1999. "The Quantification of Low Back Disorder Using Motion Measures: Methodology and Validation." *Spine* 24 (20): 2091.

Martinez-Valdes, Eduardo, Fiona Wilson, Neil Fleming, Sarah-Jane McDonnell, Alex Horgan, and Deborah Falla. 2019. "Rowers with a Recent History of Low Back Pain Engage Different Regions of the Lumbar Erector Spinae During Rowing." *Journal of Science and Medicine in Sport* 22 (11): 1206–12.

Massaly, Nicolas, Jose A Morón, and Ream Al-Hasani. 2016. "A Trigger for Opioid Misuse: Chronic Pain and Stress Dysregulate the Mesolimbic Pathway and Kappa Opioid System." *Frontiers in Neuroscience* 10: 480.

Mazzocchi, Mario. 2008. *Statistics for Marketing and Consumer Research*. Sage.

McCarthy, Christopher J, Frances A Arnall, Nikolaos Strimpakos, Anthony Freemont, and Jacqueline A Oldham. 2004. "The Biopsychosocial Classification of Non-

Specific Low Back Pain: A Systematic Review." *Physical Therapy Reviews* 9 (1): 17–30.

McEwen, Bruce S and Gianaros, Peter J. 2010. "Central role of the brain in stress and adaptation: links to socioeconomic status, health, and disease." *Annals of the New York Academy of Sciences* 1186(1): 190–222.

Meier, Michael Lukas and Vrana, Andrea and Schweinhardt, Petra. 2019. "Low back pain: the potential contribution of supraspinal motor control and proprioception." *The Neuroscientist* 25(6): 583–596.

Menache, Alberto. 2011. *Understanding Motion Capture for Computer Animation*. Elsevier.

Merletti, Roberto, and Dario Farina. 2016. *Surface Electromyography: Physiology, Engineering, and Applications*. John Wiley & Sons.

Mientjes, MIV, and JS Frank. 1999. "Balance in Chronic Low Back Pain Patients Compared to Healthy People Under Various Conditions in Upright Standing." *Clinical Biomechanics* 14 (10): 710–16.

Miki, Takahiro and Higuchi, Daisuke and Takebayashi, Tsuneo and Samukawa, Mina. 2021. "Factors associating with disability of non-specific low back pain in different subgroups: A hierarchical linear regression analysis." *Scientific reports*. Nature Publishing Group UK London. 11 (1) : 18278.

Milligan, Glenn W, and Martha C Cooper. 1987. "Methodology Review: Clustering Methods." *Applied Psychological Measurement* 11 (4): 329–54.

Mok, Nicola W, Sandra G Brauer, and Paul W Hodges. 2011. "Changes in Lumbar Movement in People with Low Back Pain Are Related to Compromised Balance." *Spine* 36 (1): E45–52.

Mörl, Falk, and Reinhard Blickhan. 2006. "Three-Dimensional Relation of Skin Markers to Lumbar Vertebrae of Healthy Subjects in Different Postures Measured by Open MRI." *European Spine Journal* 15 (6): 742–51.

Mulaik, Stanley A. 2009. *Foundations of Factor Analysis*. CRC press.

Murillo, Carlos, Eduardo Martinez-Valdes, Nicola R Heneghan, Bernard Liew, Alison Rushton, Andy Sanderson, and Deborah Falla. 2019. "High-Density Electromyography Provides New Insights into the Flexion Relaxation Phenomenon in Individuals with Low Back Pain." *Scientific Reports* 9 (1): 1–9.

Najafabadi, Maryam M and Villanustre, Flavio and Khoshgoftaar, Taghi M and Seliya, Naeem and Wald, Randall and Muharemagic, Edin. 2015. "Deep learning applications and challenges in big data analytics." *Journal of big data*. SpringerOpen. 2(1):1–21.

Nascimento, Maria CV, and Andre CPLF De Carvalho. 2011. "Spectral Methods for Graph Clustering–a Survey." *European Journal of Operational Research* 211 (2): 221–31.

Neblett, Randy, Tom G Mayer, Robert J Gatchel, Janice Keeley, Tim Proctor, and Christopher Anagnostis. 2003. "Quantifying the Lumbar Flexion–Relaxation Phenomenon: Theory, Normative Data, and Clinical Applications." *Spine* 28

(13): 1435–46.

Ng, Andrew, Michael Jordan, and Yair Weiss. 2001. "On Spectral Clustering: Analysis and an Algorithm." *Advances in Neural Information Processing Systems* 14.

Nies, N, and Patricia L Sinnott. 1991. "Variations in Balance and Body Sway in Middle-Aged Adults. Subjects with Healthy Backs Compared with Subjects with Low-Back Dysfunction." *Spine* 16 (3): 325–30.

Nishikawa, Yuichi, Kohei Watanabe, Tetsuya Takahashi, Naoya Orita, Hiroaki Kimura, Masayasu Matsumoto, and Hirofumi Maruyama. 2017. "Spatial Electromyography Distribution Pattern of the Vastus Lateralis Muscle During Ramp up Contractions in Parkinson's Disease Patients." *Journal of Electromyography and Kinesiology* 37: 125–31.

Nunally, Jum C, and I Bernstein. 1978. "Psychometric Theory, Ed." *New York McGraw*.

O'Sullivan, Peter. 2005. "Diagnosis and Classification of Chronic Low Back Pain Disorders: Maladaptive Movement and Motor Control Impairments as Underlying Mechanism." *Manual Therapy* 10 (4): 242–55.

Oliveira, Jose. 2022. "Statokinesigram Normalization." *MATLAB Central File Exchange*. https://www.mathworks.com/matlabcentral/fileexchange/51579-statoknorm-x-y.

Oliveira, José Magalhães de. 2017. "Statokinesigram Normalization Method." *Behavior Research Methods* 49 (1): 310–17.

Panjabi, Manohar M. 2003. "Clinical Spinal Instability and Low Back Pain." *Journal of Electromyography and Kinesiology* 13 (4): 371–79.

Papi, Enrica, Anthony MJ Bull, and Alison H McGregor. 2019. "Spinal Segments Do Not Move Together Predictably During Daily Activities." *Gait & Posture* 67: 277–83.

Parent, Rick, David S Ebert, David Gould, Markus Gross, Chris Kazmier, Charles John Lumsden, Richard Keiser, et al. 2009. *Computer Animation Complete: All-in-One: Learn Motion Capture, Characteristic, Point-Based, and Maya Winning Techniques*. Morgan Kaufmann.

Pedregosa, F., G. Varoquaux, A. Gramfort, V. Michel, B. Thirion, O. Grisel, M. Blondel, et al. 2011. "Scikit-Learn: Machine Learning in Python." *Journal of Machine Learning Research* 12: 2825–30.

Pijnenburg, Madelon, Simon Brumagne, Karen Caeyenberghs, Lotte Janssens, Nina Goossens, Daniele Marinazzo, Stephan P Swinnen, Kurt Claeys, and Roma Siugzdaite. 2015. "Resting-State Functional Connectivity of the Sensorimotor Network in Individuals with Nonspecific Low Back Pain and the Association with the Sit-to-Stand-to-Sit Task." *Brain Connectivity* 5 (5): 303–11.

Poitras, Stéphane, Régis Blais, Bonnie Swaine, and Michel Rossignol. 2005. "Management of Work-Related Low Back Pain: A Population-Based Survey of Physical Therapists." *Physical Therapy* 85 (11): 1168–81.

Prieto, Thomas E, Joel B Myklebust, Raymond G Hoffmann, Eric G Lovett, and Barbara M Myklebust. 1996. "Measures of Postural Steadiness: Differences Between Healthy Young and Elderly Adults." *IEEE Transactions on Biomedical Engineering* 43 (9): 956–66.

Radebold, Andrea, Jacek Cholewicki, Manohar M Panjabi, and Tushar Ch Patel. 2000. "Muscle Response Pattern to Sudden Trunk Loading in Healthy Individuals and in Patients with Chronic Low Back Pain." *Spine* 25 (8): 947–54.

Radebold, Andrea, Jacek Cholewicki, Gert K Polzhofer, and Hunter S Greene. 2001. "Impaired Postural Control of the Lumbar Spine Is Associated with Delayed Muscle Response Times in Patients with Chronic Idiopathic Low Back Pain." *Spine* 26 (7): 724–30.

Rényi, Alfréd. 1961. "On measures of entropy and information" *Proceedings of the Fourth Berkeley Symposium on Mathematical Statistics and Probability, Volume 1: Contributions to the Theory of Statistics.* University of California Press. 4 : 547–562.

Robinault, Lucien. 2021. "EMG Preprocessing Tools V1.0.0." https://github.com/TSS-22/EMG-preprocessing-tools.

Heitz, CAM and Hilfiker, R and Bachmann, LM and Joronen, H and Lorenz, T and Uebelhart, D and Klipstein, A and Brunner, Florian. 2009. "Comparison of risk factors predicting return to work between patients with subacute and chronic non-specific low back pain: systematic review." *European Spine Journal*. Springer. 18 : 1829–1835.

Robinault, Lucien and Imran, Khan Niazi and Nitika, Kumari and Imran, Amjad and Vincent, Menard and Heidi, Haavik. (in press). 2023. "Non-Specific Low Back Pain: An Inductive Exploratory Analysis through Factor Analysis and Deep Learning for Better Clustering." *MDPI* 13 (6).

Ronan, Tom and Qi, Zhijie and Naegle, Kristen M. 2016. "Avoiding common pitfalls when clustering biological data." *Science signaling*. American Association for the Advancement of Science. 9(432).

Rousseeuw, Peter J. 1987. "Silhouettes: A Graphical Aid to the Interpretation and Validation of Cluster Analysis." *Journal of Computational and Applied Mathematics* 20: 53–65.

Ruhe, Alexander and Fejer, René and Walker, Bruce. 2010. "The test–retest reliability of centre of pressure measures in bipedal static task conditions–a systematic review of the literature." *Gait & posture*. Elsevier. 32(4):436–445.

Ruhe, Alexander, René Fejer, and Bruce Walker. 2011. "Center of Pressure Excursion as a Measure of Balance Performance in Patients with Non-Specific Low Back Pain Compared to Healthy Controls: A Systematic Review of the Literature." *European Spine Journal* 20 (3): 358–68.

Samson, Monique, and Alan Crowe. 1996. "Intra-Subject Inconsistencies in Quantitative Assessments of Body Sway." *Gait & Posture* 4 (3): 252–57.

Sanderson, Andy, Eduardo Martinez-Valdes, Nicola R Heneghan, Carlos Murillo,

Alison Rushton, and Deborah Falla. 2019. "Variation in the Spatial Distribution of Erector Spinae Activity During a Lumbar Endurance Task in People with Low Back Pain." *Journal of Anatomy* 234 (4): 532–42.

Schinkel-Ivy, Alison, and Janessa DM Drake. 2015. "Which Motion Segments Are Required to Sufficiently Characterize the Kinematic Behavior of the Trunk?" *Journal of Electromyography and Kinesiology* 25 (2): 239–46.

Schofield, Deborah J, Rupendra N Shrestha, Megan E Passey, Arul Earnest, and Susan L Fletcher. 2008. "Chronic Disease and Labour Force Participation Among Older Australians." *Medical Journal of Australia* 189 (8): 447–50.

Scholkopf, Bernhard, Kah-Kay Sung, Christopher JC Burges, Federico Girosi, Partha Niyogi, Tomaso Poggio, and Vladimir Vapnik. 1997. "Comparing Support Vector Machines with Gaussian Kernels to Radial Basis Function Classifiers." *IEEE Transactions on Signal Processing* 45 (11): 2758–65.

Sebestyen, George S. 1962. *Decision-Making Processes in Pattern Recognition (ACM Monograph Series)*. Macmillan Publishing Co., Inc.

Shannon, Claude Elwood. 1948. "A Mathematical Theory of Communication." *The Bell System Technical Journal* 27 (3): 379–423.

Shi, Jianbo, and Jitendra Malik. 2000. "Normalized Cuts and Image Segmentation." *IEEE Transactions on Pattern Analysis and Machine Intelligence* 22 (8): 888–905.

Shum, Gary LK, Jack Crosbie, and Raymond YW Lee. 2005. "Effect of Low Back Pain on the Kinematics and Joint Coordination of the Lumbar Spine and Hip During Sit-to-Stand and Stand-to-Sit." *Spine* 30 (17): 1998–2004.

Shum, Gary LK, Jack Crosbie, and Raymond YW Lee. 2007. "Movement Coordination of the Lumbar Spine and Hip During a Picking up Activity in Low Back Pain Subjects." *European Spine Journal* 16 (6): 749–58.

Shum, Gary LK, Jack Crosbie, and Raymond YW Lee. 2010. "Back Pain Is Associated with Changes in Loading Pattern Throughout Forward and Backward Bending." *Spine* 35 (25): E1472–78.

Sipko, Tomasz, and MICHAŁ Kuczyński. 2013. "Intensity of Chronic Pain Modifies Postural Control in Low Back Patients." *European Journal of Pain* 17 (4): 612–20.

Sneath, Peter HA. 1957. "The Application of Computers to Taxonomy." *Microbiology* 17 (1): 201–26.

Sokal, Robert R. 1958. "A Statistical Method for Evaluating Systematic Relationships." *Univ. Kansas, Sci. Bull.* 38: 1409–38.

Solomonow, Moshe, Richard V Baratta, Anthony Banks, Curt Freudenberger, and Bing He Zhou. 2003. "Flexion–Relaxation Response to Static Lumbar Flexion in Males and Females." *Clinical Biomechanics* 18 (4): 273–79.

Song, Yuedong, Pietro Liò, et al. 2010. "A New Approach for Epileptic Seizure Detection: Sample Entropy Based Feature Extraction and Extreme Learning Machine." *Journal of Biomedical Science and Engineering* 3 (06): 556.

Soper, HE, AW Young, BM Cave, Alice Lee, and Karl Pearson. 1917. "On the Distribution of the Correlation Coefficient in Small Samples. Appendix II to the

Papers of" Student" and RA Fisher." *Biometrika* 11 (4): 328–413.
Srivastava, Nitish, Geoffrey Hinton, Alex Krizhevsky, Ilya Sutskever, and Ruslan Salakhutdinov. 2014. "Dropout: A Simple Way to Prevent Neural Networks from Overfitting." *The Journal of Machine Learning Research* 15 (1): 1929–58.
Stanton, Tasha R, Nicholas Henschke, Chris G Maher, Kathryn M Refshauge, Jane Latimer, and James H McAuley. 2008. "After an Episode of Acute Low Back Pain, Recurrence Is Unpredictable and Not as Common as Previously Thought." *Spine* 33 (26): 2923–28.
Stegeman, Dick, and Hermie Hermens. 2007. "Standards for Surface Electromyography: The European Project Surface EMG for Non-Invasive Assessment of Muscles (SENIAM)." *Enschede: Roessingh Research and Development* 10: 8–12.
Steinley, Douglas. 2003. "Local Optima in k-Means Clustering: What You Don't Know May Hurt You." *Psychological Methods* 8 (3): 294.
Steinley, Douglas. 2006. "K-Means Clustering: A Half-Century Synthesis." *British Journal of Mathematical and Statistical Psychology* 59 (1): 1–34.
Stella, X Yu, and Jianbo Shi. 2003. "Multiclass Spectral Clustering." In *Computer Vision, IEEE International Conference on*, 2:313–13. IEEE Computer Society.
Stigler, Stephen M. 1986. *The History of Statistics: The Measurement of Uncertainty Before 1900*. Harvard University Press.
Sweeney, Kevin T, Seán F McLoone, and Tomas E Ward. 2012. "The Use of Ensemble Empirical Mode Decomposition with Canonical Correlation Analysis as a Novel Artifact Removal Technique." *IEEE Transactions on Biomedical Engineering* 60 (1): 97–105.
Synnott, Aoife, Mary O'Keeffe, Samantha Bunzli, Wim Dankaerts, Peter O'Sullivan, and Kieran O'Sullivan. 2015. "Physiotherapists May Stigmatise or Feel Unprepared to Treat People with Low Back Pain and Psychosocial Factors That Influence Recovery: A Systematic Review." *Journal of Physiotherapy* 61 (2): 68–76.
Tappert, Charles C. 2019. "Who Is the Father of Deep Learning?" In *2019 International Conference on Computational Science and Computational Intelligence (CSCI)*, 343–48. IEEE.
Thurstone, Louis Leon. 1947. "Multiple-Factor Analysis; a Development and Expansion of the Vectors of Mind."
Tsantekidis, Avraam, Nikolaos Passalis, Anastasios Tefas, Juho Kanniainen, Moncef Gabbouj, and Alexandros Iosifidis. 2017. "Forecasting Stock Prices from the Limit Order Book Using Convolutional Neural Networks." In *2017 IEEE 19th Conference on Business Informatics (CBI)*, 1:7–12. IEEE.
Uçar, İlyas and Karartı, Caner and Cüce, İsa and Veziroğlu, Enes and Özüdoğru, Anıl and Koçak, Fatmanur Aybala and Dadalı, Yeliz. 2021. "The relationship between muscle size, obesity, body fat ratio, pain and disability in individuals with and without nonspecific low back pain." *Clinical Anatomy*. Wiley Online Library. 34(8):1201–1207.

Verma, Deepak, and Marina Meila. 2003. "A Comparison of Spectral Clustering Algorithms." *University of Washington Tech Rep UWCSE030501* 1: 1–18.

Villafane, Jorge H, Massimiliano Gobbo, Matteo Peranzoni, Ganesh Naik, Grace Imperio, Joshua A Cleland, and Stefano Negrini. 2016. "Validity and Everyday Clinical Applicability of Lumbar Muscle Fatigue Assessment Methods in Patients with Chronic Non-Specific Low Back Pain: A Systematic Review." *Disability and Rehabilitation* 38 (19): 1859–71.

Vogt, Lutz, Klaus Pfeifer, and Winfried Banzer. 2003. "Neuromuscular Control of Walking with Chronic Low-Back Pain." *Manual Therapy* 8 (1): 21–28.

Vogt, Lutz, Klaus Pfeifer, Martin Portscher, and Winfried Banzer. 2001. "Influences of Nonspecific Low Back Pain on Three-Dimensional Lumbar Spine Kinematics in Locomotion." *Spine* 26 (17): 1910–19.

Von Luxburg, Ulrike. 2007. "A Tutorial on Spectral Clustering." *Statistics and Computing* 17 (4): 395–416.

Von Luxburg, Ulrike, Mikhail Belkin, and Olivier Bousquet. 2008. "Consistency of Spectral Clustering." *The Annals of Statistics*, 555–86.

Weiss, Jay M, Lyn D Weiss, and Julie K Silver. 2021. *Easy EMG-e-Book: A Guide to Performing Nerve Conduction Studies and Electromyography*. Elsevier Health Sciences.

Whedon, James M, Andrew WJ Toler, Justin M Goehl, and Louis A Kazal. 2018. "Association Between Utilization of Chiropractic Services for Treatment of Low-Back Pain and Use of Prescription Opioids." *The Journal of Alternative and Complementary Medicine* 24 (6): 552–56.

Willigenburg, Nienke W, Idsart Kingma, Marco JM Hoozemans, and Jaap H van Dieën. 2013. "Precision Control of Trunk Movement in Low Back Pain Patients." *Human Movement Science* 32 (1): 228–39.

Wu, Ge, Sorin Siegler, Paul Allard, Chris Kirtley, Alberto Leardini, Dieter Rosenbaum, Mike Whittle, et al. 2002. "ISB Recommendation on Definitions of Joint Coordinate System of Various Joints for the Reporting of Human Joint Motion—Part i: Ankle, Hip, and Spine." *Journal of Biomechanics* 35 (4): 543–48.

Wu, Ge, Frans CT Van der Helm, HEJ DirkJan Veeger, Mohsen Makhsous, Peter Van Roy, Carolyn Anglin, Jochem Nagels, et al. 2005. "ISB Recommendation on Definitions of Joint Coordinate Systems of Various Joints for the Reporting of Human Joint Motion—Part II: Shoulder, Elbow, Wrist and Hand." *Journal of Biomechanics* 38 (5): 981–92.

Xie, Yihui. 2022. *Bookdown: Authoring Books and Technical Documents with r Markdown*. https://CRAN.R-project.org/package=bookdown.

Yim, Odilia, and Kylee T Ramdeen. 2015. "Hierarchical Cluster Analysis: Comparison of Three Linkage Measures and Application to Psychological Data." *The Quantitative Methods for Psychology* 11 (1): 8–21.

Zemp, Roland, Renate List, Turgut Gülay, Jean Pierre Elsig, Jaroslav Naxera, William R Taylor, and Silvio Lorenzetti. 2014. "Soft Tissue Artefacts of the

Human Back: Comparison of the Sagittal Curvature of the Spine Measured Using Skin Markers and an Open Upright MRI." *PloS One* 9 (4): e95426.

Zhang, W, K Doi, ML Giger, RM Nishikawa, and Y Wu. 1994. "A Shift-Invariant Artificial Neural Network for Detecting Clustered Microcalcifications in Digital Mammograms." *Medical Physics* 21 (5): 17–24.

Zhang, Wei, Akira Hasegawa, Kazuyoshi Itoh, and Yoshiki Ichioka. 1991. "Image Processing of Human Corneal Endothelium Based on a Learning Network." *Applied Optics* 30 (29): 4211–17.

Zhang, Wei, Jun Tanida, Kazuyoshi Itoh, and Yoshiki Ichioka. 1988. "Shift-Invariant Pattern Recognition Neural Network and Its Optical Architecture." In *Proceedings of Annual Conference of the Japan Society of Applied Physics*, 2147–51. Montreal, CA.